

Utah State University

DigitalCommons@USU

---

All Graduate Theses and Dissertations

Graduate Studies

---

8-2012

## A Mechanistic Study of Catalytic Promiscuity in Protein Phosphatase 1

Yuan Chu  
*Utah State University*

Follow this and additional works at: <https://digitalcommons.usu.edu/etd>

 Part of the [Chemistry Commons](#)

---

### Recommended Citation

Chu, Yuan, "A Mechanistic Study of Catalytic Promiscuity in Protein Phosphatase 1" (2012). *All Graduate Theses and Dissertations*. 1280.

<https://digitalcommons.usu.edu/etd/1280>

This Dissertation is brought to you for free and open access by the Graduate Studies at DigitalCommons@USU. It has been accepted for inclusion in All Graduate Theses and Dissertations by an authorized administrator of DigitalCommons@USU. For more information, please contact [digitalcommons@usu.edu](mailto:digitalcommons@usu.edu).



A MECHANISTIC STUDY OF CATALYTIC PROMISCUITY

IN PROTEIN PHOSPHATASE 1

by

Yuan Chu

A dissertation submitted in partial fulfillment  
of the requirements for the degree

of

DOCTOR OF PHILOSOPHY

in

Chemistry

Approved:

---

Alvan C. Hengge, Ph.D  
Major Professor

---

Lisa M. Berreau, Ph.D  
Committee Member

---

Cheng-Wei Tom Chang, Ph.D  
Committee Member

---

Bradley S. Davidson, Ph.D  
Committee Member

---

Marie K. Walsh, Ph.D  
Committee Member

---

Mark R. McLellan  
Vice President for Research and  
Dean of Graduate Studies

UTAH STATE UNIVERSITY  
Logan, Utah

2012

Copyright © Yuan Chu

All Rights Reserved

**ABSTRACT**

A Mechanistic Study of Catalytic Promiscuity in Protein Phosphatase 1

by

Yuan Chu, Doctor of Philosophy

Utah State University, 2012

Major Professor: Dr. Alvan C. Hengge  
Department: Chemistry and Biochemistry

“Catalytic promiscuous” enzymes, which possess additional activities besides their “native” activity, albeit with a lower efficiency than the main reaction, have become a new frontier for biochemistry and have received considerable attention. Catalytic promiscuity has been suggested to contribute to enzyme evolution through the mechanism of gene duplication followed by specialization of one of the two copies for the new function. Mimicking this evolutionary shortcut could also provide a more efficient route to changing the function of proteins by directed evolution.

The promiscuous phosphatase PP1 is a member of the phosphoprotein phosphatase (PPP) gene family, which is critical for the control of many cellular pathways by antagonizing the effects of protein phosphorylation mediated by kinases. The catalytic promiscuity of PP1 $\gamma$  WT and two mutants has been investigated with a set of monoanionic and dianionic phosphoester substrates.

PP1 $\gamma$  is an effective catalyst for the hydrolysis of both monoanionic and dianionic phosphate-ester based substrates **1-5**, with second-order rate accelerations that fall within

the narrow range of  $10^{11}$  to  $10^{13}$ . While the transition states of the uncatalyzed hydrolysis reactions of these substrates differ, those for the PP1 $\gamma$ -catalyzed reactions are similar. Thus, the enzyme catalyzes the hydrolysis of these substrates by transition states that are controlled by the active site environment more than by the intrinsic nature of the substrates. The reason for the inability of PP1 $\gamma$  to catalyze the hydrolysis of a sulfate ester is unclear, and unexpected, since the charge and transition state of this substrate are well within the range of those of the phosphorus-based substrates that are effectively catalyzed.

Inhibition experiments suggest that the PP1 $\gamma$  active site is tolerant of variations in the geometry of bound ligands. This characteristic may permit the effective catalysis even of substrates whose steric requirements may result in perturbations to the positioning of the transferring group, both in the initial enzyme-substrate complex and in the transition state.

The conservative mutation of arginine 221 to lysine results in a mutant that more effectively catalyzes monoanionic substrates than the native enzyme. The surprising result in substrate preference from a single, conservative mutation lends support to the notion that mutations following gene duplication can result in an altered enzyme with different catalytic capabilities and preferences, and may, following subsequent mutations, provide a pathway for the evolution of new enzymes.

**Public Abstract**  
**A Mechanistic Study of Catalytic Promiscuity in Protein Phosphatase 1**

Catalytic promiscuity describes the ability of an enzyme to catalyze chemically distinct reactions. This can involve forming and cleaving different type of bonds, or using more than one mechanistic pathway for the same overall bond making and breaking process. In the case, the catalytic efficiency ( $k_{\text{cat}}/K_M$ ) is usually significantly lower than the native reaction. In recent years the promiscuity of enzymes has drawn considerable attention for the insights offered into enzyme evolution, and for potential applications in enzyme engineering and biocatalysis.

The uncatalyzed hydrolyses of phosphate monoesters and diesters are extremely slow, and the same is true of sulfate esters, which are also biologically important compounds. The rate accelerations of phosphatases and sulfatases are among the most significant enzymatic rate accelerations known.

Protein phosphatase-1 (PP1), a member of the phosphoprotein phosphatase (PPP) gene family, is a metalloenzyme that utilizes a dinuclear metal center to catalyze the hydrolysis of phosphate esters using a metal-coordinated hydroxide nucleophile. Besides its native phosphate monoesterase activity, PP1 exhibits activity for aryl methylphosphonate substrates.<sup>12</sup> In this work, the promiscuity of PP1 was assessed with fluorophosphate esters, phosphorothioate esters, phosphodiester, and sulfate esters (**Figure 2**). These substrates vary in their intrinsic reactivity, the size and charge of the transferring group, and in their mechanism and transition states for uncatalyzed hydrolysis. Linear free energy relationships and kinetic isotope effects were measured, and used to assess the transition states of the PP1-catalyzed reactions compared to the uncatalyzed hydrolysis reactions.

In addition to studies with native PP1, two active site arginine residues, R221 and R96, which X-ray structures indicate interact with the transferring group, were mutated to lysine, and the effects on the catalyzed reaction with each substrate type was assessed. The results support the notion that in PP1 a single conservative mutation can selectively affect the substrate preference based on charge. A series of anionic inhibitors with geometries ranging from trigonal bipyramidal to octahedral were tested as inhibitors to further probe how geometry and charge affect affinity for the PP1 active site. The results show a surprising tolerance for geometry variations, which is consistent with the ability of PP1 to efficiently catalyze a wide range of substrates that vary in size and charge.

## ACKNOWLEDGMENTS

It is difficult to fully express my gratitude and to describe the impact Dr. Alvan C. Hengge has had on my development as a scientist. I have been unbelievably fortunate to have the opportunity to work in his laboratory. Dr. Hengge always gave me the freedom to explore on my own, and at the same time provided the guidance to recover the right direction. I also appreciate the patience and understanding that he has had over the years. In addition, I would express my thanks to Dr. Nicholas H. Williams, University of Sheffield, for his gracious help to the project.

I would also like to extend my great gratitude to my committee members, Dr. Lisa M. Berreau, Dr. Cheng-Wei Tom Chang, Dr. Bradley S. Davidson, and Dr. Marie K. Walsh. Your encouragement, assistance, and advice have made my educational experience enjoyable and informative. I am especially thankful to Dr. Lisa M. Berreau for her helpful advice in overcoming many “metal” questions. I have greatly benefited from her suggestions, without which I would have been lost in the literature.

The support of the other students in the laboratory is priceless. The days seemed to go by much easier because of you. I would especially like to thank Tiago Brandão, whose friendship will be treasured forever. Special thanks to Mark Haney for his technical assistance, language advice, inspiration, and friendship. Great colleagues, Vyacheslav Kuznetsov, Alok Shenoy, and many other lab mates not named here, made a pleasant environment to work in. Their stories made the dry experiments in the lab more enjoyable. The friendship and support of the department members cannot go without recognition. I would like to thank LuAnn Stocking, Margaret Dobrowolska, and Katarzyna Grubel for their friendship when switching group issues affected my studies.

I wouldn't be anything without the influence of some very special people who have contributed to my development in science and life. First and foremost, this second Ph.D degree would not have been possible without the constant support and encouragement from my parents and Zhiyong Yang. Their endless love and patience provide the endless source of power to conquer my fear of tough circumstances. To my parents, this achievement is in honor of you all. I would like to thank my best friend Jerpín Chong for the happiness and understanding that he brought to me. Last but not least, I want to thank Bo Li for his inspiration and company over the hardest time of writing the dissertation.

Yuan Chu

初 媛

## CONTENTS

	Page
ABSTRACT .....	iii
PUBLIC ABSTRACT .....	v
ACKNOWLEDGMENTS .....	vi
LIST OF TABLES .....	xii
LIST OF FIGURES .....	xiv
CHAPTER	
1. RESEARCH BACKGROUND .....	1
1.1. Catalytic promiscuity .....	1
1.1.1. Definition .....	1
1.1.2. Significance .....	3
1.2. Phosphoryl transfer reactions .....	4
1.2.1. Overview of phosphates and phosphoryl transfer reactions .....	4
1.2.2. Enzymatic phosphoryl transfer .....	6
1.2.3. Uncatalyzed phosphoryl transfer reaction mechanism .....	7
1.2.3.1. Mechanistic generalizations .....	7
1.2.3.2. Uncatalyzed reactions of phosphate monoester dianions .....	9
1.2.3.3. Uncatalyzed reactions of phosphorothioate monoester .....	12
1.2.3.4. Uncatalyzed reactions of phosphate diesters .....	14
1.3. Catalytic promiscuity of phosphatases .....	16
1.3.1. Catalytic promiscuity of <i>E. coli</i> alkaline phosphatase (AP) .....	16
1.3.2. Catalytic promiscuity of aryl sulfatase .....	20
1.3.3. Catalytic promiscuity of phosphonate monoester hydrolase (PMH) .....	23
1.3.4. Catalytic promiscuity of purple acid phosphatase (PAP) .....	27
1.3.5. Catalytic promiscuity of protein phosphatase 1 (PP1) .....	30
1.4. Protein phosphatase 1 .....	32
1.4.1. Brief introduction of PP1 .....	32

	ix
1.4.2. Catalytic subunit of PP1 .....	34
1.4.2.1. General features of the structure .....	35
1.4.2.2. The metal coordination geometry at the active site .....	36
1.4.2.3. Substrate binding site .....	38
1.4.2.4. Bacterially expressed catalytic subunit of PP1 .....	39
1.4.3. Proposed catalytic mechanism of PP1 .....	40
1.4.4. Mutagenesis study of catalytic subunit of PP1 .....	41
1.5. Main goal .....	45
1.6. References .....	46
<b>2. MATERIALS AND METHODS .....</b>	<b>56</b>
2.1. Substrate synthesis and characterization .....	56
2.1.1. Materials and instruments .....	57
2.1.2. Synthesis and characterization of aryl phosphorothioate bis(cyclohexyl amine) salts (2a-h) .....	57
2.1.3. Synthesis and characterization of aryl fluorophosphate monoester potassium salts (3a-f) .....	59
2.1.4. Synthesis and characterization of other substrates .....	62
2.2. Protein expression and purification .....	64
2.2.1. Materials and instruments .....	64
2.2.2. Expression and purification of PP1 $\gamma$ wild type .....	64
2.2.3. Generation of mutant proteins .....	67
2.2.4. Generation of different metal forms of PP1 $\gamma$ .....	70
2.3. Kinetic measurements .....	71
2.3.1. UV-vis spectroscopy analysis of PP1 $\gamma$ -catalyzed hydrolysis of substrate classes .....	71
2.3.2. Reverse phase-HPLC analysis of PP1 $\gamma$ -catalyzed hydrolysis of substrate classes .....	71
2.3.3. Test for sulfatase activity .....	73
2.3.4. Inhibition measurement .....	73
2.4. Isotope effect measurements .....	75
2.5. Summary .....	76
2.6. References .....	76

3. PP1 $\gamma$ EXHIBITS CATALYTIC PROMISCUITY AND HIGH CATALYTIC EFFICIENCY TOWARDS FIVE SUBSTRATE CLASSES .....	78
3.1. Introduction .....	78
3.2. Results and discussion .....	80
3.2.1. Design principles of substrate classes .....	80
3.2.2. Determination of optimal conditions for kinetic studies .....	82
3.2.3. PP1 $\gamma$ exhibits catalytic promiscuity towards all of the substrate classes except substrate 6 .....	84
3.2.4. The PP1 $\gamma$ -catalyzed hydrolysis of substrate classes 1-5 follows the same catalytic mechanism .....	87
3.2.5. The PP1 $\gamma$ -catalyzed reactions exhibit remarkably rate accelerations compared with the corresponding uncatalyzed hydrolysis reactions .....	90
3.2.6. LFER and KIE measurements indicate that the mechanism of PP1 $\gamma$ -catalyzed reactions and transition states are similar for all substrate classes .....	92
3.2.7. The binding of inhibitors is affected primarily by charge rather than size .....	97
3.2.8. <i>para</i> -Nitrophenyl sulfate is not a substrate for PP1 $\gamma$ .....	100
3.3. Summary .....	101
3.4. References .....	102
4. MUTAGENESIS AND METAL ACTIVATION STUDIES ON RECOMBINANT PP1 $\gamma$ .....	106
4.1. Introduction .....	106
4.1.1. Mutagenesis studies on recombinant PP1 $\gamma$ .....	106
4.1.2. Metal ions at the active site .....	108
4.1.3. Specific aims .....	109
4.2. Results and discussion .....	110
4.2.1. Design principle of Arg $\rightarrow$ Lys mutants .....	110
4.2.2. Kinetic properties of Arg $\rightarrow$ Lys mutants .....	111
4.2.3. Hydrolysis of substrates 1-5a by PP1 $\gamma$ mutants .....	116
4.2.4. Preliminary study on Mg <sup>2+</sup> activation of PP1 $\gamma$ .....	118
4.3. Summary .....	119
4.4. References .....	120
5. CONCLUSIONS .....	122

APPENDIX .....	xi
CURRICULUM VITAE .....	127
	176

## LIST OF TABLES

Table	page
<b>1-1</b> Kinetic isotope effects for the uncatalyzed hydrolysis of different phosphate esters. ....	11
<b>1-2</b> Kinetic parameters for <i>E. coli</i> AP-catalyzed hydrolysis of phosphodiester, sulfate monoester, phosphate monoester and phosphonate monoester. ....	20
<b>1-3</b> Kinetic parameters for the PAS-catalyzed hydrolysis of phosphodiester <b>A</b> and <b>B</b> , sulfate monoester, and phosphate monoester. ....	23
<b>1-4</b> Kinetic parameters for the <i>Bc</i> PMH-catalyzed hydrolysis of six substrate classes including phosphate monoester <b>I</b> , phosphodiester <b>II</b> , phosphate triester <b>III</b> , phosphonate monoester <b>IV</b> , sulfate monoester <b>V</b> , and sulfonate monoester <b>VI</b> . ...	26
<b>1-5</b> The kinetic parameters of wild type PP1 and mutation of active site residues predicted to bind metals. ....	42
<b>1-6</b> The kinetic parameters of wild type PP1 and mutation of active site residues predicted to bind substrates and assist catalysis. ....	43
<b>2-1</b> Phenolic leaving groups used in PP1 $\gamma$ -catalyzed hydrolysis reactions with their $pK_a$ values. ....	56
<b>2-2</b> Primers used for each specific mutation. ....	68
<b>2-3</b> Conditions for HPLC used for product analysis of enzymatic assay and substrates for the PP1 $\gamma$ -catalyzed hydrolysis reaction with their leaving group $pK_a$ values. ....	72
<b>2-4</b> Various inhibitors used in the PP1 $\gamma$ -catalyzed hydrolysis of <b>1a</b> (pNPP) at pH 7.0. ....	74
<b>3-1</b> Structures and molecular properties of the examined substrate classes. ....	81
<b>3-2</b> Effect of external manganese on PP1 $\gamma$ -catalyzed hydrolysis. ....	83
<b>3-3</b> Kinetic parameters for the hydrolysis of substrates <b>1a-5a</b> at pH 7.0 by PP1 $\gamma$ wild type. ....	84
<b>3-4</b> The kinetic $pK_a$ values for PP1 $\gamma$ -catalyzed hydrolysis of substrates <b>1a-5a</b> at 25°C derived from fits to <b>Equation 3-2</b> . ....	89

<b>3-5</b>	Substrates for the PP1 $\gamma$ -catalyzed hydrolysis reaction with their leaving group $pK_a$ values. ....	93
<b>3-6</b>	Brønsted $\beta_{lg}$ values for the PP1 $\gamma$ -catalyzed and for the uncatalyzed hydrolysis reactions of substrate classes <b>1-4</b> . ....	94
<b>3-7</b>	KIE data for uncatalyzed and PP1 $\gamma$ -catalyzed reactions. ....	95
<b>3-8</b>	Inhibition of the PP1 $\gamma$ -catalyzed hydrolysis of <b>1a</b> (pNPP) by various inhibitors at pH 7.0. ....	99
<b>4-1</b>	Catalytic parameters of pNPP hydrolysis by PP1 $\gamma$ R96K and R221K mutants at varying pH. ....	111
<b>4-2</b>	The derived kinetic $pK_a$ values for mutants of PP1 $\gamma$ . ....	112
<b>4-3</b>	Kinetic parameters and values from the hydrolysis of pNPP by the R96K mutant. ....	115
<b>4-4</b>	Catalytic efficiency ( $k_{cat}/K_M$ , $M^{-1}s^{-1}$ ) for the hydrolysis of substrates <b>1a-5a</b> at pH 7.0 by wild type and arginine mutants of PP1 $\gamma$ . ....	117

## LIST OF FIGURES

Figure	page
<b>1-1</b> Catalytic promiscuity is one type of enzyme promiscuity. ....	2
<b>1-2</b> In substrate promiscuity, enzymes perform the same chemical transformation with different substrates. ....	3
<b>1-3</b> The structures of phosphoryl groups and various types of phosphate esters. ....	5
<b>1-4</b> Diagram illustration of phosphoryl transfer. ....	6
<b>1-5</b> The transfer of the phosphoryl group from a phosphorylated protein to water is catalyzed by protein phosphatase. ....	7
<b>1-6</b> Three distinct reaction mechanisms for phosphate esters uncatalyzed hydrolysis reactions, dissociative (A) and associative (B) mechanistic extremes, and the concerted pathway (C). ....	8
<b>1-7</b> pH-rate profile for <i>para</i> -nitrophenyl phosphate monoester (pNPP) at 39 °C, ionic strength 1.0, on adjusted scale $k_{\text{hyd}} \times 10^7 \text{ min}^{-1}$ . ....	9
<b>1-8</b> (A) Hydrolysis rates for pNPP dianions at 39 °C, as a function of the $\text{p}K_{\text{a}}$ of the conjugate acid the leaving group. (B) Second-order rate constants for reactions of amines with pNPP dianion at 39°C and ionic strength 1.0, plotted against the $\text{p}K_{\text{a}}$ of the attacking amine. ....	10
<b>1-9</b> More-O’Ferrall-Jencks diagrams for phosphate monoester dianions (A) and phosphate diester (B) hydrolysis in solution. ....	12
<b>1-10</b> pH-rate profile for <i>para</i> -nitrophenyl phosphorothioate monoester (pNPPT) at 39 °C. ....	13
<b>1-11</b> (A) Hydrolysis rates for pNPPT dianions at 37 °C, as a function of the $\text{p}K_{\text{a}}$ of the conjugate acid the leaving group. (B) Eyring plot for the aqueous hydrolysis of pNPPT dianion. ....	14
<b>1-12</b> (A) Influence of buffer pH on rate constant for hydrolysis of $\text{Np}_2\text{P}$ (■) at 25 °C and $\text{Np}_2^*\text{P}$ (●) at 250 °C. (B) Linear free energy relationship between the second-order rate constant for hydroxide-catalyzed hydrolysis of methyl 2,4-dinitrophenyl phosphate diesters at 25 °C and the $\text{p}K_{\text{a}}$ of the conjugate acid of the leaving group. ....	15

<b>1-13</b>	(A) Active site structure of <i>E. coli</i> AP. (B) Transition state model for phosphoryl transfer by <i>E. coli</i> AP based on X-ray structure of this enzyme. ....	16
<b>1-14</b>	Proposed phosphoryl transfer mechanism catalyzed by <i>E. coli</i> AP. ....	17
<b>1-15</b>	A stereo view of the intermolecular contacts between protein residues and sulfate in the active site region of PAS base upon the crystal structure. ....	21
<b>1-16</b>	Proposed catalytic mechanism for PAS using a sulfate monoester as the substrate. ....	21
<b>1-17</b>	(A) The active site structure of <i>Bc</i> PMH. (B) Proposed mechanism for phosphonate monoester hydrolysis by <i>Bc</i> PMH. ....	24
<b>1-18</b>	(A) Crystal structure of rat purple acid phosphatase shows the di-nuclear iron center with bound sulfate ion. (B) A view of the di-iron center and the active site of rat purple acid phosphatase as seen in the crystals. ....	28
<b>1-19</b>	A view of the active site of PP1 with bound phosphate monoester as the hypothetical model according to the crystal structure. ....	31
<b>1-20</b>	The three families, phosphoprotein phosphatases (PPP), metal-dependent protein phosphatases (PPM), and aspartate-based phosphatases (FCP/SCP), of protein serine/threonine phosphatases. ....	33
<b>1-21</b>	Nucleotide and amino-acid sequence of the human PP1 $\gamma$ 1 and PP1 $\gamma$ 2 gene and comparison to the amino acid sequences of human PP1 $\alpha$ . ....	35
<b>1-22</b>	(A) Topology diagram showing the catalytic site of the secondary structural of PP1. (B) Structure of the catalytic subunit of PP1 bound to okadaic acid. ....	36
<b>1-23</b>	(A) Crystal structure of the active site of PP1 from literature. (B) Crystal structure of the catalytic site showing metal ions (cyan spheres) and tungstate binding sites from literature. ....	37
<b>1-24</b>	Conserved coordination of the binuclear metal center in the PPP superfamily. ....	38
<b>1-25</b>	The proposed PP1-catalyzed hydrolysis mechanism according to the crystal structure. ....	41
<b>2-1</b>	Structures of designed substrate classes. ....	56
<b>2-2</b>	(A) Chromatogram of the purification of PP1 $\gamma$ on HiTrap Heparin column at 280 nm. (B) SDS-PAGE of fractions 47-54 from HiTrap Heparin column. ....	65

2-3	(A) Chromatogram of the purification of PP1 $\gamma$ on HiTrap Q sepharose column at 280 nm. (B) SDS-PAGE of fractions 11-16 from Q sepharose column. ....	66
2-4	(A) Chromatogram of the purification of PP1 $\gamma$ on HiTrap SP sepharose column at 280 nm. (B) SDS-PAGE of fractions 31-37 from SP sepharose column. ....	67
2-5	Analytical 1% agarose gel stained with ethidium bromide showing the overlap extension PCR of wild type PP1 $\gamma$ to produce the R96K mutant. ....	69
2-6	Substrates pNPP and pNPPT with the positions indicated at which isotope effects were measured. ....	75
3-1	pH-rate profiles of $k_{cat}/K_M$ for the hydrolysis of five different substrate classes catalyzed by PP1 $\gamma$ . ....	87
3-2	pH-rate profiles of $k_{cat}$ for the hydrolysis of two different substrate classes catalyzed by PP1 $\gamma$ . ....	88
3-3	Brønsted plot for the PP1 $\gamma$ -catalyzed hydrolysis of four substrate classes. ....	93
4-1	(A) Crystal structure of the catalytic site showing metal ions (cyan spheres) and tungstate binding sites. (B) Schematic diagram of the active site of PP1 $\gamma$ and proposed reaction mechanism involving nucleophilic attack by bridging hydroxide. ....	106
4-2	Phosphatase activity of reactivation PP1 by different metal ion. ....	109
4-3	Comparison of the pH dependence of $\log(k_{cat}/K_M)$ for pNPP hydrolysis by wild type PP1 $\gamma$ (■), the R96K (●), and the R221K (⊕) mutants. ....	113
4-4	Comparison of the pH dependence of $\log(k_{cat})$ for pNPP hydrolysis by PP1 $\gamma$ R96K (●) and R221K (⊕) mutants. ....	114
4-5	Comparison of the pH dependence of $\log(1/K_M)$ for pNPP hydrolysis by PP1 $\gamma$ R96K (●) and R221K (⊕) mutants. ....	116
4-6	Dependence of $k_{cat}/K_M$ on pH for the hydrolysis of pNPP by PP1 Mn(II) form (■) and by PP1 Mg(II) form (⊥). ....	119

## CHAPTER 1

### RESEARCH BACKGROUND

#### 1.1 Catalytic promiscuity

##### 1.1.1 Definition

Promiscuous enzymes can perform additional functions besides their “native” activities, challenging the textbook adage “one enzyme, one activity.” During the past decade, enzyme promiscuity received considerable attention. Increasing evidence suggests that promiscuous activities of enzymes can provide insight into an important question: protein evolution.

For example, organophosphorus triesters, like paraoxon, are not naturally occurring compounds. They have been used in pesticides in large quantities for no longer than 80 years. Catalytically “perfect” enzymes, like phosphotriesterase from *Pseudomonas diminuta*<sup>1</sup> whose catalytic efficiency ( $k_{\text{cat}}/K_{\text{M}}$ ) is as high as  $10^8 \text{ M}^{-1} \text{ s}^{-1}$ , exist for hydrolyzing paraoxon despite the fact that it has only been exposed to the environment within the last century. How can an enzyme detoxify antibiotics and environmental toxins that have been in the environment for a far shorter time than the billions of years assumed to be necessary for the development of essential enzymes? Catalytic promiscuity equips a protein with a second head-start activity that can be adapted without compromising the original activity. The lower activities might already be sufficient to support a metabolic function.

Catalytic promiscuity, also referred to as cross-reactivity, poly-reactivity, or moonlighting, is defined as the ability of enzyme active sites to catalyze chemically

distinct reactions that involve forming and cleaving different types of bonds and/or proceeding with different mechanism or pathway of bond making and breaking, albeit with a lower efficiency than the main reaction.<sup>2</sup> The promiscuous reaction may be the same class of reaction as the native activity, but the bonds made and broken, or the transition states, might differ between the native and promiscuous functions. For example (**Figure 1-1**), to possess the catalytic promiscuity of both phosphodiesterase and sulfatase activity, an enzyme with the native activity of phosphate diesters hydrolysis must tolerate the different reaction centers and retain the ability to stabilize the transition state of the bond making and breaking processes in sulfate monoester hydrolysis. Furthermore, the transition states involved in these two hydrolysis reactions are different: phosphate diesters pass through a tight transition state while sulfate esters proceed through a loose transition state.

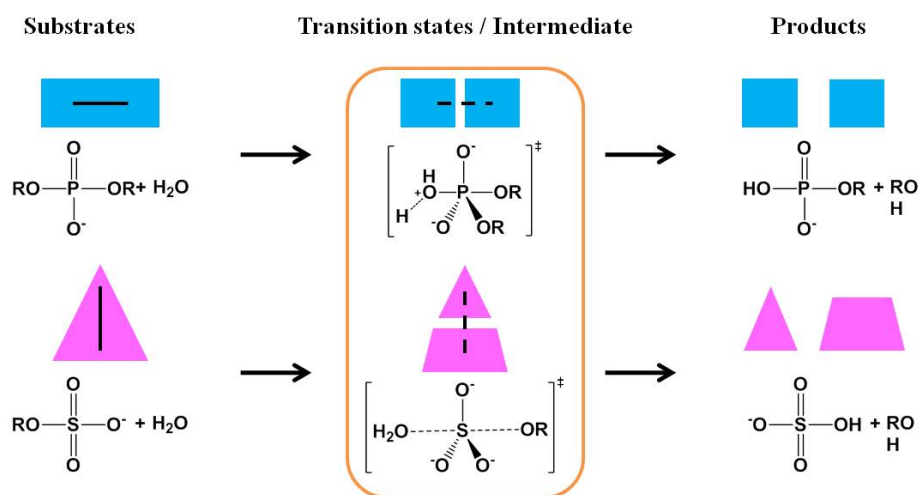


**Figure 1-1.** Catalytic promiscuity is one type of enzyme promiscuity.

In contrast, substrate promiscuity is the ability of enzymes to perform the same chemical reaction on different substrates. For instance, many hydrolases accept a wide range of substrates with different substituents, which are shown as a blue circle and pink

triangle in **Figure 1-2**), but always tackle the same chemical functionality which is represented by the blue rectangle in **Figure 1-2**.

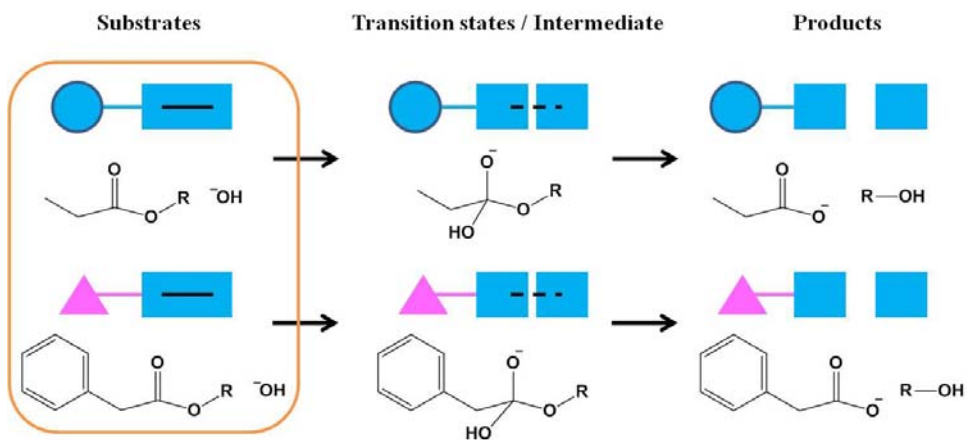


**Figure 1-2.** In substrate promiscuity, enzymes perform the same chemical transformation with different substrates.

As of this writing, about two dozen catalytically promiscuous proteins have been identified.<sup>3-8</sup> Generally, promiscuous activities share the main active site features with the native activity.<sup>6</sup> It is well known that enzymatic active sites are reactive environments, already crowded with a range of potential nucleophiles, electrophiles, acids, bases, metal ions, and sometimes other cofactors beneficial for catalysis. Sometimes conformational changes in the active site enable the same enzyme to accommodate different reactions.<sup>9,10</sup>

### 1.1.2 Significance

Catalytic promiscuity has been suggested to contribute to enzyme evolution, through the mechanism of gene duplication followed by specialization of one of the two copies for the new function. Mimicking this evolutionary shortcut could also provide a more efficient route to changing the function of proteins by directed evolution.<sup>11</sup>

The catalytic promiscuity of enzymes has drawn considerable attention in terms of enzyme evolution, enzyme engineering, and biocatalysis. The evolutionary aspect of promiscuity was first discussed in detail by Jensen<sup>12</sup> and then by O'Brien and Herschlag.<sup>3</sup> It has been proposed that promiscuity might provide a starting point for divergent evolution after gene duplication based upon the fact that many enzymes have remarkably broad substrate specificities. If a duplicated gene's product already has some low level of activity toward a new biological function, once the activity reaches the threshold for which a selectable advantage is conferred, evolutionary pressure then has a higher probability of adapting and improving the new activity through natural selection. Several successes in protein engineering also support the potential role of catalytic promiscuity in the evolution of new enzymatic activities. These results show that a single or a few point mutations can substantially improve the ability of enzymes to carry out new reactions. Catalytic promiscuity has been exploited in biocatalysis.<sup>5</sup> A classic example is yeast pyruvate decarboxylase, used in industry, which not only decarboxylates pyruvate but also forms a carbon-carbon bond between acetaldehyde and benzaldehyde.<sup>13,14</sup>

## **1.2 Phosphoryl transfer reactions**

### **1.2.1 Overview of phosphates and phosphoryl transfer reactions**

Phosphoryl groups are derivatives of phosphoric acid, a strong acid that is commonly used in the laboratory (**Figure 1-3**). Phosphoric acid is triprotic, which has three protons available to donate, with  $pK_a$  values of 2.1, 7.2, and 12.3, respectively. At the physiological pH of approximately 7.3, all phosphoric acid species in solution will have donated at least one proton, and more than half will have donated two. The average

charge on the phosphate ion is slightly higher than -1.5. The fully deprotonated conjugate base of phosphoric acid is called a phosphate ion, or inorganic phosphate (often abbreviated “P<sub>i</sub>”). When two phosphate groups are linked to each other, the ion is called “phosphate anhydride”. When a phosphate ion is attached to a carbon atom on an organic molecule, the whole species is called a phosphate monoester. Phosphate monoester dianions and phosphate monoester monoanions are two forms that exist under the physiological condition in solution. Phosphate monoesters appear throughout the biochemical world. Phosphorylated proteins are also phosphate monoesters. When a single phosphate is linked to two organic groups, the term “phosphate diester” is used. The best known examples of phosphate diesters are the linkage connecting DNA and RNA. Oxygen atoms in phosphate groups are referred to either “bridging” or “non-bridging”, depending on their position.

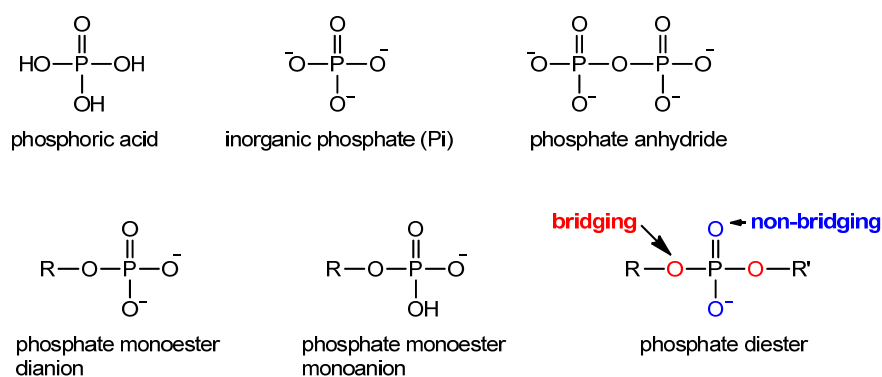


**Figure 1-3.** The structures of phosphoryl groups and various types of phosphate esters.

Phosphoryl transfer is the name given to the chemical process of the transfer of the phosphoryl group from a phosphate ester or anhydride to a nucleophile. **Figure 1-4** illustrates the transfer of a single phosphate group from R<sub>2</sub> to R<sub>1</sub>. Both the phosphate monoester bond and the phosphodiester linkages are incredibly stable at neutral pH. The

uncatalyzed rate for spontaneous methyl phosphate dianion hydrolysis is  $2 \times 10^{-20} \text{ s}^{-1}$  at  $25 \text{ }^\circ\text{C}$ .<sup>15</sup> The half-life of cleavage of phosphodiester linkages of RNA, destabilized by the neighboring 2'-hydroxyl group, is estimated to be about 4 years.<sup>16</sup> Moreover, the half-life of the hydrolysis of dimethyl phosphate, which is taken as a model for the phosphodiester linkages in DNA, is about 140,000 years<sup>17</sup> in the pH-independent range near neutrality. By contrast, phosphatases and diesterases catalyze these same hydrolysis reactions very rapidly.

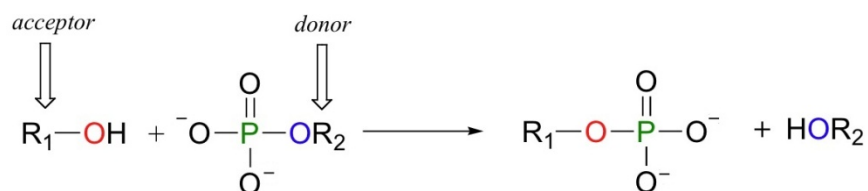


**Figure 1-4.** Diagram illustration of phosphoryl transfer.

### 1.2.2 Enzymatic phosphoryl transfer

Protein dephosphorylation and phosphorylation, executed by phosphatases and kinases, respectively, have been studied for decades because this process functions as a switch between active and inactive states for many proteins. Nearly all aspects of cell life are regulated by reversible protein phosphorylation. Some examples include metabolic processes, gene regulation, cell cycle control, transport and secretory processes, the organization of the cytoskeleton, and cell adhesion. This net dephosphorylation reaction is catalyzed by phosphatases. The formation of phosphate esters is termed phosphorylation, and is accomplished in biological systems by kinases. The figure below (**Figure 1-5**) illustrates the transfer of an inorganic phosphate (Pi) from a phosphorylated protein by protein phosphatase.

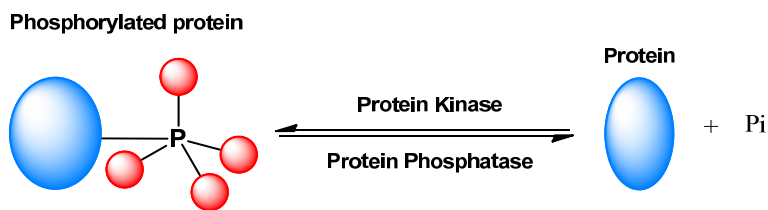


**Figure 1-5.** The transfer of the phosphoryl group from a phosphorylated protein to water is catalyzed by protein phosphatase.

Protein phosphatases can be divided into three main subclasses based upon their substrate specificity and protein structures. Non-specific phosphatases include alkaline phosphatases and acid phosphatases, which hydrolyze a wide range of substrates *in vivo*. Protein serine/threonine phosphatases and protein tyrosine phosphatases specifically dephosphorylate phosphorylated serine/threonine or phosphorylated tyrosine residues. Small molecule specific phosphatases catalyze the hydrolysis of small molecules such as glucose 6-phosphate and inositol monophosphate. Phosphatases are extremely efficient enzymes, with  $k_{\text{cat}}$  values 10 or more orders of magnitude greater than the rate constants for the corresponding uncatalyzed hydrolysis reactions. In order to understand how such huge rate accelerations are achieved, it is important to understand the mechanism and transition state structures of both the background and enzyme-catalyzed hydrolysis.

### 1.2.3 Uncatalyzed phosphoryl transfer reaction mechanism

#### 1.2.3.1 Mechanistic generalizations

The importance of phosphate esters in nature has been one of the reasons for continued interest in the mechanism of phosphoryl transfer that these compounds undergo. The fact that phosphate esters undergo phosphoryl transfer by a range of mechanisms depending primarily on the alkylation state (mono-, di-, or triester) of the

reactant is fascinating to scientists. Three limiting mechanisms have been observed for uncatalyzed hydrolysis reactions of phosphate esters, shown in **Figure 1-6**.

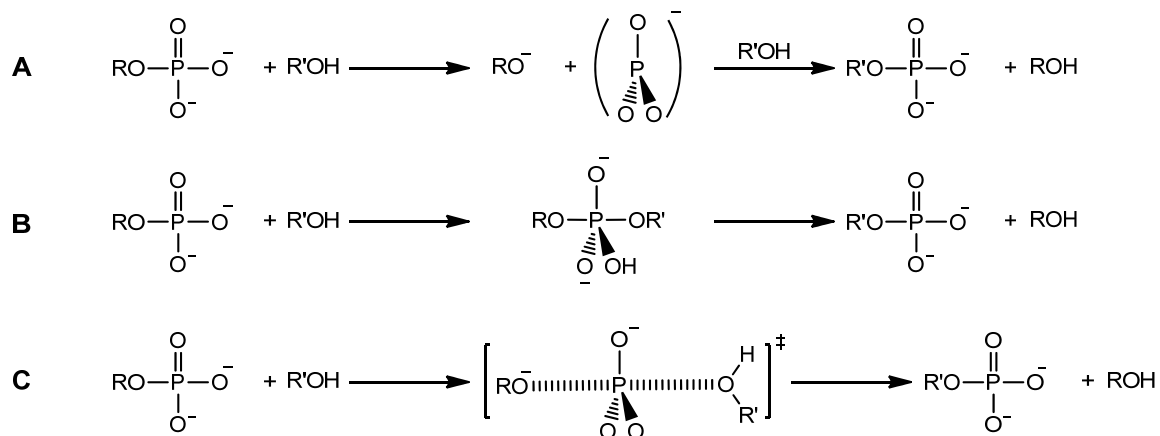


**Figure 1-6.** Three distinct reaction mechanisms for phosphate esters uncatalyzed hydrolysis reactions, dissociative (A) and associative (B) mechanistic extremes, and the concerted pathway (C).

Mechanism A is a dissociative,  $S_N1$ -type two-step mechanism, and designated  $D_N + A_N$  in the IUPAC nomenclature.<sup>18</sup> In this mechanism, a stable  $\text{PO}_3^-$  ion (metaphosphate) is formed that is attacked by a nucleophile in a subsequent step. Mechanism B is an associative, two-step mechanism ( $A_N + D_N$ ). In this mechanism a stable pentacoordinate intermediate, called a phosphorane is formed in the addition–elimination pathway. Mechanism C is concerted ( $A_N D_N$ ) with no intermediate. The transition state could have tight or loose character (be associative or dissociative) depending upon the synchronicity between bond formation to the nucleophile and bond cleavage to the leaving group. In principle, this transition state could lie at any point between the mechanistic extremes. In a loose (or dissociative) transition state the sum of the bond orders to the nucleophile and leaving group is less than 1; in a tight (or associative) transition state this sum is greater

than 1. The transition state shown in the concerted mechanism of **Figure 1-6** is drawn to indicate dissociative character, which is characteristic of the uncatalyzed reactions of phosphate monoesters.

### 1.2.3.2 Uncatalyzed reactions of phosphate monoester dianions

A large body of evidence indicates that phosphate monoester dianions undergo phosphoryl transfer via a concerted mechanism with a loose transition state.<sup>19,20</sup> The pH-rate profile for hydrolysis of *para*-nitrophenyl phosphate monoester (pNPP) (**Figure 1-7**) shows a maximum rate around pH 4, which corresponds to the hydrolysis of the monoanion.<sup>21</sup> For pH 4-7, the proportion of dianion increases and the rate of reactions decrease. When pH is above 7, the rate of reactions eventually reaches a pH independent plateau, which corresponds to the hydrolysis of the dianion.

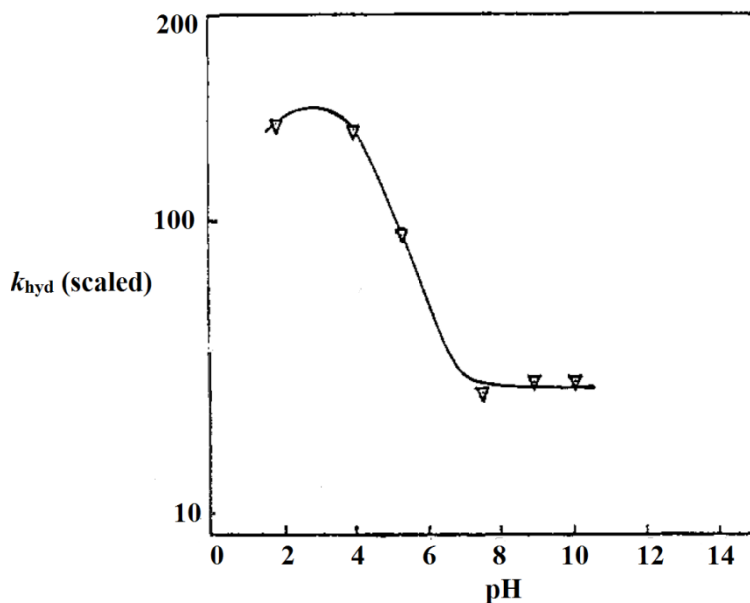


**Figure 1-7.** pH-rate profile for *para*-nitrophenyl phosphate monoester (pNPP) at 39 °C, ionic strength 1.0, on adjusted scale  $k_{\text{hyd}} \times 10^7 \text{ min}^{-1}$ .<sup>21</sup>

The high sensitivity of the rate of hydrolysis of the dianions to the  $pK_a$  of the leaving group, as measured by the slope in **Figure 1-8 A** ( $\beta_{lg}=-1.23$ ),<sup>21</sup> indicates that bond breaking is well advanced in the transition state. Meanwhile, the small dependencies of rates on nucleophile basicity ( $\beta_{nuc}=0.2$ )<sup>22</sup> shown in **Figure 1-8 B** imply a small degree of bond forming with the nucleophile. An Eyring plot of the rate constant for the hydrolysis of the dianion at three temperatures give values of  $\Delta H^*$  and  $\Delta S^*$  of 30.6 kcal/mole and +0.35 e.u., respectively. Near zero entropies of activation also support a loose transition state for pNPP dianion hydrolysis.

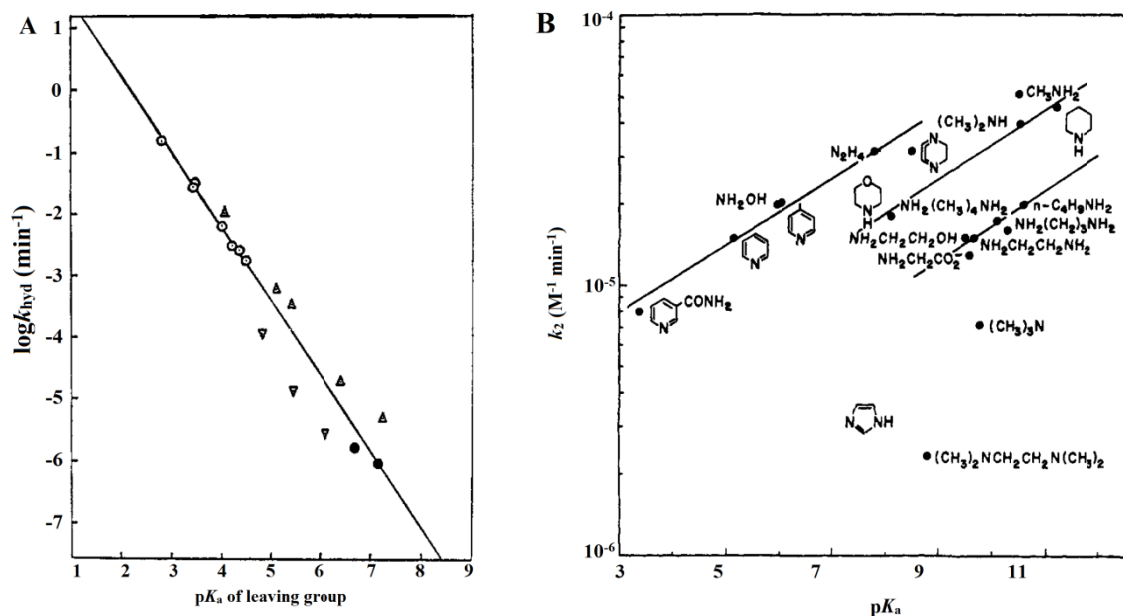


**Figure 1-8** (A) Hydrolysis rates for pNPP dianions at 39 °C, as a function of the  $pK_a$  of the conjugate acid the leaving group.<sup>21</sup> (B) Second-order rate constants for reactions of amines with pNPP dianion at 39°C and ionic strength 1.0, plotted against the  $pK_a$  of the attacking amine.<sup>22</sup>

The kinetic isotope effect (KIE) data for pNPP dianion<sup>23</sup> hydrolysis further supports the loose transition state developed during the uncatalyzed hydrolysis reaction

(Table 1-1). When the phosphoryl group in pNPP dianion is made chiral using  $^{16}\text{O}$ ,  $^{17}\text{O}$ , and  $^{18}\text{O}$ , phosphoryl transfer occurs with inversion of configuration. This result confirms that pNPP dianion hydrolysis reaction is not stepwise, and there is no evidence for the formation of free metaphosphate.<sup>24</sup>

**Table 1-1.** Kinetic isotope effects for the uncatalyzed hydrolysis of different phosphate esters.

Phosphate esters	$^{15}\text{N } k$	$^{18}\text{O } k_{\text{bridge}}$	$^{18}\text{O } k_{\text{nonbridge}}$
4-nitrophenyl phosphate dianion (pNPP) <sup>23</sup>	1.0028±0.0002	1.0189±0.0005	0.9994±0.0005
4-nitrophenyl phosphorothioate dianion (pNPPT) <sup>25</sup>	1.0027±0.0001	1.0237±0.0007	1.0135±0.0013
3,3-dimethylbutyl 4-nitrophenyl phosphate diester <sup>26</sup>	1.0016±0.0002	1.0059±0.0005	0.9949±0.0006
4-tert-butylphenyl 4-nitrophenyl phosphate diester <sup>27</sup>	1.0010±0.0001	1.0046±0.0008	1.0040±0.0001

More-O’Ferrall-Jencks diagrams<sup>28,29</sup> in **Figure 1-9** represent the position of the transition states for the solution reactions of phosphate monoesters relative to the limiting extremes in a two-dimensional way.<sup>30</sup> The reactants and products are located in the lower left and upper right corners, respectively. Bond fission to the leaving group is shown along the horizontal axis, and bond formation to the nucleophile along the vertical axis. Stepwise mechanisms proceed along the lower right and upper left corners. The transition state of pNPP dianion is characterized by a metaphosphate-like phosphoryl group, and in the lower right region of the More-O’Ferrall-Jencks diagram (**Figure 1-9 A**).

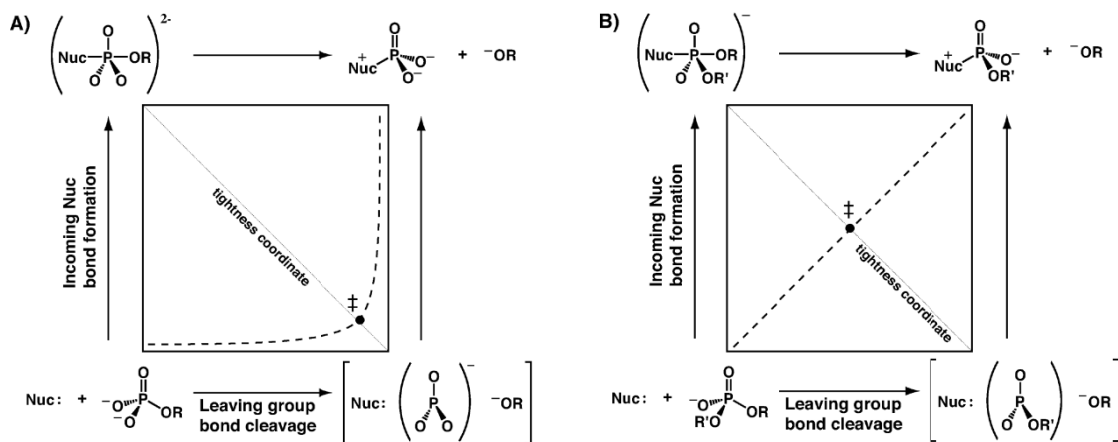


**Figure 1-9.** More-O'Ferrall-Jencks diagrams for phosphate monoester dianions (A) and phosphate diester (B) hydrolysis in solution.<sup>30</sup>

### 1.2.3.3 Uncatalyzed reactions of phosphorothioate monoester

Phosphorothioate monoesters, in which a non-bridging oxygen atom of the phosphate group is replaced by a sulfur atom, have been used to probe kinetic and stereochemical aspects of phosphoryl transfer. This simple change leads to charge distribution on phosphorothioate monoesters different from that on phosphate monoesters. For the phosphorothioate monoester dianion, the sulfur atom has a localized negative charge, whilst the other negative charge is delocalized between two non-bridging oxygens.<sup>31</sup>

The pH-rate profile for hydrolysis of *para*-nitrophenyl phosphorothioate monoester (pNPPT)<sup>31</sup> (**Figure 1-10**) is similar to that of the pNPP monoester. However, pNPPT exhibit approximately 10-60 folds enhanced chemical reactivity in solution, as compared to pNPP. This inverse thio effect (the ratio of the rate of phosphate ester vs phosphorothioate ester reaction) can be rationalized by the higher electronegativity of oxygen as compared to sulfur.<sup>32</sup>

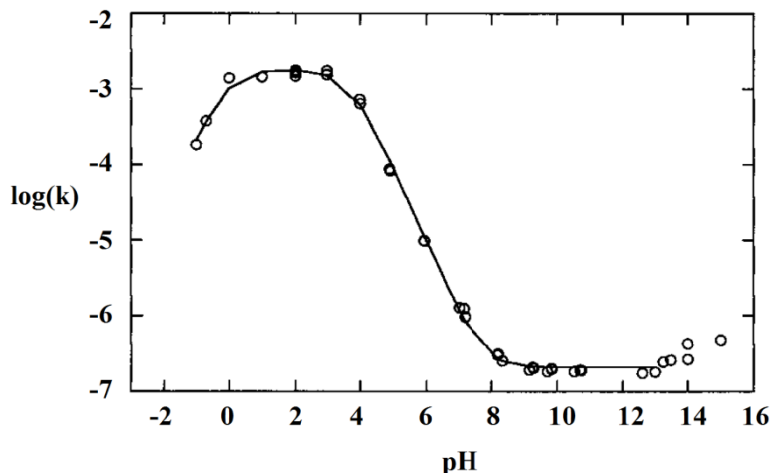


**Figure 1-10.** pH-rate profile for *para*-nitrophenyl phosphorothioate monoester (pNPPT) at 39 °C.<sup>31</sup>

The value of  $\beta_{lg}$  for the uncatalyzed hydrolysis of a series of aryl phosphorothioate monoester dianions was determined as -1.1 (**Figure 1-11 A**).<sup>33</sup> This value is consistent with a dissociative transition state essentially identical to that of phosphate monoester hydrolysis. The racemic product obtained from hydrolysis and ethanolysis of chiral *para*-nitrophenyl [ $O^{16}$ ,  $O^{18}$ ] phosphorothioate monoester indicate the formation of free thiometaphosphate as an intermediate. Kinetic isotope effect data for pNPPT dianion have been determined (**Table 1-1**).<sup>25</sup> The KIEs are similar to those for hydrolysis of the pNPP dianion, indicating the transition states of both reactions are similar with large leaving group bond fission. An Eyring plot of the rate constant for the hydrolysis of the pNPPT dianion (**Figure 1-11 B**) at four temperatures give values of  $\Delta H^*$  and  $\Delta S^*$  of  $37.0 \pm 1.0$  kcal/mole and  $+29 \pm 3$  e.u., respectively.<sup>31</sup> The hydrolysis of the pNPPT dianion exhibits a much more favorable  $\Delta S^*$  than for pNPP as a result of the different reaction mechanism. The pNPPT dianion reacts by a fully dissociative ( $D_N + A_N$ ) mechanism which avoids the entropic cost of recruiting a solvent molecule into the

transition state of the rate-limiting step, while the pNPP dianion proceeds through a concerted mechanism with a loose transition state.

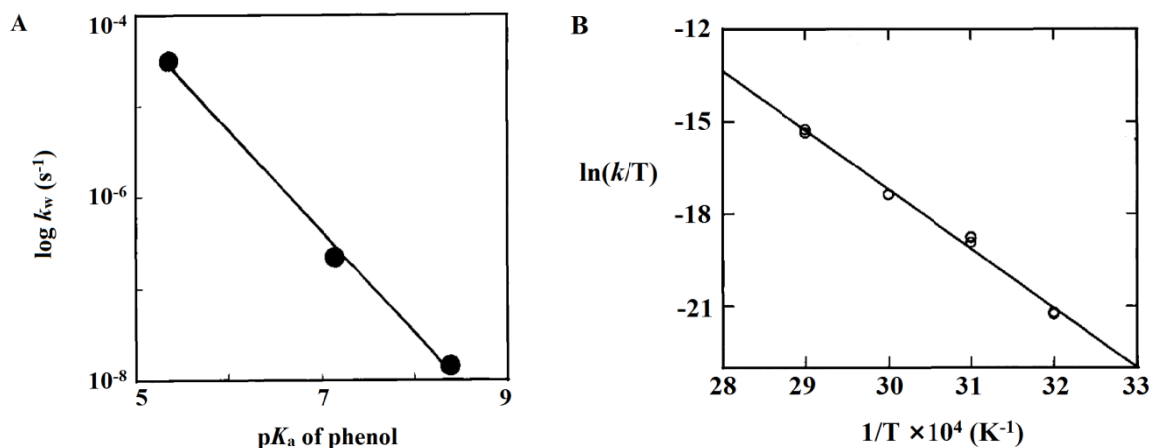


**Figure 1-11** (A) Hydrolysis rates for pNPPT dianions at 37 °C, as a function of the  $pK_a$  of the conjugate acid the leaving group.<sup>33</sup> (B) Eyring plot for the aqueous hydrolysis of pNPPT dianion.<sup>31</sup>

#### 1.2.3.4 Uncatalyzed reactions of phosphate diesters

Rate constants obtained for hydrolysis of two types of phosphate diesters over the range from pH 6.5 to 13 are shown in **Figure 1-12 A**.<sup>34</sup> A  $\beta_{lg}$  value of -0.76 for aryl phosphate diesters has been reported (**Figure 1-12 B**).<sup>35</sup> This value is smaller than that of phosphate monoesters, and is consistent with a more associative transition state. The reported  $\beta_{nuc}$  value of 0.31 for the nucleophilic attack of oxyanion nucleophiles on a range of methyl 2,4-dinitrophenyl phosphate diesters is also consistent with a more associative transition state.<sup>36</sup>

KIE data has been measured for the alkaline hydrolysis of a range of phosphate diesters at 70°C and 95 °C,<sup>37-39</sup> and a range of KIE values for diesters are found in a review of phosphoryl and sulfonyl transfer reactions (**Table 1-1**).<sup>40</sup> The KIE data show

reduced  $^{15}\text{N}$   $k$  and  $^{18}\text{O}$   $k_{\text{bridge}}$  isotope effects compared to the values for monoester hydrolysis, which is consistent with a more associative mechanism. However the  $^{15}\text{N}$   $k$  value of 1.0016 for 3,3-dimethylbutyl 4-nitrophenyl phosphate indicates that the P-O bond is substantially broken in the transition state.<sup>37</sup> KIE data has also been measured for the attack of hydroxide on 4-tert-butylphenyl 4-nitro phenyl phosphate diester.<sup>26</sup> The partially broken P-O bond and the dependence of hydroxide in the rate limiting step indicate that the reaction is concerted rather than a fully associative two step process. The transition state for phosphate diester hydrolysis is synchronous, roughly midway between the extremes (**Figure 1-9 B**).

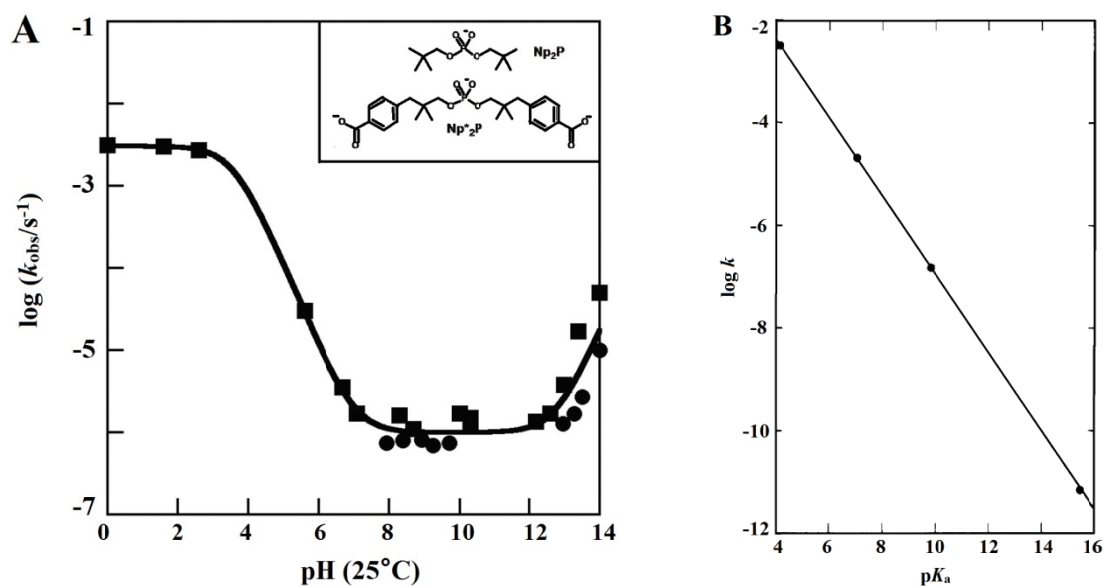


**Figure 1-12.** (A) Influence of buffer pH on rate constant for hydrolysis of Np<sub>2</sub>P (■) at 25 °C and Np<sub>2</sub>\*P (●) at 250 °C.<sup>34</sup> (B) Linear free energy relationship between the second-order rate constant for hydroxide-catalyzed hydrolysis of methyl 2,4-dinitrophenyl phosphate diesters at 25 °C and the pK<sub>a</sub> of the conjugate acid of the leaving group.<sup>41</sup>

### 1.3 Catalytic promiscuity of phosphatases

#### 1.3.1 Catalytic promiscuity of *E. coli* alkaline phosphatase (AP)

*E. coli* alkaline phosphatase, the prototypical member of the alkaline phosphatase superfamily, is a non-specific phosphate monoester hydrolase which has been extensively studied.<sup>42-44</sup>

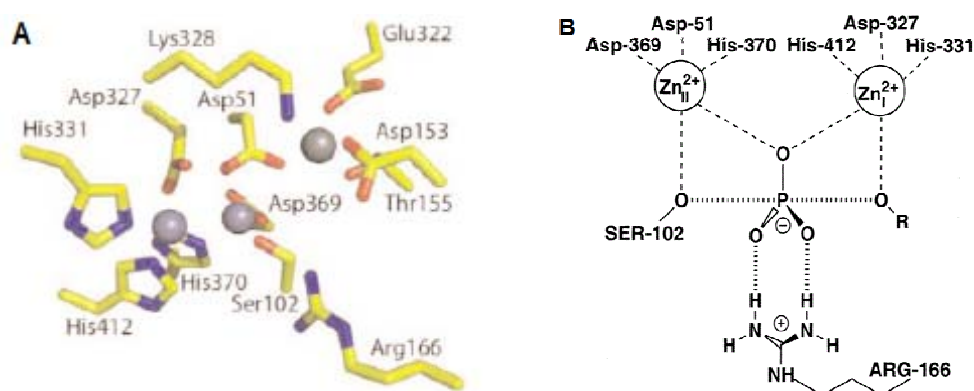


**Figure 1-13.** (A) Active site structure of *E. coli* AP.<sup>45</sup> (B) Transition state model for phosphoryl transfer by *E. coli* AP based on X-ray structure of this enzyme.<sup>46</sup> The two zinc ions are about 4Å apart.

The structural information for *E. coli* AP includes structures with inorganic phosphate (Pi) product bound both covalently and noncovalently and with a pentavalent vanadyl transition state analogue.<sup>45-47</sup> **Figure 1-13 A** shows the active site structure of *E. coli* AP. Structural and mechanistic work has led to the following transition state model for active site interactions (**Figure 1-13 B**). These structures suggest that the central roles for the two Zn<sup>2+</sup> ions in the catalytic mechanism are to simultaneously activate the nucleophile and stabilize the leaving group. *E. coli* AP also contains Mg<sup>2+</sup> as the third metal ion in the active site. The role of the Mg<sup>2+</sup> ion has been the subject of some debate

and has been proposed to have a structural role, or to provide a general base in the form of an  $\text{Mg}^{2+}$ -coordinated hydroxide, or to coordinate and stabilize the transferring phosphoryl group during catalysis. Removal of the  $\text{Mg}^{2+}$ -binding site by mutagenesis has a large effect on phosphate monoester hydrolysis, and on its promiscuous sulfate ester hydrolysis activity, but no significant effect on the promiscuous phosphate diester hydrolysis.<sup>48</sup>

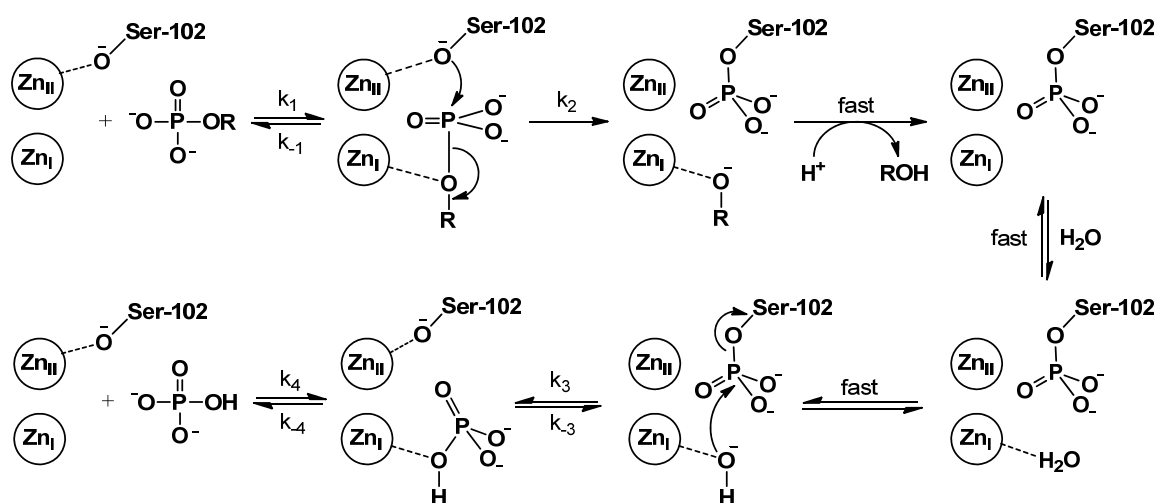


**Figure 1-14.** Proposed phosphoryl transfer mechanism catalyzed by *E. coli* AP.<sup>43</sup>

A large body of kinetic data and biochemical characterization has established a two-step reaction mechanism with formation of a covalent enzyme-phosphate intermediate (**Figure 1-14**).<sup>42-44</sup> In the first chemical step ( $k_2$ , **Figure 1-14**),  $\text{Zn}_{\text{II}}$  is thought to facilitate formation of the more reactive serine alkoxide, and  $\text{Zn}_{\text{I}}$  is thought to stabilize the developing negative charge on the leaving group. In the second chemical step ( $k_3$ , **Figure 1-14**), which is analogous to the reverse of the first step,  $\text{Zn}_{\text{I}}$  would facilitate generation of a hydroxide molecule for attack on the phosphoryl group and  $\text{Zn}_{\text{II}}$  would stabilize the serine leaving group. Arg166 at the active site interacts with the other

two non-bridging phosphoryl oxygen atoms. The guanidinium group of this conserved arginine plays a role in binding and in transition state stabilization. It has been widely speculated that phosphatases render the transition state tighter, or more associative, due to coordination of the non-bridging oxygen atoms of the phosphoryl group to such positively charged groups in the active site.

O'Brien and Herschlag pioneered the detection of catalytic promiscuity of *E. coli* AP.<sup>49</sup> In addition to the highly proficient native phosphate monoesterase activity of AP, it has sulfate monoesterase,<sup>49</sup> phosphate diesterase,<sup>50</sup> and phosphonate monoesterase<sup>50</sup> activities. One report has also suggested that AP possesses the ability to oxidize phosphite to phosphate.<sup>51</sup>

Although these reactions share the same trigonal–bipyramidal transition state, there are remarkable variations in the nature of the reaction center as well as in the substrate and transition state. Diverse substrates have small differences in steric bulk; it is thought that diesters are accommodated by movement of the arginine side chain. The substrate charges range from 0 to –2. During the hydrolysis reaction, nucleophiles attack phosphorus or sulfur at the reaction center. In solution, phosphate and sulfate monoester hydrolysis reactions occur with similar rate constants, and both reactions proceed through a loose transition state, whereas phosphate diester and phosphonate monoesters undergo tighter, more associative transition states. Prior linear free energy relationship and isotope effect results suggest that the transition states for AP-catalyzed reactions of phosphate and sulfate esters are still “loose,” whereas the transition states for phosphate diester and phosphonate monoester are still “tight”.<sup>30</sup> In other words, the transition states for various

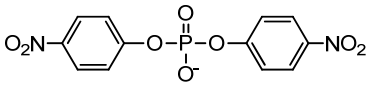
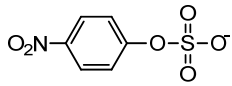
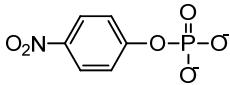
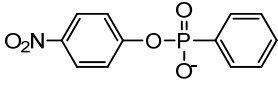
AP-catalyzed reactions are indistinguishable from the corresponding uncatalyzed hydrolysis reactions.

All of the catalytic mechanisms are presumed to involve nucleophilic attack by Ser102 and stabilization of the negatively charged intermediate by the active site  $\text{Zn}^{2+}$  ions. The steric and electrostatic diversity of the substrates affect the bonding and charge distribution in the transition states. Data suggest that electrostatic interactions between the non-bridging oxygen atoms and the bimetallo  $\text{Zn}^{2+}$  center are very important. The lower charge density on the non-bridge oxygen atoms on the transferred group in sulfate esters and phosphate diesters accounts for much of the decreased stabilization of the transition state relative to phosphoryl transfer. The presence of two  $\text{Zn}^{2+}$  ions approximately 4 Å apart might enable the catalytic promiscuity of AP, as two divalent metal ions about this distance apart is a central feature of known phosphomonoesterases, phosphodiesterases, and phosphotriesterases.

The AP-catalyzed phosphate monoester hydrolysis proceeds through a loose transition state with a  $>10^{17}$ -fold rate enhancement relative to the rate of the uncatalyzed reaction, whereas phosphate diester and phosphonate monoester hydrolysis proceeds through a tighter, associative transition states with  $10^{11}$  and  $10^{10}$ -fold rate enhancements, respectively (**Table 1-2**). According to transition state theory, enzymatic rate enhancements arise from preferential stabilization of the transition state relative to the ground state. Consequently, the specificity of an enzyme for a particular reaction depends on its ability to recognize and stabilize the transition state for that reaction. Thus, the smaller rate enhancement for phosphate diester and phosphonate monoester hydrolysis indicates that the AP active site binds the tighter transition state for diester hydrolysis

more weakly than it binds the loose transition state for monoester hydrolysis. The rate enhancements for sulfate ester hydrolysis are  $10^9$ -fold even though sulfate ester hydrolysis proceeds through a loose transition state. This might be caused by weaker interaction between non-bridging oxygen atoms with the metal ions and R166, because of the reduced charge on the transferring group. AP remarkably accepts these substrates with much more discrimination (12.3 kcal/mol) between transition states.

**Table 1-2.** Kinetic parameters for *E. coli* AP-catalyzed hydrolysis of phosphodiester, sulfate monoester, phosphate monoester and phosphonate monoester. Rate constants for enzymatic reactions and solution reactions are from literature sources.<sup>49,50</sup>

substrates	$k_{\text{cat}}/K_M$ , ( $M^{-1}s^{-1}$ )	$(k_{\text{cat}}/K_M)/k_w$
 <i>para</i> -nitrophenyl phosphodiester	$5 \times 10^{-2}$	$3.0 \times 10^{11}$
 <i>para</i> -nitrophenyl sulfate monoester	$1 \times 10^{-2}$	$1.1 \times 10^9$
 <i>para</i> -nitrophenyl phosphate monoester	$3.0 \times 10^7$	$1.1 \times 10^{18}$
 phosphonate monoester	$3 \times 10^{-2}$	$4 \times 10^{10}$

### 1.3.2 Catalytic promiscuity of arylsulfatase

Arylsulfatases, on the basis of high structural homology revealed by structural data, are members of the AP superfamily.<sup>52,53</sup> *Pseudomonas aeruginosa* arylsulfatase (PAS) has been identified as an arylsulfatase and is classified as a member of the alkaline

phosphatase (AP) superfamily<sup>54,55</sup> in the SCOP database.<sup>56</sup> This assignment is based on high structural homology between PAS and the prototypical member of this superfamily, *E. coli* AP. The crystal structure of PAS has been determined at 1.3 Å (**Figure 1-15**).<sup>57</sup>

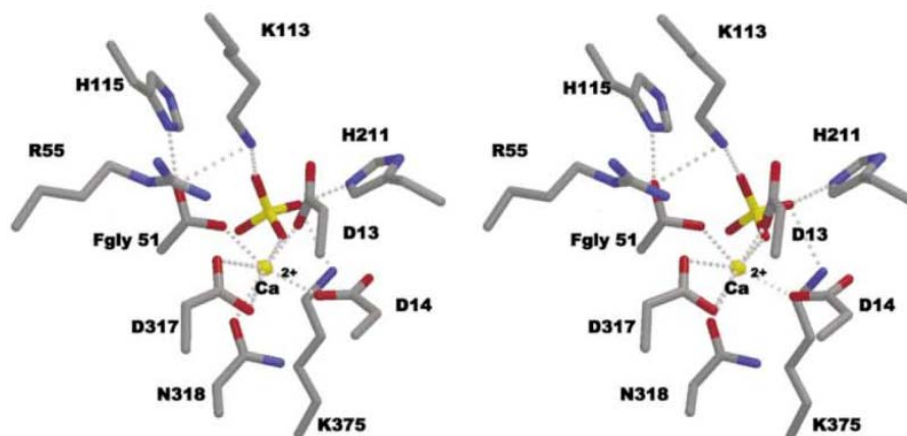


**Figure 1-15.** A stereo view of the intermolecular contacts between protein residues and sulfate in the active site region of PAS base upon the crystal structure.<sup>57</sup>

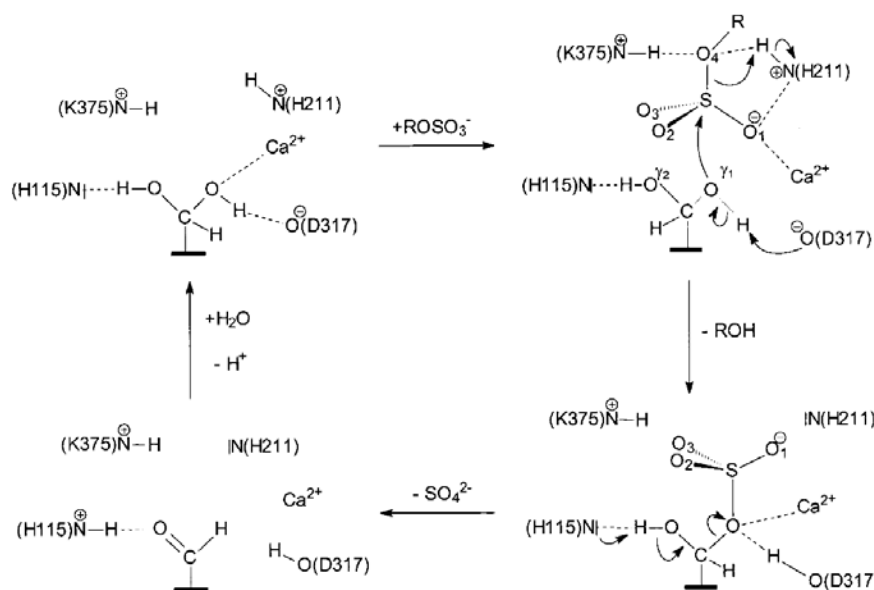


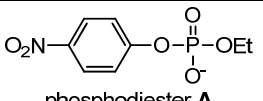
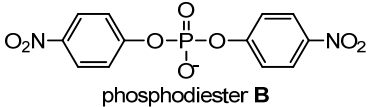
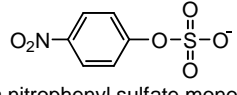
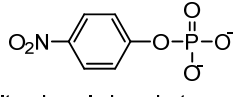
**Figure 1-16.** Proposed catalytic mechanism for PAS using a sulfate monoester as the substrate.<sup>57</sup>

According to the crystal structure and kinetic studies, the catalytic mechanism of PAS has been proposed as shown in **Figure 1-16**. In its active site, a cysteine is post-translationally oxidized to a C $\alpha$ -formylglycine (FGly) whose hydrated form coordinates to a calcium ion. This metal positions and activates the FGly for nucleophilic attack on the sulfur center of the substrate.<sup>57</sup> The oxidation of cysteine (or serine in other sulfatases) is carried out by a range of modification systems,<sup>58-62</sup> although the specific modification machinery for PAS is not known.

Several experimental observations suggest that while PAS acts as a sulfatase *in vivo*, it also exhibits phosphate monoesterase and diesterase activities.<sup>63,64</sup> PAS catalyzes the hydrolysis of phosphate monoesters with multiple turnovers and shows a remarkably high rate acceleration of  $10^{13}$  relative to the nonenzymatic hydrolysis [ $(k_{\text{cat}}/K_{\text{M}})/k_{\text{w}}$ ]. The promiscuous phosphodiesterase activity of PAS was reported with an even higher proficiency of  $10^{18}$ , which is comparable to the proficiency of its native sulfatase activity ( $4 \times 10^{18}$ ) (see **Table 1-3**). Considering the fact that hydrolysis of phosphate monoester and diester in solution occur via somewhat different transition states, PAS seems to display a greater selectivity for substrate structure than for transition-state characteristics. However, the nature of the transition states for PAS-catalyzed reactions remains to be determined. Phosphate monoester dianions and sulfate monoesters have similar bond lengths, geometries, and transition state charge changes but differ in substrate charge and the identity of atoms undergoing bonding changes. PAS remarkably accepts these substrates with little discrimination (7.4 kcal/mol) in transition state binding. The magnitudes and relative similarities of the kinetic parameters also suggest that a

functional switch from sulfatase to phosphatase activities is feasible, either by gene duplication or by direct evolution via an intermediate enzyme with dual specificity.

**Table 1-3.** Kinetic parameters for the PAS-catalyzed hydrolysis of phosphodiester **A** and **B**, sulfate monoester, and phosphate monoester.<sup>63</sup>

substrates	$k_{\text{cat}}$ ( $\text{s}^{-1}$ )	$K_{\text{M}}$ ( $\mu\text{M}$ )	$k_{\text{cat}}/K_{\text{M}}$ , ( $\text{M}^{-1}\text{s}^{-1}$ )	$(k_{\text{cat}}/K_{\text{M}})/k_{\text{w}}$ [b]
 phosphodiester <b>A</b>	0.073 $\pm 0.004$	617 $\pm$ 61	119 $\pm$ 7	$6.5 \times 10^{15}$
 phosphodiester <b>B</b>	0.55 $\pm$ 0.02	2.2 $\pm$ 0.3	(2.5 $\pm$ 0.3) $\times 10^5$	$1.3 \times 10^{18}$
 <i>para</i> -nitrophenyl sulfate monoester	14.2 $\pm$ 0.6	0.29 $\pm$ 0.03	(4.9 $\pm$ 0.8) $\times 10^7$	$4.3 \times 10^{18}$
 <i>para</i> -nitrophenyl phosphate monoester	0.023 $\pm 0.001$	29.1 $\pm$ 2.0	790 $\pm$ 58	$1.6 \times 10^{13}$

[a] Reaction conditions: 25 °C, 0.1 M Tris-HCl (pH 8.0), 0.5 mg mL<sup>-1</sup> bovine serum albumin (BSA), 0.5 M NaCl (for **A** and **B**). [b] For hydrolytic reactions, the second-order rate constant  $k_{\text{w}}$  for the uncatalyzed reaction is taken as  $k_{\text{uncat}}/55 \text{ M}$ . Values for  $k_{\text{uncat}}/\text{s}^{-1}$  at 25 °C, pH 8.0,  $1.0 \times 10^{-12}$  (**A**),  $1.1 \times 10^{-11}$  (**B**),  $6.2 \times 10^{-10}$  (sulfate monoester),  $2.7 \times 10^{-9}$  (phosphate monoester).

### 1.3.3 Catalytic promiscuity of phosphonate monoester hydrolase (PMH)

Phosphonate monoester hydrolases (PMH) capable of hydrolyzing *para*-nitrophenyl phenylphosphonate have been characterized as a new member of the AP superfamily<sup>65</sup> because of the close homology of the  $\alpha/\beta$  core structure to AP and PAS. Two phosphonate monoester hydrolases (PMH) characterized so far are *R*/PMH from

*Rhizobium leguminosarum*<sup>66</sup> and *BcPMH* from *Burkholderia caryophylli*.<sup>67</sup> The crystal structure of *BcPMH* is almost identical to *R/PMH*, and shows high homology to arylsulfatases with conservation of the core  $\alpha/\beta$ -fold, the mononuclear active site and most of the active-site residues. (**Figure 1-17 A**)

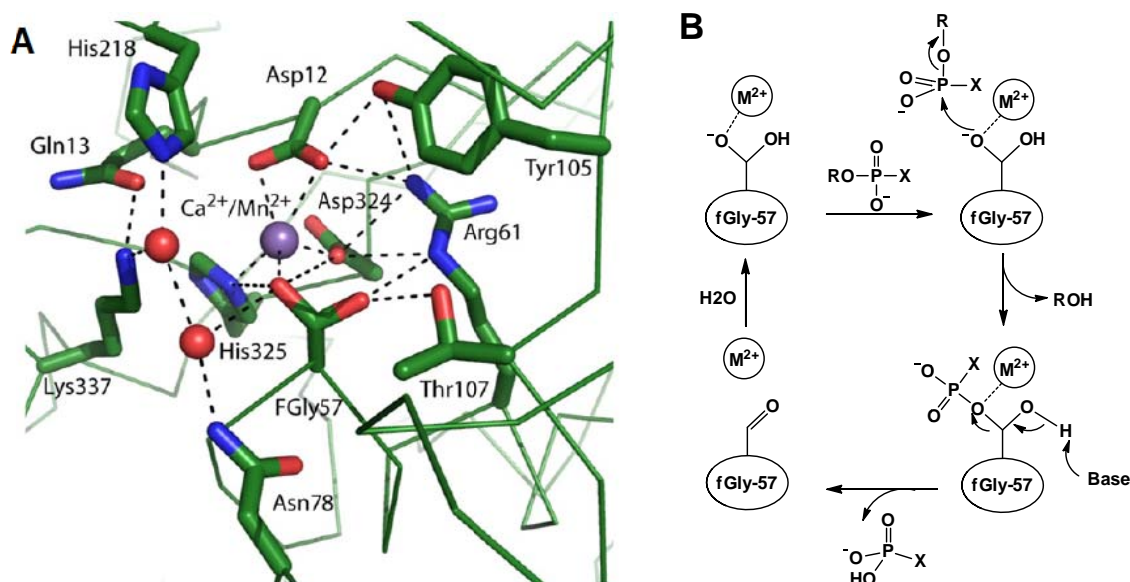


**Figure 1-17.** (A) The active site structure of *BcPMH*.<sup>68</sup> (B) Proposed mechanism for phosphonate monoester hydrolysis by *BcPMH*.<sup>68</sup> X represents methyl or ethyl group.

Mass spectrometry, mutational evidence, MALDI-TOF analysis, fluorophore labeling and the crystal structure strongly suggest that *BcPMH* uses a formylglycine as the catalytic nucleophile even though it is not a sulfatase. The double-displacement mechanism proposed for *BcPMH* catalyzed reactions is shown in **Figure 1-17 B**. The nucleophile fGly57 is in its active hydrated form, stabilized by the metal and hydrogen bonds to Thr107, Arg61, His325 and Asp324. The bound substrate is coordinated by the active site Asn78, His218, Lys337 and the nucleophile fGly57. Asp324 and the metal ion activate the nucleophile that performs the attack on the phosphorus atom. His218 donates

a proton to the alcohol-leaving group; Asn78 and Lys337 stabilize the buildup of negative charge on the non-bridging oxygen atoms. The covalent intermediate is subsequently cleaved by breaking one of the fGly hydrate bonds resulting in the formation of the aldehyde. The proton is probably transferred to an incoming water molecule. Phosphonate/phosphate monoester is released and the gem-diol regenerated by hydration of the aldehyde function.

*R*/PMH hydrolyses phosphonate monoesters and phosphate diesters with similar efficiency. *R*/PMH exhibits a high level of activity towards *para*-nitrophenyl phenyl phosphonate with a  $k_{\text{cat}}/K_{\text{m}}$  of  $5300 \pm 600 \text{ M}^{-1} \text{ s}^{-1}$  at the optimum pH of 7.5.<sup>66</sup> A promiscuous phosphodiesterase activity towards *para*-nitrophenyl ethyl phosphate diester ( $k_{\text{cat}}/K_{\text{m}} = 4100 \pm 1000 \text{ M}^{-1} \text{ s}^{-1}$ ) was also detected. Compared to the uncatalyzed rates, *R*/PMH accelerates hydrolysis of *para*-nitrophenyl phenyl phosphonate roughly  $10^{12}$ -fold and hydrolysis of *para*-nitrophenyl ethyl phosphate diester  $10^{13}$ -fold ( $k_{\text{cat}}/k_{\text{uncat}}$ ).<sup>66</sup>

*Bc*PMH, similar to the highly homologous *R*/PMH, is able to efficiently hydrolyze six different substrate classes including phosphate mono-, di-, and triesters, phosphonate monoesters, sulfate monoesters, and sulfonate monoesters.<sup>67</sup> Isotope-labeling experiments analyzed by mass spectrometry prove that all six reactions proceed through an identical reaction sequence involving nucleophilic attack on the various phosphorus and sulfur centers, following by breaking the ester bond to the leaving group. The coincidence of pH-rate profiles for five substrate classes (except substrate **3**) suggest that their conversions are catalyzed by the same active site and by following the mechanism proposed for phosphonate monoester hydrolysis<sup>66</sup> (**Figure 1-17 B**).

**Table 1-4.** Kinetic parameters for the *Bc*PMH-catalyzed hydrolysis of six substrate classes including phosphate monoester **I**, phosphodiester **II**, phosphate triester **III**, phosphonate monoester **IV**, sulfate monoester **V**, and sulfonate monoester **VI**. Rate constants for solution reactions are from literature sources.<sup>49,50</sup>

Substrate structures	R group	$k_{cat}$ (s <sup>-1</sup> )	$K_M$ ( $\mu$ M)	$k_{cat}/K_M$ , (M <sup>-1</sup> s <sup>-1</sup> )	$(k_{cat}/K_M)/k_w$ [b]
$\begin{array}{c} \text{O} \\ \parallel \\ \text{R}-\text{O}-\text{P}-\text{O}^- \\   \\ \text{O}^- \\ \text{I} \end{array}$	<b>a</b> :R=Phe	$(2.1 \pm 0.2) \times 10^{-4}$	$0.33 \pm 0.03$	$0.63 \pm 0.08$	$3.16 \times 10^{11}$
	<b>b</b> :R=4-NO <sub>2</sub> Phe	$(7.7 \pm 0.1) \times 10^{-3}$	$0.35 \pm 0.02$	$22 \pm 1$	$2.51 \times 10^{10}$
$\begin{array}{c} \text{O} \\ \parallel \\ \text{R}-\text{O}-\text{P}-\text{O}-\text{R}' \\   \\ \text{O}^- \\ \text{II} \end{array}$	<b>a</b> :R=R'=Phe	$2.12 \pm 0.02$	$0.071 \pm 0.004$	$(3.0 \pm 0.2) \times 10^4$	$3.98 \times 10^{19}$
	<b>b</b> :R=4-NO <sub>2</sub> Phe, R'=Et	$5.8 \pm 0.1$	$0.63 \pm 0.04$	$(9.2 \pm 0.6) \times 10^3$	$2.00 \times 10^{18}$
$\begin{array}{c} \text{O} \\ \parallel \\ \text{R}-\text{O}-\text{P}-\text{O}-\text{R}' \\   \\ \text{O}-\text{R}'' \\ \text{III} \end{array}$	<b>b</b> :R=4-NO <sub>2</sub> Phe, R'=R''=Et	$>3.7 \times 10^{-5}$	$>2.4$	$(1.6 \pm 0.1) \times 10^{-2}$	$1.58 \times 10^7$
$\begin{array}{c} \text{O} \\ \parallel \\ \text{R}-\text{O}-\text{P}-\text{R}' \\   \\ \text{O}^- \\ \text{IV} \end{array}$	<b>a</b> :R=R'=Phe	$1.58 \pm 0.04$	$1.23 \pm 0.09$	$(1.3 \pm 0.1) \times 10^3$	$3.98 \times 10^{17}$
	<b>b</b> :R=4-NO <sub>2</sub> Phe, R'=Phe	$2.73 \pm 0.06$	$0.19 \pm 0.02$	$(1.5 \pm 0.1) \times 10^4$	$5.01 \times 10^{16}$
$\begin{array}{c} \text{O} \\ \parallel \\ \text{R}-\text{O}-\text{S}-\text{O}^- \\ \parallel \\ \text{O} \\ \text{V} \end{array}$	<b>a</b> :R=Phe	$(1.0 \pm 0.1) \times 10^{-4}$	$58 \pm 5$	$(1.7 \pm 0.3) \times 10^{-3}$	$2.00 \times 10^{11}$
	<b>b</b> :R=4-NO <sub>2</sub> Phe	$(4.0 \pm 0.1) \times 10^{-2}$	$68 \pm 4$	$0.59 \pm 0.04$	$3.16 \times 10^{10}$
$\begin{array}{c} \text{O} \\ \parallel \\ \text{R}-\text{O}-\text{S}-\text{R}' \\ \parallel \\ \text{O} \\ \text{VI} \end{array}$	<b>a</b> :R=R'=Phe	$(7.0 \pm 0.3) \times 10^{-4}$	$0.51 \pm 0.09$	$1.4 \pm 0.2$	$5.01 \times 10^{11}$
	<b>b</b> :R=4-NO <sub>2</sub> Phe, R'=Phe	$(1.2 \pm 0.1) \times 10^{-2}$	$0.24 \pm 0.03$	$49 \pm 7$	$5.01 \times 10^{11}$

The half lives of the uncatalyzed reactions for the six substrate classes identified above range from 200 days to 10<sup>5</sup> years at neutral pH, and *Bc*PMH exhibits remarkable second-order rate accelerations ( $(k_{cat}/K_M)/k_w$ ), ranging from 10<sup>7</sup> to as high as 10<sup>19</sup> (Table

1-4). Among the reported cases of catalytic promiscuity, *BcPMH* is the most efficient promiscuous enzyme and is even more efficient than PAS.<sup>63</sup> The second-order rate accelerations  $[(k_{\text{cat}}/K_{\text{M}})/k_{\text{w}}]$  by *BcPMH* differ up to 12 orders of magnitude.

The range and magnitude of promiscuous activities suggest that *BcPMH* is an enzyme in which high reactivity is combined with a relative lack of specificity. Even though the transition state information about *BcPMH*-catalyzed hydrolysis reactions is not known, the authors conjecture that the enzymatic transition states are not substantially changed from those of the uncatalyzed reactions as has been suggested as the most straightforward solution to lower the thermodynamic barrier for the promiscuous reactions.

#### 1.3.4 Catalytic promiscuity of purple acid phosphatase (PAP)

Purple acid phosphatases (PAPs) are metalloenzymes that utilize a dinuclear metal center to catalyze the hydrolysis of phosphate esters and anhydrides under acidic conditions.

The active site structure of PAPs has been well studied and characterized, as well as the metal centers. The X-ray structures have been reported for the PAP from kidney bean,<sup>69</sup> rat bone,<sup>70</sup> pig,<sup>71</sup> and sweet potato.<sup>72</sup> Seven invariant amino acid ligands to the metal center and the conserved  $\text{Fe}^{3+}$  are found in all PAP active sites (**Figure 1-18**). The second metal ion varies with the source of the enzyme and is always divalent. Mammalian PAPs are monomeric and have  $\text{Fe}^{3+}\text{-Fe}^{2+}$  centers, whereas most plant PAPs are dimeric with  $\text{Fe}^{3+}\text{-Zn}^{2+}$  centers. A PAP isolated from sweet potato contains a  $\text{Fe}^{3+}\text{-Mn}^{2+}$  center.<sup>73,74</sup> The structure of the kidney bean PAP shows the two metal ions at a distance of 3.1 Å, with a monodentate bridging Asp164.

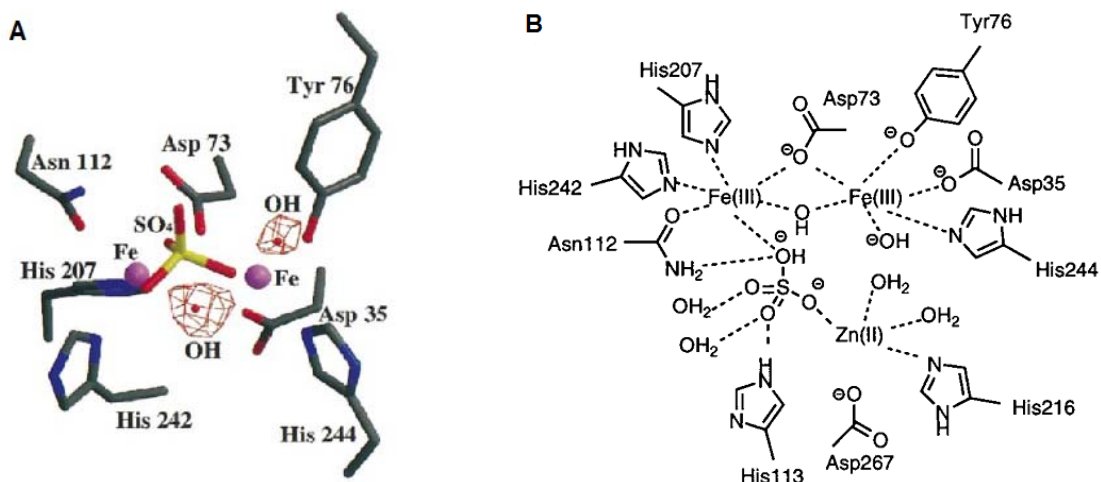


**Figure 1-18.** (A) Crystal structure of rat purple acid phosphatase shows the di-nuclear iron center with bound sulfate ion.<sup>70</sup> (B) A view of the di-iron center and the active site of rat purple acid phosphatase as seen in the crystals. Dotted lines indicate hydrogen bonds or coordination to metal ions.<sup>75</sup>

In contrast to the well-known structural information on PAPs, the details of the catalytic mechanism are much less certain. It is generally believed that catalysis begins with the rapid coordination of substrate to the divalent metal ion.<sup>76,77</sup> The stereochemical course of the reaction occurs with inversion of configuration at phosphorus, which supports the direct transfer of the phosphoryl group to water.<sup>78</sup> The identity of the nucleophile is still under debate. In one proposal, substrate binds to the metal centers either in monodentate fashion using a terminal Fe<sup>3+</sup>-bound hydroxide as the nucleophile, or in a bidentate way using the bridging-hydroxide as the nucleophile.<sup>72,79</sup> In an alternative mechanism, the Fe<sup>3+</sup>-bound hydroxide could function as a general base to deprotonate a water molecule not directly bound to the metal center.<sup>80,81</sup> The possibility has been raised that the second p*K*<sub>a</sub> observed in the pH-rate profile (~6.9) might reflect a conserved histidine residue that protonates the leaving group during catalysis. The

structure of the kidney bean enzyme shows His296 in a location consistent with such a function.<sup>82</sup>

Purple acid phosphatases (PAPs) are reported to exhibit diesterase activity as a secondary catalytic activity, besides their native monoesterase activity.<sup>79</sup> The PAPs from pig and from red kidney bean are reported to lack the ability to hydrolyze diesters such as bis(*para*-nitrophenyl) phosphate bearing a large second ester group,<sup>83</sup> while they can efficiently hydrolyze diesters bearing smaller second ester groups, such as methyl *para*-nitrophenyl phosphate and ethyl *para*-nitrophenyl phosphate.<sup>79</sup> The kinetic results give insights into the sequential steps involved in binding and hydrolysis by the metal center. Methyl *para*-nitrophenyl phosphate is converted to methyl phosphate monoester, which is the initial product, and then hydrolyzed to inorganic phosphate without being released into solution. The turnover number for this reaction is faster than that for the reaction of free methyl phosphate. This is consistent with a mechanism for monoester hydrolysis consisting of initial coordination to the divalent metal, followed by slower partially rate-limiting displacement of hydroxide from Fe<sup>3+</sup> to give the catalytically active bidentately bound substrate. The reaction with the diester substrate is proposed to proceed by coordination to the divalent metal ion followed by nucleophilic attack by the Fe<sup>3+</sup>-coordinated terminal hydroxide to give a bidentately bound monoester, which is then poised for attack by the bridging hydroxide. This mechanism eliminates the need for the second, slow binding event in monoester hydrolysis.

The Schenk group has shown that the iron ion in the unique Fe<sup>3+</sup>-Mn<sup>2+</sup> center in the novel PAP from sweet potato can be replaced by Mn<sup>2+</sup>, and form a catalytically active, unprecedented antiferromagnetically coupled homodivalent Mn<sup>2+</sup>-Mn<sup>2+</sup> center.<sup>84</sup> This is

the first homodivalent, catalytically active form of a PAP, which challenges the currently accepted paradigm that PAPs require a heterovalent, dinuclear metal-ion center for catalysis. However, although the enzyme is still active, it no longer functions as an acid phosphatase, having optimal activity at neutral pH. The results presented in this study demonstrate the importance of having a trivalent metal ion for acid phosphatase activity, thus increasing the understanding of the role of the chromophoric metal ion as an activator of the nucleophile in acid hydrolysis. Furthermore, the results also indicate that PAPs may have evolved from distantly related divalent dinuclear metallohydrolases that operate under pH neutral conditions by stabilization of a trivalent–divalent metal-ion core.

### 1.3.5 Catalytic promiscuity of protein phosphatase 1 (PP1)

Protein phosphatase-1 (PP1) is one example of a serine/threonine phosphatase that exhibits catalytic promiscuity. The crystal structures of apo and tungstate-bound forms of PP1 are known,<sup>85</sup> as well as the microcystin and okadaic acid bound forms of PP1.<sup>86,87</sup> Based on the structure of PP1 complexes to tungstate, the bridging hydroxide ion has been proposed to be the nucleophile<sup>86</sup> (see **Figure 1-19**). Experimental data indicate the catalytic reaction proceeds via a single direct phosphoryl transfer without participation of a phosphoenzyme intermediate. The reaction is thought to follow an  $A_N D_N$  mechanism in which nucleophilic attack is concerted and in line with departure of the leaving group. The crystal structure and catalysis mechanism of PP1 will be particularly illustrated in detail in **Chapter 1.4.2** and **Chapter 1.4.3**.

Besides its native phosphate monoesterase activity, PP1 also shows a promiscuous hydrolytic activity toward aryl methylphosphonate substrates.<sup>88</sup> For the monoester substrate pNPP, the transition state implied by the KIEs and LFER in the

enzymatic reactions is loose, which is similar to that of the uncatalyzed reactions. For *para*-nitrophenyl methylphosphonate (pNPMP) substrate, the transition state implied by the KIEs in the enzymatic reactions is still loose, which is different from the tight transition state in uncatalyzed reactions. LFER and KIE data reflect partial charge neutralization of the leaving group by a general acid, most likely the histidine 125, conserved near the active site in all members of the PPP family.

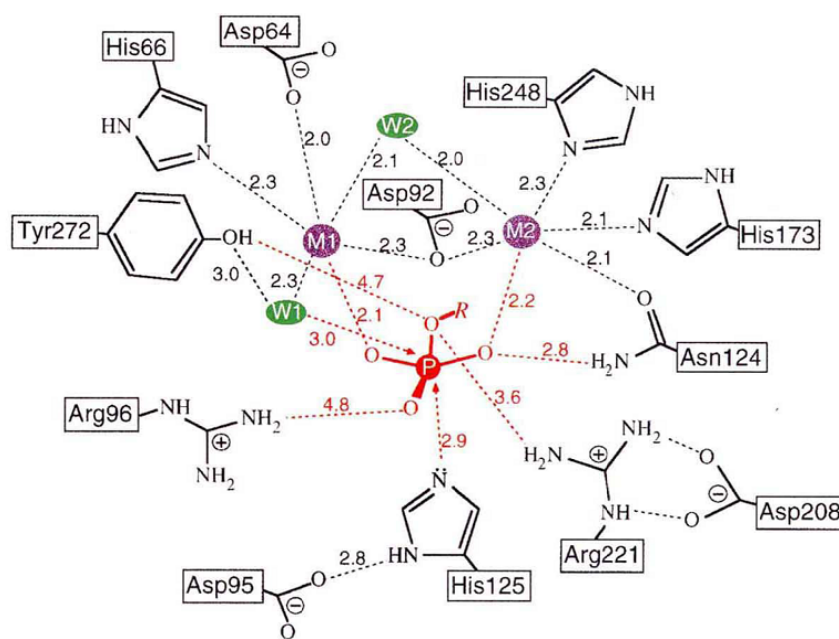


**Figure 1-19.** A view of the active site of PP1 with bound phosphate monoester as the hypothetical model according to the crystal structure. Dotted lines indicate hydrogen bonds or coordination bonds.<sup>86</sup>

The overall data from linear free energy relationships (LFER) and kinetic isotope effects (KIE) imply that the transition states of the PP1-catalyzed reactions of the two substrates are much more similar to one another than are the transition states of the

respective uncatalyzed reactions, as well as the similar catalytic proficiency for hydrolyzing both reactions.

## 1.4 Protein phosphatase 1

### 1.4.1 Brief introduction of PP1

Phosphate serine/threonine phosphatases, which dephosphorylate phosphoserine and phosphothreonine residues in proteins, are classified into three superfamilies including phosphoprotein phosphatases (PPP), metal-dependent protein phosphatases (PPM), and aspartate-based phosphatases (FCP/SCP).<sup>89,90</sup> Protein phosphatase 1 (PP1) is a representative member of PPP superfamily. The PPP superfamily also includes other members such as PP2A, PP2B (commonly known as calcineurin), PP4, PP5, PP6, and PP7 (**Figure 1-20**). Three characteristic sequence motifs, GDxHG, GDxVDRG, and GNHE (G, glycine; D, aspartic acid; x, any amino acid; H, histidine; V, valine; R, arginine; N, asparagines; E, glutamic acid) within the conserved 30 kD catalytic domain are contained in all PPP family members.

PP1 is ubiquitously expressed in all eukaryotic cells. Recent data suggest that mammals contain as many as 650 distinct PP1 complexes,<sup>91</sup> indicating that PP1 catalyzes the majority of protein dephosphorylation events in eukaryotic cells. The cellular processes involving PP1 include meiosis and cell division, apoptosis, protein synthesis, metabolism, cytoskeletal reorganization, and the regulation of membrane receptors and channels. Its history and enzymology have been extensively reviewed.<sup>92-95</sup> Each functional PP1 enzyme consists of a catalytic subunit and a regulatory subunit. The catalytic subunits of PP1 do not exist as free monomers in eukaryotic cells, but they

associate with different regulatory subunits to form a variety of distinct multimeric holoenzymes. The catalytic subunit of PP1 is highly conserved among all eukaryotes. Sequencing results indicate that the catalytic subunits of mammalian PP1s are 76-88% and 90% identical with plant and fungi PP1s, respectively. Remarkably, human PP1 $\beta$  is 100% identical with rat, mouse, rabbit and chicken and 97% identical with the zebra fish, goldfish and Atlantic salmon enzymes.<sup>96</sup>

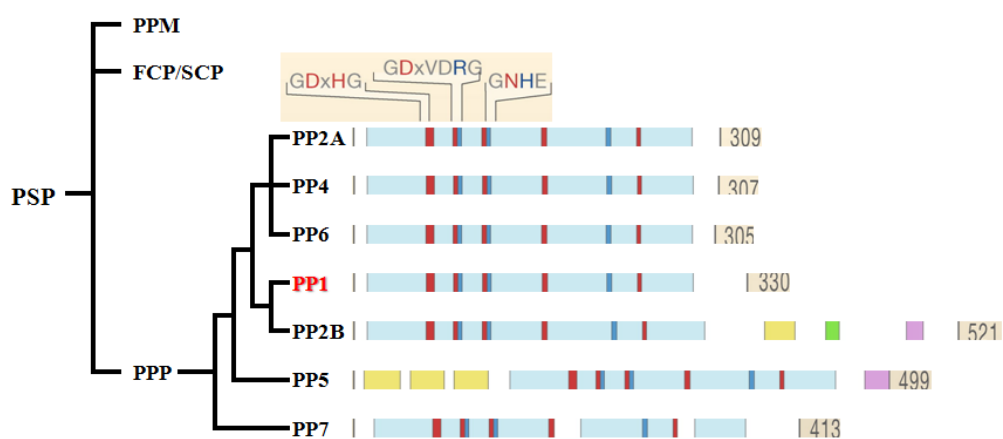


**Figure 1-20.** The three families, phosphoprotein phosphatases (PPP), metal-dependent protein phosphatases (PPM), and aspartate-based phosphatases (FCP/SCP), of protein serine/threonine phosphatases.<sup>97</sup> The catalytic core domains of each protein in PPP gene family are indicated below the diagram. Signature sequence motifs are labeled above the diagram.

Contrary to the highly conserved catalytic subunits, at least 100 putative PP1-binding regulatory subunits have been identified, while full complement of regulatory subunits remains unknown.<sup>98</sup> The large variety of regulatory subunits is not structurally related and has distinct effects on the activity and substrate specificity. Therefore, the interactions between the catalytic subunit and specific regulatory subunits are central to

the functions of PP1. Thus, PP1 represents a large family of biochemically diverse enzymes that have individual high specificity but share a common catalytic subunit.

Physiological substrates of PP1 can be classified into two groups based upon their affinity for the catalytic subunits, exemplified by the tumor suppressor BRCA1 which has high affinity docking sites for PP1 and glycogen phosphorylase which has only weak interactions with the catalytic subunit.<sup>99</sup> Thus, substrate selection by PP1 clearly depends on phosphatase docking motifs and subcellular targeting subunits. It has been suggested that binding of PP1 substrates required interactions with the acidic groove of PP1, as well as with the active site, and the hydrophobic groove.<sup>100</sup> In addition, large numbers of natural molecular toxins from different organisms have been identified that are capable of binding to PP1 and directly inhibiting the catalytic activity of PP1. These toxins include cyclic hepta-peptide microcystins,<sup>101</sup> okadaic acid,<sup>102</sup> and calyculin A,<sup>103</sup> as well as nodularins,<sup>104</sup> tautomycin,<sup>105</sup> fostriecin,<sup>106</sup> and cantharidin.<sup>107</sup> All these inhibitors bind to PP1 at a conserved site in the c terminal region with the sequence FSAPNYCXXXXN.<sup>108</sup>

The phosphate monoester bond is incredibly stable at neutral pH, with a half life estimated at  $10^{12}$  years. The catalytic subunit of PP1 accelerates the rate of hydrolysis of the phosphate monoester bond by a factor of  $10^{21}$ .<sup>15</sup> This makes PP1 one of the most efficient enzymes known.

#### **1.4.2 Catalytic subunit of PP1**

Mammals have three PP1 genes, encoding four isoforms PP1 $\alpha$ , PP1 $\gamma$ , PP1 $\beta/\delta$  of the PP1 catalytic subunit. Two splice variants can be generated from the PP1 $\gamma$  gene, PP1 $\gamma$ 1 and PP1 $\gamma$ 2.<sup>94</sup> All four isoforms are highly homologous and only differ in the C-terminal domain.

The sequence and chromosomal localization of human PP1 $\gamma$ , which is used in this work, has been identified (**Figure 1-21**).<sup>109</sup> The gene for human PP1 $\gamma$  is localized to chromosome 12 by analysis of somatic cell hybrid DNA and mapped to bands q24.1–q24.2 by in situ hybridization. These data show that although PP1 $\gamma$ 1 and PP1 $\gamma$ 2 are 94% and 93% identical to PP1 $\alpha$  respectively, the PP1 $\gamma$  gene is not closely linked to the PP1 $\alpha$  gene, which has been mapped to chromosome 11.

PP1 $\alpha$	<b>MADLDKLNIDSIIQRLLLEV</b> RGSKPGKNVQLQENEIRGLCLKSREIFLSQPIILLELEAPLKICGDIHGQYYDLLRLFEYGG	80
PP1 $\gamma$ 1	MADLDKLNIDSIIQRLLLEV <b>RGSKPGKNVQLQENEIRGLCLKSREIFLSQPIILLELEAPLKICGDIHGQYYDLLRLFEYGG</b>	80
PP1 $\gamma$ 2	MADLDKLNIDSIIQRLLLEV <b>RGSKPGKNVQLQENEIRGLCLKSREIFLSQPIILLELEAPLKICGDIHGQYYDLLRLFEYGG</b>	80
PP1 $\alpha$	<b>FPPESNYLFLGDYVDRGKQ</b> SLETICLLLAYKIKYPENFFLLRGNRECCASINRIYGFYDECKRRYNIKLNKWTFTDCFNCLP	160
PP1 $\gamma$ 1	FPPESNYLFLGDYVDRGKQ <b>SLETICLLLAYKIKYPENFFLLRGNRECCASINRIYGFYDECKRRYNIKLNKWTFTDCFNCLP</b>	160
PP1 $\gamma$ 2	FPPESNYLFLGDYVDRGKQ <b>SLETICLLLAYKIKYPENFFLLRGNRECCASINRIYGFYDECKRRYNIKLNKWTFTDCFNCLP</b>	160
PP1 $\alpha$	<b>IAAIVDEKIFCCCHGGLSPDLQ</b> SMEQIRIRMRPTDVPDQGLLCDLLWSDPDKDVLGWGENDRGVSTFFGAEVVAKFLHKHD	240
PP1 $\gamma$ 1	IAAIVDEKIFCCCHGGLSPDLQ <b>SMEQIRIRMRPTDVPDQGLLCDLLWSDPDKDVLGWGENDRGVSTFFGAEVVAKFLHKHD</b>	240
PP1 $\gamma$ 2	IAAIVDEKIFCCCHGGLSPDLQ <b>SMEQIRIRMRPTDVPDQGLLCDLLWSDPDKDVLGWGENDRGVSTFFGAEVVAKFLHKHD</b>	240
PP1 $\alpha$	<b>LDLICRAHQVVEDGYEFFAKR</b> QLVTLFSAPNYCGEFDNAGAMMSVDETLMCSFQILKPAKPKKPKN	320
PP1 $\gamma$ 1	LDLICRAHQVVEDGYEFFAKR <b>QLVTLFSAPNYCGEFDNAGAMMSVDETLMCSFQILKPAKPKKPKN</b> -----ATRPVT	311
PP1 $\gamma$ 2	LDLICRAHQVVEDGYEFFAKR <b>QLVTLFSAPNYCGEFDNAGAMMSVDETLMCSFQILKPAKPKKPKN</b> -----ATRPVT	311
PP1 $\alpha$	<b>PPRN--SAKAKR</b>	330
PP1 $\gamma$ 1	PP <b>NGMITKQAKR</b>	323
PP1 $\gamma$ 2	PP <b>VASGLNPSIQKASNYRNNTVLYE</b>	337

**Figure 1-21.** Nucleotide and amino-acid sequence of the human PP1 $\gamma$ 1 and PP1 $\gamma$ 2 gene<sup>109</sup> and comparison to the amino-acid sequences of human PP1 $\alpha$ .<sup>110</sup> Identical amino acids are boxed.

#### 1.4.2.1 General features of the structure

The crystal structures of apo PP1 $\gamma$  and its complex with tungstate<sup>85</sup>, PP1 $\alpha$ :microcystins,<sup>86</sup> PP1 $\gamma$ :okadaic acid,<sup>87</sup> PP1 $\gamma$ :calyculin A,<sup>111</sup> PP1 $\gamma$ :motuporin and PP1 $\gamma$ :dihydromicrocystin-LA,<sup>112</sup> PP1 $\gamma$ :nodularin-R, and PP1 $\gamma$ :tautomycin<sup>113</sup> have been reported. The overall and secondary structures of PP1 are similar to each other.

X-ray data for human PP1 $\gamma$  complexed with tungstate show that PP1 adopts a compact elliptical structure composed of 10  $\alpha$ -helices and 3- $\beta$  sheets with a  $\beta$ -sandwich

wedged between two  $\alpha$ -helical domains (**Figure 1-22 A**).<sup>85,86</sup> On the molecular surface, three shallow surface grooves (c-terminal groove, hydrophobic groove and acidic groove) follow the domain boundaries and converge at the catalytic center, forming a Y-shaped surface feature (**Figure 1-22 B**).<sup>111</sup> Toxins such as microcystin and okadaic acid are associated tightly with the hydrophobic groove and the acidic groove through the bifurcation point. C-terminal residues of PP1 are likely to be responsible for binding inhibitors and the targeting subunit.

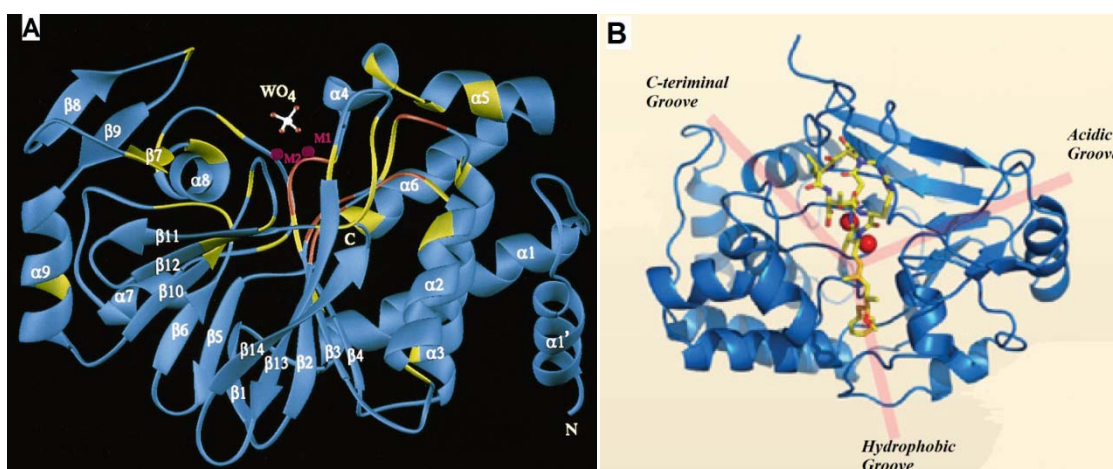


**Figure 1-22.** (A) Topology diagram showing the catalytic site of the secondary structural of PP1.<sup>85</sup> (B) Structure of the catalytic subunit of PP1 bound to okadaic acid. A Y-shaped surface groove is defined by the three domains of PP1.<sup>111</sup>

#### 1.4.2.2 The metal coordination geometry at the active site

In common with many phosphatases, the active site, identified from the positions of the inhibitor tungstate ion, is located in a shallow groove on the surface formed at the C-terminus of  $\beta$ -strands of the  $\beta$ -sheets 1 and 2 (**Figure 1-22 A**). The crystallographic data demonstrate that PP1 contains two metal ions that are close to each other, near the C-termini of the  $\beta$ -strands of the  $\beta$ - $\alpha$ - $\beta$ - $\alpha$ - $\beta$  unit.<sup>86</sup> Two metal ions, identified as  $Mn^{2+}$  and

$\text{Fe}^{2+}$  (iron) by proton-induced X-ray emission spectroscopy, are located in the active site at the three-way joint of the  $\beta$  sandwich and the two helical domains.<sup>85</sup> The Egloff group tentatively assigned metal sites 1 and 2 as  $\text{Fe}^{2+}$  and  $\text{Mn}^{2+}$  binding sites, respectively. The distance between the two metal ions is 3.3 Å; this close approach is facilitated by a carboxylate oxygen of Asp92 and a water molecule or hydroxyl ion (W2), each of which form a bridge between the two metals.

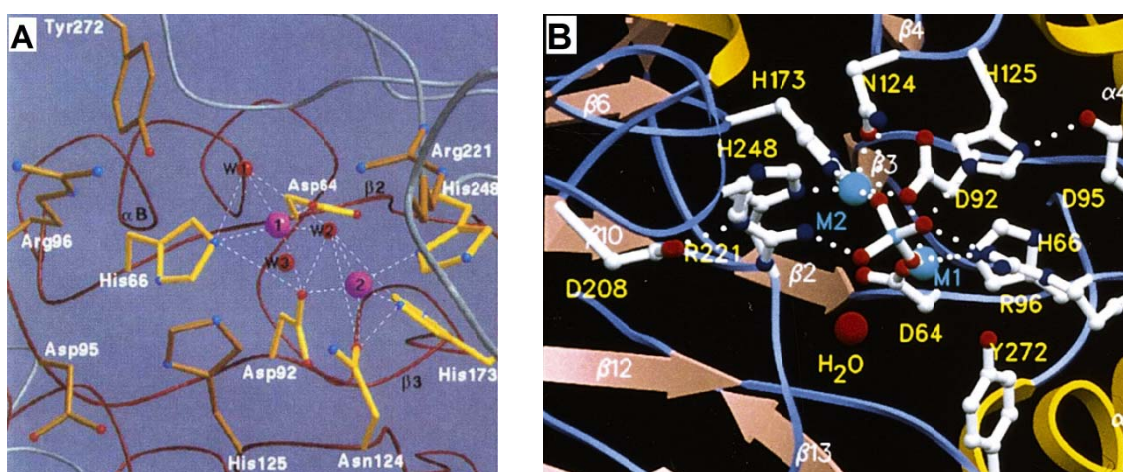


**Figure 1-23.** (A) Crystal structure of the active site of PP1 from literature.<sup>86</sup> Metal ions 1 and 2 (purple) and waters W1, W2 and W3 (red) are drawn as spheres. (B) Crystal structure of the catalytic site showing metal ions (cyan spheres) and tungstate binding sites from literature.<sup>85</sup> The tungstate-associated water molecule is shown as a red sphere.

The only agreement about the metal coordination geometry achieved so far is the M2 ( $\text{Mn}^{2+}$ ) coordinated by five ligands which are the side-chains of Asn124, His173 and His248, a carboxylate oxygen of Asp92, and a bridging water molecule or hydroxyl group. Goldberg group suggested that M2 adopted a distorted trigonal bipyramidal arrangement,<sup>86</sup> while Egloff group suggested that the arrangement of ligands to M2 corresponds to square pyramid geometry with Asn124 as the axial ligand. For the M1,

Goldberg group suggest that M1 was also coordinated by a total of five ligands and adopted square-pyramidal arrangement (**Figure 1-23 A**), while the Egloff group suggested M1 coordinated three protein ligands, Asp64, His66 and Asp92 and a water molecule in a trigonal pyramid geometry<sup>85</sup> (**Figure 1-23 B**).

The residues coordinating the metal centers are highly conserved in all members of the PPP family (**Figure 1-24**), suggesting a common mechanism of metal-catalyzed reaction in the protein family.

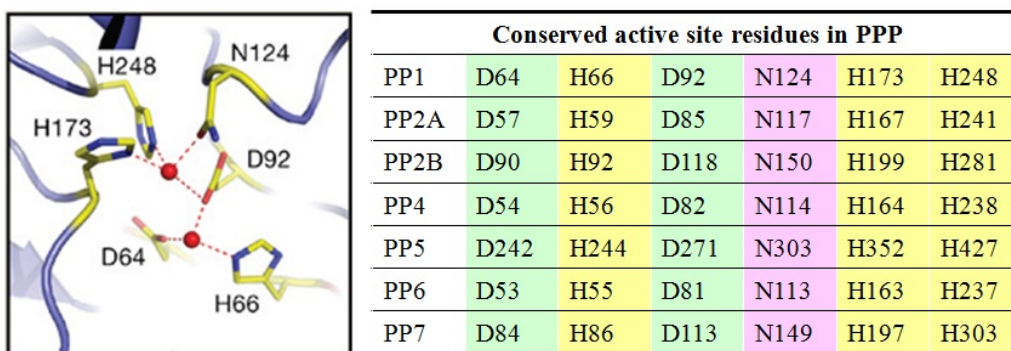


**Figure 1-24.** Conserved coordination of the binuclear metal center in the PPP superfamily.<sup>97</sup> The metal-binding scheme of PP1 where six highly conserved amino acids bind to the two metal ions is indicated on the left. The corresponding metal-binding residues from other PPP superfamily members are shown on the right.

#### 1.4.2.3 Substrate binding site

The crystal structure of PP1 $\gamma$  complexed with tungstate provides valuable information about substrate binding to the active site. Tungstate is bound at the dinuclear metal site resulting in displacement of one bridging water molecule. Each metal is coordinated by a different tungstate oxygen atom (O1 and O2). The two remaining oxygen atoms are more accessible to solvent (O3 and O4), one of which would

correspond to the seryl or threonyl side-chain oxygen atom. (**Figure 1-23 B**) The guanidinium groups of Arg96 and Arg221 form salt bridges with O1 and O3, respectively. A salt bridge between the side-chain of the residue Asp208 and Arg221 helps maintain the conformation of Arg221 for interaction with the substrate.

A salt bridge is formed between Asp95 on the C terminal strand of  $\beta$ 3, and the His125 residue on the C terminal strand of  $\beta$ 4. This salt bridge between the two domains may help stabilize the structure of PP1 $\gamma$ , and is also thought to position the His125 residue in the correct orientation to act as a general acid.

When tungstate is bound at the active site, the bridging hydroxide is positioned 3.7 Å away from the W atom of the tungstate, and would be ideally positioned to act as a nucleophile if the substrate binds in the same manner as tungstate. The bridging hydroxide is also located at an angle of almost 180 degrees to the tungstate oxygen which forms a hydrogen bond to His125, and it was suggested that this oxygen might correspond to the phosphoryl oxygen of the leaving group when a substrate is bound. Inspection of the structure shows that with closer approach of the water/hydroxyl molecule, W, O1, O2 and O3 atoms in WO<sub>4</sub> could possibly adopt a planar arrangement by distorting the tetrahedral geometry.

#### **1.4.2.4 Bacterially expressed catalytic subunit of PP1**

To obtain sufficient amounts of the catalytic subunit of PP1 to perform biochemical and biophysical studies, and also to provide a means for the study of structure-function relationships, it would be desirable to establish a system for the expression of the enzyme in *E. coli*. Initial attempts at expression of recombinant PP1 in the pET vector in the BL21 strain of *E. Coli* were unsuccessful, as although the protein

was readily over expressed, it was in the form of insoluble inclusion bodies.<sup>114,115</sup> The insoluble protein could be solubilized by refolding, but only exhibited 5 % of the expected activity. Zhang et al were able to successfully express considerable quantities of recombinant PP1 using the pTACTAC plasmid vector pCW in DH5 $\alpha$  *E. Coli* in the presence of manganese chloride at 28 °C.<sup>115</sup> Recombinant PP1 requires the addition of Mn<sup>2+</sup> to the growth media in order to express, and so it is presumed that the active site in the enzyme contains two Mn<sup>2+</sup> ions.<sup>114,115</sup>

There are several remarkable differences between PP1 prepared from natural resources and recombinant PP1. First, the catalytic subunits of PP1 from natural sources do not exist as free monomers but recombinant PP1 does. Second, the catalytic activity of native PP1 does not depend on the concentration of additional divalent metal ions, such as Mn<sup>2+</sup>, while recombinant PP1 requires the addition of Mn<sup>2+</sup> to the growth media in order to express and to the buffer solution to maintain full catalytic activity. The last difference is that native PP1 has high substrate selectivity and specificity, but recombinant PP1 has been referred to as promiscuous because of its low specificity. Recombinant PP1 can dephosphorylate small molecules such as pNPP.<sup>85</sup> However, the catalytic subunit that is purified from mammalian tissues does not act on these atypical substrates. The greater selectivity of the native enzyme may arise because the metals that are incorporated in the active site (Mn<sup>2+</sup> and Fe<sup>2+</sup>) differ from those of the bacterially expressed enzyme (Mn<sup>2+</sup>).

### 1.4.3 Proposed catalytic mechanism of PP1

On the basis of the structural data, a mechanism for PP1-catalyzed hydrolysis reaction was proposed in which the substrate binds to the active site in the same manner

as tungstate, and is attacked by the bridging hydroxide (**Figure 1-25**). The mechanism proposed is a concerted one, and the leaving group is protonated by the His125 residue, concomitant to the formation of the nucleophile-phosphorous bond. The role of the conserved Arg96 and Arg221 residues is suggested to help substrate binding and to stabilize the transition state.<sup>85</sup>

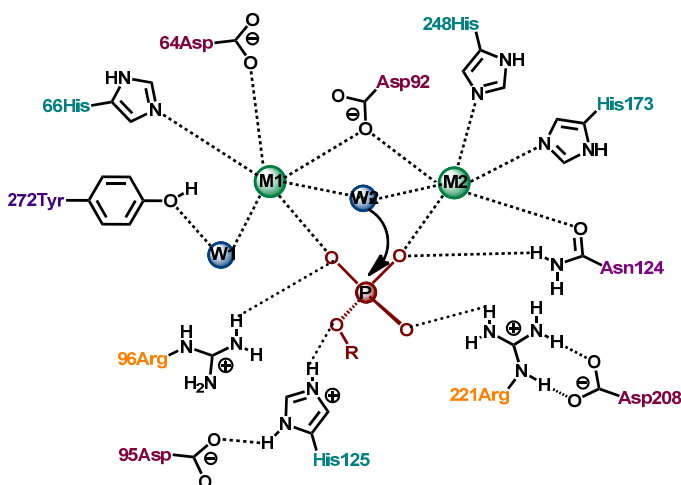


**Figure 1-25.** The proposed PP1-catalyzed hydrolysis mechanism according to the crystal structure.<sup>88</sup>

#### 1.4.4 Mutagenesis study of catalytic subunit of PP1

Potential target amino acids for mutagenesis can be classified into three groups: active site residues predicted to coordinate to the metal ions; active site residues predicted to bind substrates or facilitate catalysis; and residues located out of the active site. The data in **Table 1-5** show that mutation of D64, H66, D92 and H248 result in significantly reduced catalytic activity. This is consistent with their role as metal chelating ligands. However, the mutant N124D only shows up to 10-fold reduction in  $k_{\text{cat}}$  in both reports. The N124D and N124A mutants give contrasting results, as the N124D shows little

decrease in  $k_{\text{cat}}$ , while N124A mutant exhibits a dramatic loss in  $k_{\text{cat}}$ . To further explore the function of N124, the pH-rate profile of N124D and N124A mutants were determined. N124D mutant shows a bell-shaped profile with a pH optimum of 6.5, while wild type having a pH optimum of 7.5. N124A mutant displays a monophasic curve showing slight increase in activity up to pH 7 and much larger increase in activity after pH 7.

**Table 1-5.** The kinetic parameters of wild type PP1 and mutation of active site residues predicted to bind metals. Phosphorylase *a* was used as the substrate. The data shown in the top part of the table was cited from Lee group;<sup>116</sup> data in the bottom part of table was cited from Huang group.<sup>117</sup>

Enzyme	$k_{\text{cat}}$ , ( $\text{s}^{-1}$ )	$K_{\text{M}}$ , ( $\mu\text{M}$ )	$k_{\text{cat}}/K_{\text{M}}$ , ( $\text{M}^{-1}\text{s}^{-1} \times 10^{-6}$ )
Wild type	14.255	3.5	4.072
D64N	0.00050	2.4	0.00021
H66N	0.00246	2.4	0.0013
H66K	No detectable activity		
D92N	0.0028	10	0.00028
N124D	2.67	6.6	0.404
N124A	0.0026	7.4	0.00035
H248N	0.018	5.8	0.0032
H248K	0.00058	4.8	0.00012
Wild type	39	10.6	3.63
N124D	3.1	19.8	0.16
H248N	0.5	5.1	0.10

The explanation for the surprising properties of N124 is that this residue is not only involved in metal binding but also as a ligand binding to substrate oxygen or the

penta-coordinate phosphate intermediate or transition state during catalysis. The shift in the pH optimum of N124D was interpreted as reflecting the protonation of a phosphorous oxygen combined with an effect on the  $pK_a$  for dissociation of the metal bound water. The apparent  $pK_a$  of the basic limb (7.3) was consistent with the expected  $pK_a$  for the deprotonation of the substrate. The monophasic behavior of N124A mutant was interpreted as resulting from the elimination of the carbonyl function of N124 which is involved in metal binding and in binding to the phosphorus oxygen. Therefore, a greater concentration of hydroxide being available in solution would act as the nucleophile.

**Table 1-6.** The kinetic parameters of wild type PP1 and mutants of active site residues predicted to bind substrates and assist catalysis. Phosphorylase *a* was used as the substrate. The data shown in top part of the table was cited from Lee's group;<sup>116</sup> data in the bottom part of table was cited from Huang's group.<sup>117</sup>

Enzyme	$k_{cat}$ , (s <sup>-1</sup> )	$K_M$ , (μM)	$k_{cat}/K_M$ , (M <sup>-1</sup> s <sup>-1</sup> × 10 <sup>-6</sup> )
Wild type	14.255	3.5	4.072
D95N	0.171	3	0.057
R96E	0.054	8.9	0.0061
Wild type	39	10.6	3.63
D95A	0.02	5.8	0.0073
R96A	0.09	6.9	0.013
R221S	0.2	105.0	0.002

The crystal structures of PP1 suggest that R96 and R221 bind to substrate oxygens and may contribute to substrate binding as well as to stabilization of the

hypothetical penta-coordinate transition state.<sup>85,86</sup> Mutagenesis of the residues R96 and R221 mainly reduce the  $k_{\text{cat}}$  so that leading to between 300 and 700-fold reduction in catalytic efficiency ( $k_{\text{cat}}/K_{\text{M}}$ ) (**Table 1-6**). R96 mutants (R96A and R96E) did not exhibit much change in the  $K_{\text{M}}$ , while R221S show a significant reduction in  $K_{\text{M}}$ . The remarkable decrease in  $k_{\text{cat}}$  is consistent with these two residues having a role in catalysis. The mutagenesis data are also suggestive of a more important role for R96 in stabilization of the transition state than substrate binding. Even though these two residues are very important for substrate binding and catalysis, no pH dependencies of R96 and R221 mutants have been reported.

H125 was predicted to serve as a general acid to neutralize the negative charge developed in the leaving group.<sup>85,86</sup> Systematic mutation of H125 to F (Phenylalanine), C (Cysteine), Y (Tyrosine), S (serine), G (Glycine), D (Aspartic acid), V (Valine) and A (Alanine) all produced insoluble proteins except mutants H125A and H125S, neither of which exhibited detectable activity. These results could be due to misfolding of the protein, or could suggest that the positioning of the H125 residue is important for catalysis.

According to the crystal structure, D95 is buried in the active site with a carboxyl oxygen forming a hydrogen bond with H125. The catalytic role of D95 would be confining the position of H125 and stabilizing its protonated state. The D95A and D95N mutants are expressed, and show huge reduction in  $k_{\text{cat}}$  but no significant reduction in  $K_{\text{M}}$ . The results confirm the important function of D95 in catalysis.

## 1.5 Main goal

Even though Jensen recognized in 1976 that the catalytic promiscuity of proteins can provide a solution to the protein-evolution dilemma, and there has been an increasing systematic analysis of enzyme promiscuity in recent years combining not only newly discovered enzymes, but also numerous historic examples from earlier studies in which the phenomenon of promiscuity was not explicitly discussed as such, deep research into catalytic promiscuity of proteins is still urgently needed. So far, about two dozen catalytic promiscuous proteins have been identified, which are not sufficient to explore and explain enzyme evolution.

Secondly, the existence of enzyme catalytic promiscuity raises an important question: how do specificity and promiscuity coincide with a single active site? Generally, promiscuous activities share the main active site features with the native activity. The specificity and selectivity of an enzyme for a particular substrate or reaction depends on its ability to recognize and stabilize the transition state for that substrate during the reaction, and characterization of the structure of the transition state is a critical step for protein to distinguish between different substrates. So far, major efforts are still focusing on discovering new examples of catalytic promiscuous enzymes and their substrates. In only one example of the catalytic promiscuous enzymes shown in **Chapter 1.3** has the mechanistic aspect of catalytic promiscuity been explored.

The main goals of this project were to:

- (1) Measure and compare the catalytic effectiveness of PP1 in the hydrolysis of several new substrate classes;

- (2) Compare the mechanism and transition state of the PP1-catalyzed hydrolysis reactions with the respective uncatalyzed hydrolysis reactions for each substrate class;
- (3) Examine how two active site arginine residues contribute to the respective promiscuous activities of one substrate class over another;
- (4) Learn the origin of the catalytic rate acceleration by PP1.

The specific aims would help answer the following fundamental questions:

- (1) By comparing the catalytic efficiency ( $k_{\text{cat}}/K_{\text{M}}$ ), transition state affinities ( $k_{\text{w}}/(k_{\text{cat}}/K_{\text{M}})$ ), linear free energy relationships (LFER) and kinetic isotope effect (KIE) for the various substrate classes, insights will be gained into how the electronic and geometric nature of the substrates affect catalysis.
- (2) By comparing the catalytic efficiency ( $k_{\text{cat}}/K_{\text{M}}$ ) transition state affinities ( $k_{\text{w}}/(k_{\text{cat}}/K_{\text{M}})$ ) for various PP1 mutants, the energetic importance of specific residues and how these active site residues contribute to the various hydrolytic activities of PP1 will be revealed.
- (3) By comparing inhibition constants and the mode of inhibition for a set of oxyanions as a function of charge and geometry, an understanding of how these factors affect affinity and the binding mode at the active site will be gained.

## 1.6 References

- (1) Benning, M. M.; Shim, H.; Raushel, F. M.; Holden, H. M. *Biochemistry* **2001**, *40*, 2712-2722.
- (2) Babbie, A. C.; Bandyopadhyay, S.; Olguin, L. F.; Hollfelder, F. *Angew Chem. Int. Ed. Engl.* **2009**, *48*, 3692-3694.
- (3) O'Brien, P. J.; Herschlag, D. *Chem. Biol.* **1999**, *6*, R91-R105.

- (4) Copley, S. D. *Curr. Opin. Chem. Biol.* **2003**, *7*, 265-272.
- (5) Bornscheuer, U. T.; Kazlauskas, R. J. *Angew Chem. Int. Ed. Engl.* **2004**, *43*, 6032-6040.
- (6) Khersonsky, O.; Roodveldt, C.; Tawfik, D. S. *Curr. Opin. Chem. Biol.* **2006**, *10*, 498-508.
- (7) Hult, K.; Berglund, P. *Trends Biotech.* **2007**, *25*, 231-238.
- (8) Jonas, S.; Hollfelder, F. *Pure and Applied Chemistry* **2009**, *81*, 731-742.
- (9) James, L. C.; Tawfik, D. S. *Trends Biochem. Sci.* **2003**, *28*, 361-368.
- (10) Gamage, N. U.; Tsvetanov, S.; Duggleby, R. G.; McManus, M. E.; Martin, J. L. *J. Biol. Chem.* **2005**, *280*, 41482-41486.
- (11) Aharoni, A.; Gaidukov, L.; Khersonsky, O.; Mc, Q. G. S.; Roodveldt, C.; Tawfik, D. S. *Nat. Genet.* **2005**, *37*, 73-76.
- (12) Jensen, R. A. *Annu. Rev. Microbiol.* **1976**, *30*, 409-425.
- (13) C. Neuberg, J. H. *Biochem. Z.* **1921**, *115*, 282-310.
- (14) Crout, D. H. G.; Dalton, H.; Hutchinson, D. W.; Miyagoshi, M. *J. Chem. Soc., Perkin Trans. I* **1991**, 1329-1334.
- (15) Lad, C.; Williams, N. H.; Wolfenden, R. *Proc Natl Acad Sci U S A* **2003**, *100*, 5607-5610.
- (16) Thompson, J. E.; Kutateladze, T. G.; Schuster, M. C.; Venegas, F. D.; Messmore, J. M.; Raines, R. T. *Bioorg. Chem.* **1995**, *23*, 471-481.
- (17) Wolfenden, R.; Ridgway, C.; Young, G. *J. Am. Chem. Soc.* **1998**, *120*, 833-834.
- (18) Guthrie, R. D.; Jencks, W. P. *Acc. Chem. Res.* **1989**, *22*, 343-349.

- (19) Thatcher, G. R. J.; Kluger, R. *Advances in Physical Organic Chemistry* **1989**, *25*, 99-265.
- (20) Hengge, A. C. *Comprehensive Biological Catalysis: A Mechanistic Reference*, Wiley, 1998; Vol. 1.
- (21) Kirby, A. J.; Varvoglis, A. G. *J. Am. Chem. Soc.* **1967**, *89*, 415-423.
- (22) Kirby, A. J., Jencks, W. P. *J. Am. Chem. Soc.* **1965**, *87*, 3209-3216.
- (23) Hengge, A. C.; Edens, W. A.; Elsing, H. *J. Am. Chem. Soc.* **1994**, *116*, 5045-5049.
- (24) Herschlag, D.; Jencks, W. P. *J. Am. Chem. Soc.* **1989**, *111*, 7579-7586.
- (25) Catrina, I. E.; Hengge, A. C. *J. Am. Chem. Soc.* **2003**, *125*, 7546-7552.
- (26) Hengge, A. C.; Tobin, A. E.; Cleland, W. W. *J. Am. Chem. Soc.* **1995**, *117*, 5919-5926.
- (27) Cassano, A. G.; Anderson, V. E.; Harris, M. E. *J. Am. Chem. Soc.* **2002**, *124*, 10964-10965.
- (28) O'Ferrall, R. A. M. *J. Chem. Soc. B* **1970**, 274-277.
- (29) Jencks, W. P. *Chem. Rev.* **1972**, *72*, 705-718.
- (30) Zalatan, J. G.; Herschlag, D. *J. Am. Chem. Soc.* **2006**, *128*, 1293-1303.
- (31) Catrina, I. E.; Hengge, A. C. *J. Am. Chem. Soc.* **1999**, *121*, 2156-2163.
- (32) Zhang, Y. L.; Hollfelder, F.; Gordon, S. J.; Chen, L.; Keng, Y. F.; Wu, L.; Herschlag, D.; Zhang, Z. Y. *Biochemistry* **1999**, *38*, 12111-23.
- (33) Hollfelder, F.; Herschlag, D. *Biochemistry* **1995**, *34*, 12255-12264.
- (34) Schroeder, G. K.; Lad, C.; Wyman, P.; Williams, N. H.; Wolfenden, R. *Proc Natl Acad Sci U S A* **2006**, *103*, 4052-5.

- (35) Chin, J.; Banaszczyk, M.; Jubian, V.; Zou, X. *J. Am. Chem. Soc.* **1989**, *111*, 186-190.
- (36) Kirby, A. J.; Younas, M. *J. Chem. Soc. B.* **1970**, 1165-1170.
- (37) Hengge, A. C.; Cleland, W. W. *J. Am. Chem. Soc.*, **1990**, *112*, 7421-7422.
- (38) Hengge, A. C.; Cleland, W. W. *J. Am. Chem. Soc.*, **1991**, *113*, 5835-5841.
- (39) Hengge, A. C.; Tobin, A. E.; Cleland, W. W. *J. Am. Chem. Soc.*, **1995**, *117*, 5919-5926.
- (40) Hengge, A. C. *Acc. Chem. Res.* **2002**, *35*, 105-112.
- (41) Chin, J.; Banaszczyk, M.; Jubian, V.; Zou, X. *J. Am. Chem. Soc.* **1989**, *111*, 186-190.
- (42) Coleman, J. E. *Annu. Rev. Biophys. Biomol. Struct.* **1992**, *21*, 441-483.
- (43) Holtz, K. M.; Kantrowitz, E. R. *FEBS Lett* **1999**, *462*, 7-11.
- (44) O'Brien, P. J.; Herschlag, D. *Biochemistry* **2002**, *41*, 3207-3225.
- (45) Kim, E. E.; Wyckoff, H. W. *J. Mol. Biol.* **1991**, *218*, 449-464.
- (46) Holtz, K. M.; Stec, B.; Kantrowitz, E. R. *J. Biol. Chem.* **1999**, *274*, 8351-8354.
- (47) Murphy, J. E.; Stec, B.; Ma, L.; Kantrowitz, E. R. *Nat. Struct. Biol.* **1997**, *4*, 618-622.
- (48) Zalatan, J. G.; Fenn, T. D.; Herschlag, D. *J. Mol. Biol.* **2008**, *384*, 1174-1189.
- (49) O'Brien, P. J.; Herschlag, D. *J. Am. Chem. Soc.* **1998**, *120*, 12369-12370.
- (50) O'Brien, P. J.; Herschlag, D. *Biochemistry* **2001**, *40*, 5691-5699.
- (51) Yang, K. C.; Metcalf, W. W. *Proc Natl Acad Sci U S A* **2004**, *101*, 7919-7924.
- (52) Bond, C. S.; Clements, P. R.; Ashby, S. J.; Collyer, C. A.; Harrop, S. J.; Hopwood, J. J.; Guss, J. M. *Structure* **1997**, *5*, 277-289.

- (53) Lukatela, G.; Krauss, N.; Theis, K.; Selmer, T.; Gieselmann, V.; von Figura, K.; Saenger, W. *Biochemistry* **1998**, *37*, 3654-3664.
- (54) Galperin, M. Y.; Bairoch, A.; Koonin, E. V. *Protein Sci.* **1998**, *7*, 1829-1835.
- (55) Galperin, M. Y.; Jedrzejewski, M. J. *Proteins* **2001**, *45*, 318-324.
- (56) Murzin, A. G.; Brenner, S. E.; Hubbard, T.; Chothia, C. *J. Mol. Biol.* **1995**, *247*, 536-540.
- (57) Boltes, I.; Czapinska, H.; Kahnert, A.; von Bulow, R.; Dierks, T.; Schmidt, B.; von Figura, K.; Kertesz, M. A.; Uson, I. *Structure* **2001**, *9*, 483-491.
- (58) Dierks, T.; Schmidt, B.; von Figura, K. *Proc Natl Acad Sci U S A* **1997**, *94*, 11963-11968.
- (59) Dierks, T.; Lecca, M. R.; Schlotterhose, P.; Schmidt, B.; von Figura, K. *EMBO J.* **1999**, *18*, 2084-2091.
- (60) Sardiello, M.; Annunziata, I.; Roma, G.; Ballabio, A. *Hum. Mol. Genet.* **2005**, *14*, 3203-3217.
- (61) Benjdia, A.; Deho, G.; Rabot, S.; Berteau, O. *FEBS Lett* **2007**, *581*, 1009-1014.
- (62) Benjdia, A.; Leprince, J.; Guillot, A.; Vaudry, H.; Rabot, S.; Berteau, O. *J. Am. Chem. Soc.* **2007**, *129*, 3462-3463.
- (63) Babbitt, A. C.; Bandyopadhyay, S.; Olguin, L. F.; Hollfelder, F. *Angew Chem. Int. Ed. Engl.* **2009**, *48*, 3692-3694.
- (64) Olguin, L. F.; Askew, S. E.; O'Donoghue, A. C.; Hollfelder, F. *J. Am. Chem. Soc.* **2008**, *130*, 16547-16555.
- (65) Kelly, S. J.; Butler, L. G. *Biochem. Biophys. Res. Commun.* **1975**, *66*, 316-321.

- (66) Jonas, S.; van Loo, B.; Hyvonen, M.; Hollfelder, F. *J. Mol. Biol.* **2008**, *384*, 120-136.
- (67) Dotson, S. B.; Smith, C. E.; Ling, C. S.; Barry, G. F.; Kishore, G. M. *J. Biol. Chem.* **1996**, *271*, 25754-25761.
- (68) van Loo, B.; Jonas, S.; Babbie, A. C.; Benjdia, A.; Berteau, O.; Hyvonen, M.; Hollfelder, F. *Proc Natl Acad Sci U S A* **2010**, *107*, 2740-2745.
- (69) Strater, N.; Klabunde, T.; Tucker, P.; Witzel, H.; Krebs, B. *Science* **1995**, *268*, 1489-1492.
- (70) Lindqvist, Y.; Johansson, E.; Kaija, H.; Vihko, P.; Schneider, G. *J. Mol. Biol.* **1999**, *291*, 135-147.
- (71) Guddat, L. W.; McAlpine, A. S.; Hume, D.; Hamilton, S.; de Jersey, J.; Martin, J. L. *Structure* **1999**, *7*, 757-767.
- (72) Schenk, G.; Gahan, L. R.; Carrington, L. E.; Mitic, N.; Valizadeh, M.; Hamilton, S. E.; de Jersey, J.; Guddat, L. W. *Proc Natl Acad Sci U S A* **2005**, *102*, 273-278.
- (73) Schenk, G.; Ge, Y.; Carrington, L. E.; Wynne, C. J.; Searle, I. R.; Carroll, B. J.; Hamilton, S.; de Jersey, J. *Arch. Biochem. Biophys.* **1999**, *370*, 183-189.
- (74) Schenk, G.; Boutchard, C. L.; Carrington, L. E.; Noble, C. J.; Moubaraki, B.; Murray, K. S.; de Jersey, J.; Hanson, G. R.; Hamilton, S. *J. Biol. Chem.* **2001**, *276*, 19084-19088.
- (75) Lindqvist, Y.; Johansson, E.; Kaija, H.; Vihko, P.; Schneider, G. *J. Mol. Biol.* **1999**, *291*, 135-147.
- (76) Aquino, M. A. S.; Lim, J. S.; Sykes, A. G. *J. Chem. Soc., Dalton Trans.* **1992**, 2135-2136.

- (77) Twitchett, M. B.; Schenk, G.; Aquino, M. A. S.; Yiu, D. T. Y.; Lau, T. C.; Sykes, A. G. *Inorg. Chem.* **2002**, *41*, 5787-5794.
- (78) Mueller, E. G.; Crowder, M. W.; Averill, B. A.; Knowles, J. R. *J. Am. Chem. Soc.* **1993**, *115*, 2974-2975.
- (79) Cox, R. S.; Schenk, G.; Mitic, N.; Gahan, L. R.; Hengge, A. C. *J. Am. Chem. Soc.* **2007**, *129*, 9550-9558.
- (80) Merckx, M.; Averill, B. A. *J. Am. Chem. Soc.* **1999**, *121*, 6683-6689.
- (81) Strater, N.; Lipscomb, W. N.; Klabunde, T.; Krebs, B. *Angew Chem. Int. Ed. Engl.* **1996**, *35*, 2024-2055.
- (82) Klabunde, T.; Strater, N.; Frohlich, R.; Witzel, H.; Krebs, B. *J. Mol. Biol.* **1996**, *259*, 737-748.
- (83) Schlosnagle, D. C.; Bazer, F. W.; Tsibris, J. C.; Roberts, R. M. *J. Biol. Chem.* **1974**, *249*, 7574-7579.
- (84) Mitic, N.; Noble, C. J.; Gahan, L. R.; Hanson, G. R.; Schenk, G. *J. Am. Chem. Soc.* **2009**, *131*, 8173-8179.
- (85) Egloff, M. P.; Cohen, P. T.; Reinemer, P.; Barford, D. *J. Mol. Biol.* **1995**, *254*, 942-959.
- (86) Goldberg, J.; Huang, H. B.; Kwon, Y. G.; Greengard, P.; Nairn, A. C.; Kuriyan, J. *Nature* **1995**, *376*, 745-753.
- (87) Maynes, J. T.; Bateman, K. S.; Cherney, M. M.; Das, A. K.; Luu, H. A.; Holmes, C. F.; James, M. N. *J. Biol. Chem.* **2001**, *276*, 44078-44082.
- (88) McWhirter, C.; Lund, E. A.; Tanifum, E. A.; Feng, G.; Sheikh, Q. I.; Hengge, A. C.; Williams, N. H. *J. Am. Chem. Soc.* **2008**, *130*, 13673-13682.

- (89) Jackson, M. D.; Denu, J. M. *Chem. Rev.* **2001**, *101*, 2313-2340.
- (90) Barford, D.; Das, A. K.; Egloff, M. P. *Annu. Rev. Biophys. Biomol. Struct.* **1998**, *27*, 133-64.
- (91) Janssens, V.; Longin, S.; Goris, J. *Trends Biochem. Sci.* **2008**, *33*, 113-121.
- (92) Cohen, P. *Annu. Rev. Biochem.* **1989**, *58*, 453-508.
- (93) Bollen, M.; Peti, W.; Ragusa, M. J.; Beullens, M. *Trends Biochem. Sci.* **2010**, *35*, 450-458.
- (94) Ceulemans, H.; Bollen, M. *Physiol. Rev.* **2004**, *84*, 1-39.
- (95) Cohen, P. T. J. *J. Cell. Sci.* **2002**, *115*, 241-256.
- (96) Moorhead, G. B.; De Wever, V.; Templeton, G.; Kerk, D. *Biochem. J.* **2009**, *417*, 401-409.
- (97) Shi, Y. *Cell* **2009**, *139*, 468-84.
- (98) Moorhead, G. B.; Trinkle-Mulcahy, L.; Ulke-Lemee, A. *Nat. Rev. Mol. Cell Biol.* **2007**, *8*, 234-244.
- (99) Hubbard, M. J.; Cohen, P. *Eur. J. Biochem.* **1989**, *186*, 711-716.
- (100) Lee Y.C., Z. L., Zhao S., Wei Q., Zhang J., Zhi Q.Q., Belmonte E.R., *Frontiers in Bioscience* **1999**, *4*, 270-285.
- (101) Gullledgea, B. M.; Aggena, J. B.; Huangb, H. B.; Nairnc, A. C.; Chamberlin, A. R. *Curr. Med. Chem.* **2002**, *9*, 1991-2003.
- (102) Dounay, A. B.; Forsyth, C. J. *Curr. Med. Chem.* **2002**, *9*, 1939-1980.
- (103) Kato, Y.; Fusetani, N.; Matsunaga, S.; Hashimoto, K.; Fujita, S.; Furuya, T. *J. Am. Chem. Soc.* **1986**, *108*, 2780-2781.

- (104) Honkanen, R. E.; Dukelow, M.; Zwiller, J.; Moore, R. E.; Khatra, B. S.; Boynton, A. L. *Mol. Pharmacol* **1991**, *40*, 577-583.
- (105) Cheng, X. C.; Kihara, T.; Kusakabe, H.; Magae, J.; Kobayashi, Y.; Fang, R. P.; Ni, Z. F.; Shen, Y. C.; Ko, K.; Yamaguchi, I.; et al. *J. Antibiot. (Tokyo)* **1987**, *40*, 907-909.
- (106) Stampwala, S. S.; Bunge, R. H.; Hurley, T. R.; Willmer, N. E.; Brankiewicz, A. J.; Steinman, C. E.; Smitka, T. A.; French, J. C. *J. Antibiot. (Tokyo)* **1983**, *36*, 1601-1605.
- (107) Wang, G. S. *J. Ethnopharmacol* **1989**, *26*, 147-162.
- (108) Zhang, L. F.; Zhang, Z. J.; Long, F. X.; Lee, E. Y. C. *Biochemistry* **1996**, *35*, 1606-1611.
- (109) Barker, H. M.; Craig, S. P.; Spurr, N. K.; Cohen, P. T. *Biochim. Biophys. Acta* **1993**, *1178*, 228-233.
- (110) Barker, H. M.; Jones, T. A.; Silva, E. F. D.; Spurr, N. K.; Sheer, D.; Cohen, P. T. *W. Genomics* **1990**, *7*, 159-166.
- (111) Kita, A.; Matsunaga, S.; Takai, A.; Kataiwa, H.; Wakimoto, T.; Fusetani, N.; Isobe, M.; Miki, K. *Structure* **2002**, *10*, 715-724.
- (112) Maynes, J. T.; Luu, H. A.; Cherney, M. M.; Andersen, R. J.; Williams, D.; Holmes, C. F.; James, M. N. *J. Mol. Biol.* **2006**, *356*, 111-120.
- (113) Kelker, M. S.; Page, R.; Peti, W. *J. Mol. Biol.* **2009**, *385*, 11-21.
- (114) Browner, M. F.; Rasor, P.; Tugendreich, S.; Fletterick, R. J. *Protein Engineering* **1991**, *4*, 351-357.

- (115) Zhang, Z. J.; Bai, G.; Deanszirattu, S.; Browner, M. F.; Lee, E. Y. C. *J. Biol. Chem.* **1992**, *267*, 1484-1490.
- (116) Zhang, J.; Zhang, Z.; Brew, K.; Lee, E. Y. *Biochemistry* **1996**, *35*, 6276-6282.
- (117) Huang, H. B.; Horiuchi, A.; Goldberg, J.; Greengard, P.; Nairn, A. C. *Proc Natl Acad Sci U S A* **1997**, *94*, 3530-3535.

## CHAPTER 2

## MATERIALS AND METHODS

## 2.1 Substrate synthesis and characterization

In this work, a set of functional group modifications were made in the transferring group of the hydrolysis reactions (**Figure 2-1**). **Table 2-1** shows phenolic leaving groups used in PP1 $\gamma$ -catalyzed hydrolysis reactions with their  $pK_a$  values.<sup>1</sup>

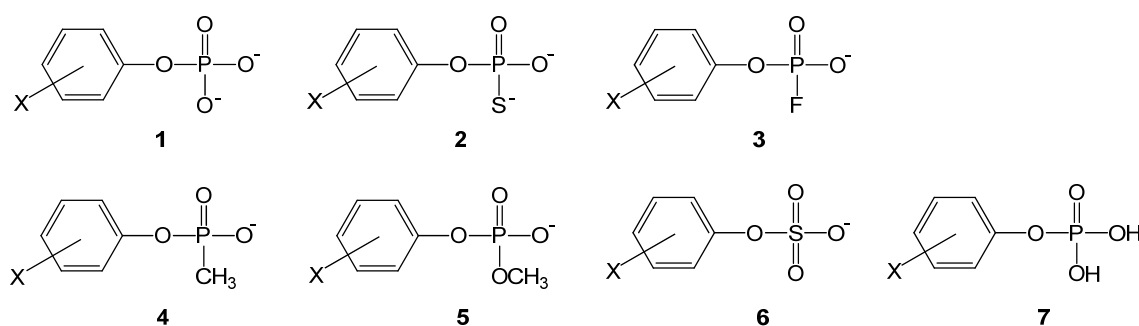


**Figure 2-1.** Structures of designed substrate classes.

**Table 2-1.** Phenolic leaving groups used in PP1 $\gamma$ -catalyzed hydrolysis reactions with their  $pK_a$  values.<sup>1</sup>

Phenyl substituent (X)	Label	$pK_a$
4-NO <sub>2</sub>	<b>a</b>	7.14
4-CN	<b>b</b>	7.95
3-CN	<b>c</b>	8.61
4-Cl	<b>d</b>	9.38
3-Cl	<b>e</b>	9.02
H-	<b>f</b>	9.95
3-NO <sub>2</sub>	<b>g</b>	8.35
4-Cl, 3-NO <sub>2</sub>	<b>h</b>	7.78

### 2.1.1 Materials and instruments

All chemical reagents and solvents were commercial products and were used as received unless otherwise noted. Thiophosphoryl chloride was distilled under nitrogen before use. Pyridine was distilled from calcium hydride. Acetonitrile was dried over anhydrous  $K_2CO_3$  for 24h, followed by distillation. NMR spectra were performed on a JEOL ECX-300 (proton at 300 MHz) with an Oxford 54-mm-bore magnet. Phosphoric acid and trichlorofluoromethane were used as external standard for  $^{31}P$  NMR and  $^{19}F$  NMR, separately.

### 2.1.2 Synthesis and characterization of aryl phosphorothioate bis(cyclohexyl amine) salts (2a-h)

Aryl phosphorothioate bis(cyclohexyl amine) salts were prepared and purified as previously reported<sup>2,3</sup> except that thiophosphoryl chloride was used instead of phosphoryl chloride as the starting material. Compounds **2a-h** were previously reported but with different counterions. The NMR spectra of **2a-h** match the reported results and are shown in **Appendix A1-A17**.

#### *4-nitrophenyl phosphorothioate bis(cyclohexyl amine) salt (2a)*

$^1H$  NMR (300 MHz,  $D_2O$ )  $\delta$  8.09 (2H, d,  $J = 9.3$  Hz), 7.27 (2H, d,  $J = 8.3$  Hz), 2.99 (2H, m), 1.94-1.75 (4H, m), 1.73-1.57 (4H, m), 1.56-1.43 (2H, m), 1.29-0.93 (10H, m);  $^{31}P$  NMR (122 MHz,  $D_2O$ )  $\delta$  41.46; Anal. Calcd for  $C_{18}H_{32}N_3O_5SP$ : C, 49.94; H, 7.45; N, 9.70; Found: C, 50.00; H, 7.25; N, 9.68

#### *4-cyanophenyl phosphorothioate bis(cyclohexyl amine) salt (2b)*

$^1\text{H}$  NMR (300 MHz,  $\text{D}_2\text{O}$ )  $\delta$  7.57 (2H, d,  $J = 8.6$  Hz), 7.24 (2H, d,  $J = 7.9$  Hz), 2.99 (2H, m), 1.94-1.75 (4H, m), 1.73-1.57 (4H, m), 1.56-1.43 (2H, m), 1.29-0.93 (10H, m);  $^{31}\text{P}$  NMR (122 MHz,  $\text{D}_2\text{O}$ )  $\delta$  41.33

*3-cyanophenyl phosphorothioate bis(cyclohexyl amine) salt (2c)*

$^1\text{H}$  NMR (300 MHz,  $\text{D}_2\text{O}$ )  $\delta$  7.50 (1H, s), 7.46-7.30 (3H, m), 2.99 (2H, m), 1.82 (4H, m), 1.65 (4H, m), 1.52-1.48 (2H, m), 1.28-0.95 (10H, m);  $^{31}\text{P}$  NMR (122 MHz,  $\text{D}_2\text{O}$ )  $\delta$  41.83

*4-chlorophenyl phosphorothioate bis(cyclohexyl amine) salt (2d)*

$^1\text{H}$  NMR (300 MHz,  $\text{D}_2\text{O}$ )  $\delta$  7.18 (2H, d,  $J = 9.1$  Hz), 7.07 (2H, d,  $J = 8.9$  Hz), 2.99 (2H, m), 1.94-1.75 (4H, m), 1.73-1.57 (4H, m), 1.56-1.43 (2H, m), 1.29-0.93 (10H, m);  $^{31}\text{P}$  NMR (122 MHz,  $\text{D}_2\text{O}$ )  $\delta$  41.57

*3-chlorophenyl phosphorothioate bis(cyclohexyl amine) salt (2e)*

$^1\text{H}$  NMR (300 MHz,  $\text{D}_2\text{O}$ )  $\delta$  7.27-6.93 (4H, m), 2.99 (2H, m), 1.82 (4H, m), 1.65 (4H, m), 1.52-1.48 (2H, m), 1.28-0.95 (10H, m);  $^{31}\text{P}$  NMR (122 MHz,  $\text{D}_2\text{O}$ )  $\delta$  41.63

*phenyl phosphorothioate bis(cyclohexyl amine) salt (2f)*

$^1\text{H}$  NMR (300 MHz,  $\text{D}_2\text{O}$ )  $\delta$  7.25-6.98 (5H, m), 2.99 (2H, m), 1.82 (4H, m), 1.65 (4H, m), 1.52-1.48 (2H, m), 1.28-0.95 (10H, m);  $^{31}\text{P}$  NMR (122 MHz,  $\text{D}_2\text{O}$ )  $\delta$  41.36

*3-nitrophenyl phosphorothioate bis(cyclohexyl amine) salt (2g)*

$^1\text{H}$  NMR (300 MHz,  $\text{D}_2\text{O}$ )  $\delta$  8.00 (1H, d,  $J = 1.4$  Hz), 7.82 (1H, d,  $J = 7.2$  Hz), 7.49 (1H, d,  $J = 8.2$  Hz), 7.39 (1H, t,  $J = 8.3$  Hz), 2.99 (2H, m), 1.82 (4H, m), 1.65 (4H, m), 1.52-1.48 (2H, m), 1.28-0.95 (10H, m);  $^{31}\text{P}$  NMR (122 MHz,  $\text{D}_2\text{O}$ )  $\delta$  41.96

*4-chloro-3-nitrophenyl phosphorothioate bis(cyclohexyl amine) salt (2h)*

$^1\text{H}$  NMR (300 MHz,  $\text{D}_2\text{O}$ )  $\delta$  7.79 (1H, s), 7.45-7.35 (2H, m), 2.99 (2H, m), 1.94-1.75 (4H, m), 1.73-1.57 (4H, m), 1.56-1.43 (2H, m), 1.29-0.93 (10H, m);  $^{31}\text{P}$  NMR (122 MHz,  $\text{D}_2\text{O}$ )  $\delta$  42.14

**2.1.3 Synthesis and characterization of aryl fluorophosphate monoester potassium salts (3a-f)**

Potassium salts of aryl fluorophosphate monoesters were prepared from 2,4-dinitrofluorobenzene and appropriate aryl phosphoric acids (**7a-f**) via triethylamine with subsequent hydrolysis.<sup>4,5</sup> A typical procedure, described for phenyl fluorophosphate monoester potassium salt, was as follows. Phenyl phosphate bis(cyclohexyl amine) salt was dissolved in a minimum amount of water. The solution was then cooled, strongly acidified with sulfuric acid, and extracted with diethyl ether. The diethyl ether extract was combined and evaporated, yielding phenyl phosphoric acid as a thick syrup. The crude phenyl phosphoric acid (10 mmol, 1.74 g), 2,4-dinitrofluorobenzene (12 mmol, 2.23 g), and triethylamine (23 mmol, 3.2 mL) were stirred in dry acetonitrile (10 mL) at room temperature for 24 h. The solvent was evaporated; the product was dissolved in 25 mL water and treated with amberlite IR120 (H) in an ice bath. After filtration, the filtrate was washed with diethyl ether, and neutralized with potassium carbonate. The crude yellow product was obtained after lyophilization. The pure product was recrystallized from methanol/acetone/diethyl ether. **3b** and **3c** were newly reported compounds and their NMR spectra and elemental results (EA) are shown in **Appendix A18-A24**. The NMR spectra for the other substrates (**3a**, **3d-f**) match the literature data and are shown in **Appendix A25-A35**.

*4-nitrophenyl phosphoric acid (7a)*

$^1\text{H}$  NMR (300 MHz,  $\text{D}_2\text{O}$ )  $\delta$  8.03 (2H, d,  $J = 9.3$  Hz), 7.13 (2H, d,  $J = 9.3$  Hz);  $^{31}\text{P}$  NMR (122 MHz,  $\text{D}_2\text{O}$ )  $\delta$  -4.28

*4-nitrophenyl fluorophosphate potassium salt (3a)*

$^1\text{H}$  NMR (300 MHz,  $\text{D}_2\text{O}$ )  $\delta$  8.18 (2H, d,  $J = 8.9$  Hz), 7.27 (2H, d,  $J = 9.0$  Hz);  $^{31}\text{P}$  NMR (122 MHz,  $\text{D}_2\text{O}$ )  $\delta$  -7.62, -15.41 ( $J_{\text{PF}} = 945$  Hz);  $^{19}\text{F}$  NMR (283 MHz,  $\text{D}_2\text{O}$ )  $\delta$  -73.64, -76.98 ( $J_{\text{PF}} = 945$  Hz)

*4-cyanophenyl phosphoric acid (7b)*

$^1\text{H}$  NMR (300 MHz,  $\text{D}_2\text{O}$ )  $\delta$  7.63 (2H, d,  $J = 8.6$  Hz), 7.19 (2H, d,  $J = 7.9$  Hz);  $^{31}\text{P}$  NMR (122 MHz,  $\text{D}_2\text{O}$ )  $\delta$  -4.19

*4-cyanophenyl fluorophosphate potassium salt (3b)*

$^1\text{H}$  NMR (300 MHz,  $\text{D}_2\text{O}$ )  $\delta$  7.68 (2H, d,  $J = 6.2$  Hz), 7.21 (2H, d,  $J = 8.6$  Hz);  $^{31}\text{P}$  NMR (122 MHz,  $\text{D}_2\text{O}$ )  $\delta$  -7.39, -15.17 ( $J_{\text{PF}} = 945$  Hz);  $^{19}\text{F}$  NMR (283 MHz,  $\text{D}_2\text{O}$ )  $\delta$  -73.73, -77.08 ( $J_{\text{PF}} = 945$  Hz); Anal. Calcd for  $\text{C}_7\text{H}_4\text{FKNO}_3\text{P}$ : C, 35.15; H, 1.69; N, 5.86; Found: C, 34.87; H, 1.50; N, 5.75

*3-cyanophenyl phosphoric acid (7c)*

$^1\text{H}$  NMR (300 MHz,  $\text{D}_2\text{O}$ )  $\delta$  7.47-7.23 (4H, m);  $^{31}\text{P}$  NMR (122 MHz,  $\text{D}_2\text{O}$ )  $\delta$  -3.77

*3-cyanophenyl fluorophosphate potassium salt (3c)*

$^1\text{H}$  NMR (300 MHz,  $\text{D}_2\text{O}$ )  $\delta$  7.53-7.33 (4H, m);  $^{31}\text{P}$  NMR (122 MHz,  $\text{D}_2\text{O}$ )  $\delta$  -6.87, -14.65 ( $J_{\text{PF}} = 945$  Hz);  $^{19}\text{F}$  NMR (283 MHz,  $\text{D}_2\text{O}$ )  $\delta$  -74.26, -77.60 ( $J_{\text{PF}} = 945$  Hz);

*4-chlorophenyl phosphoric acid (7d)*

$^1\text{H}$  NMR (300 MHz,  $\text{D}_2\text{O}$ )  $\delta$  7.22 (2H, d,  $J = 8.9$  Hz), 7.02 (2H, d,  $J = 8.9$  Hz);  $^{31}\text{P}$  NMR (122 MHz,  $\text{D}_2\text{O}$ )  $\delta$  -3.63

*4-chlorophenyl fluorophosphate potassium salt (3d)*

$^1\text{H}$  NMR (300 MHz,  $\text{D}_2\text{O}$ )  $\delta$  7.29 (2H, d,  $J = 8.3$  Hz), 7.05 (2H, d,  $J = 8.6$  Hz);  $^{31}\text{P}$  NMR (122 MHz,  $\text{D}_2\text{O}$ )  $\delta$  -6.40, -14.13 ( $J_{\text{PF}} = 945$  Hz);  $^{19}\text{F}$  NMR (283 MHz,  $\text{D}_2\text{O}$ )  $\delta$  -74.62, -77.97 ( $J_{\text{PF}} = 945$  Hz); Anal. Calcd for  $\text{C}_6\text{H}_4\text{ClFKO}_3\text{P}$ : C, 28.99; H, 1.62; Found: C, 28.97; H, 1.49

*3-chlorophenyl phosphoric acid (7e)*

$^1\text{H}$  NMR (300 MHz,  $\text{D}_2\text{O}$ )  $\delta$  7.24-6.92 (4H, m);  $^{31}\text{P}$  NMR (122 MHz,  $\text{D}_2\text{O}$ )  $\delta$  -3.77

*3-chlorophenyl fluorophosphate potassium salt (3e)*

$^1\text{H}$  NMR (300 MHz,  $\text{D}_2\text{O}$ )  $\delta$  7.28-7.21 (1H, m), 7.17-7.11 (2H, m), 7.01 (1H, d,  $J = 8.3$  Hz);  $^{31}\text{P}$  NMR (122 MHz,  $\text{D}_2\text{O}$ )  $\delta$  -6.56, -14.33 ( $J_{\text{PF}} = 945$  Hz);  $^{19}\text{F}$  NMR (283 MHz,  $\text{D}_2\text{O}$ )  $\delta$  -74.41, -77.75 ( $J_{\text{PF}} = 945$  Hz)

*phenyl phosphoric acid (7f)*

$^1\text{H}$  NMR (300 MHz,  $\text{CD}_3\text{CN}$ )  $\delta$  7.39-7.31 (2H, m), 7.28-7.13 (3H, m);  $^{31}\text{P}$  NMR (122 MHz,  $\text{D}_2\text{O}$ )  $\delta$  -4.26

*phenyl fluorophosphate potassium salt (3f)*

$^1\text{H}$  NMR (300 MHz,  $\text{D}_2\text{O}$ )  $\delta$  7.31 (2H, t,  $J = 7.6$  Hz), 7.18-7.07 (3H, m);  $^{31}\text{P}$  NMR (122 MHz,  $\text{D}_2\text{O}$ )  $\delta$  -6.07, -13.80 ( $J_{\text{PF}} = 945$  Hz);  $^{19}\text{F}$  NMR (283 MHz,  $\text{D}_2\text{O}$ )  $\delta$  -74.50, -77.84 ( $J_{\text{PF}} = 945$  Hz)

### 2.1.4 Synthesis and characterization of other substrates

#### *4-nitrophenyl phosphate monoester bis(cyclohexylamine) salt (1a)*

4-Nitrophenyl phosphate monoester bis(cyclohexyl amine) salts were prepared and purified as previously reported.<sup>3</sup> The NMR spectra for **1a** match the literature data and are shown in **Appendix A36-A37**.

<sup>1</sup>H NMR (300 MHz, D<sub>2</sub>O) δ 8.08 (2H, d, *J* = 9.3 Hz), 7.18 (2H, d, *J* = 8.6 Hz), 2.99 (2H, m), 1.94-1.75 (4H, m), 1.73-1.57 (4H, m), 1.56-1.43 (2H, m), 1.29-0.93 (10H, m); <sup>31</sup>P NMR (122 MHz, D<sub>2</sub>O) δ 0.21

#### *4-nitrophenyl methylphosphonate sodium salt (4a)*

4-Nitrophenyl methylphosphonate sodium salt was prepared according to literature.<sup>6</sup> The NMR spectra for **4a** are shown in **Appendix A38-A40**.

<sup>1</sup>H NMR (300 MHz, D<sub>2</sub>O) δ 8.14 (2H, d, *J* = 8.9 Hz), 7.20 (2H, d, *J* = 9.3 Hz), 1.34 (3H, d, *J* = 16.9 Hz); <sup>31</sup>P NMR (122 MHz, D<sub>2</sub>O) δ -25.77; <sup>13</sup>C NMR (76 MHz, D<sub>2</sub>O) δ 157.44, 143.54, 125.85, 121.27, 12.23 (d, *J* = 139 Hz)

#### *Methyl 4-nitrophenyl phosphate diester (5a)*

The sodium salt of methyl 4-nitrophenyl phosphate diester was prepared using a modification of a literature procedure.<sup>7</sup> 4-Nitrophenol (3.0 g, 21.6 mmol) in dry pyridine (10 mL) was added dropwise to phosphoryl chloride (2.0 mL, 21.5 mmol) which was previously mixed with dry pyridine (25 mL). After addition was finished, the mixture was stirred for another 45 min at room temperature. Methanol (1.6 mL, 40 mmol) was added very slowly to the mixture. Another 2 h refluxing was applied. The reaction solution was filtrated to remove pyridine hydrochloride as white solid. The filtrate was

poured into 20 mL of cold water. The resulting solution was titrated down to pH 4-5 with hydrochloric acid and extracted with dichloromethane. Removal of the solvent yielded the neutral form of methyl 4-nitrophenyl phosphate diester. The crude product was re-dissolved in 20 mL of water and titrated to about pH 9 with sodium carbonate. The pale yellow product was obtained after lyophilization. The pure product was obtained by recrystallization with acetone/methanol. The NMR spectra for **5a** match the literature data and are shown in **Appendix A41-A42**.

$^1\text{H}$  NMR (300 MHz,  $\text{D}_2\text{O}$ )  $\delta$  8.15 (2H, d,  $J = 8.9$  Hz), 7.23 (2H, d,  $J = 8.6$  Hz), 3.58 (3H, d,  $J = 11.4$  Hz);  $^{31}\text{P}$  NMR (122 MHz,  $\text{D}_2\text{O}$ )  $\delta$  -3.03

#### *4-nitrophenyl sulfate potassium salt (6a)*

Pyridine- $\text{SO}_3$  complex (1.0 g, 6.3 mmol) was dissolved in anhydrous pyridine (7 mL), and the solution heated to 65°C. Then 4-nitrophenol (500 mg, 3.6 mmol) was added. After 10 min, 8 mL of benzene was added and the mixture was stirred at 90°C under nitrogen for 4 h. After this time, an additional 10 mL of benzene was added, and the reaction mixture was allowed to cool to room temperature, and then cooled further in an ice bath. The resulting precipitate was collected by filtration and re-dissolved in 0.1 N KOH. This solution (which had a pH of ~5) was washed with 75 mL of diethyl ether twice. The water volume was reduced by rotary evaporation until the volume was about 40 mL. The resulted solution was placed in the refrigerator overnight. The potassium salt of 4-nitrophenyl sulfate was collected by filtration and identified as clean compound by NMR. The  $^1\text{H}$  NMR spectrum for **6a** matches the literature data and is shown in **Appendix A43**.

$^1\text{H}$  NMR (300 MHz,  $\text{D}_2\text{O}$ )  $\delta$  8.18 (2H, d,  $J = 9.0$  Hz), 7.36 (2H, d,  $J = 9.3$  Hz).

## 2.2 Protein expression and purification

### 2.2.1 Materials and instruments

The plasmid pCWOri+ encoding the 37 kDa form of human wild type PP1 $\gamma$  is a generous gift from Dr Williams. (University of Sheffield) *E. coli* DH5 $\alpha$  was supplied by Invitrogen Ltd. All primers were synthesised by Integrated DNA Technologies. *NdeI*, *Hind III*, *T4 DNA ligase* and *Deep vent polymerase* were purchased from Fermentas Molecular Biology (Thermo Scientific). QIAquick gel extraction kit (Qaigen, Cat. No. 28704) was used for DNA purification and extraction. QIAprep spin miniprep kit (Qaigen, Cat. No. 27106) was used for the mutant plasmid DNA isolation from the cell culture. HiTrap Heparin column, Q sepharose column and SP sepharose column were purchased from GE Healthcare. All buffer solutions for protein purifications were filtered passing 0.45  $\mu$ m membrane before use. 1 mM MnCl<sub>2</sub> was added to the expression media and all purification buffers.

### 2.2.2 Expression and purification of PP1 $\gamma$ wild type

Expression in *E. coli* DH5 $\alpha$  and purification was accomplished by a slight modification of the previously described method.<sup>8</sup> Briefly, the plasmid pCWOri+ was used to transform competent *E. coli* DH5 $\alpha$  cells. Single colonies from *E. coli* DH5 $\alpha$  cells were taken from cells plated on LB/ampicillin plates and used to inoculate 20 mL cultures in LB/ampicillin media which were grown overnight at 37°C. These were then used to inoculate 2 liter cultures (LB/ampicillin media containing 1 mM MnCl<sub>2</sub>) and grown at 37°C until the absorbance at 600 nm reached a value of about 0.6. IPTG was then added to a final concentration of 1.0 mM, and the culture was grown at room

temperature for about 22 h. The cells were harvested by centrifugation at 8,000 RPM for 30 min. Typical yields of cell pellet were in the range 8-10 gram per liter culture.

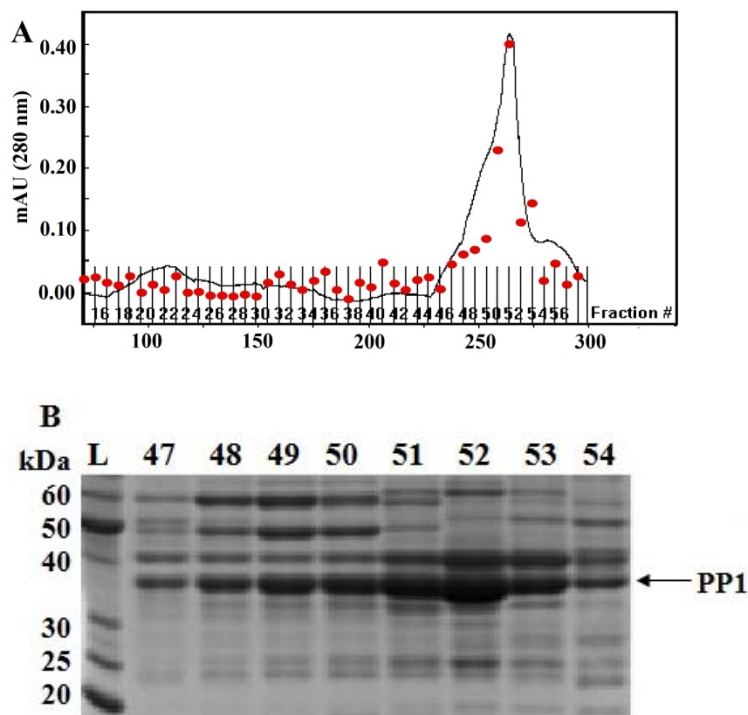


**Figure 2-2.** (A) Chromatogram of the purification of PP1 $\gamma$  on HiTrap Heparin column at 280 nm. The phosphatase activities (●) of each fraction were determined with pNPP at pH 7.0. (B) SDS-PAGE of fractions 47-54 from HiTrap Heparin column. L: Ladder. Lanes 47-54 correspond to the indicated fractions in the chromatogram. These fractions were combined and purified further.

The next steps were carried out at 4 °C. The resulting pellet (10 g) was resuspended in 25 mL of buffer A (0.1 mM EGTA, 25 mM triethanol amine, 1 mM MnCl<sub>2</sub>, 0.1% v/v 2-mercaptoethanol, 5% v/v glycerol, 3% by mass Brij 35, pH 7.5) containing protease inhibitors (2 mM benzamidine and 2  $\mu$ g/mL each of aprotinin, pepstatin, and leupeptin). The cells were lysed by sonication and spun down at 45 000

rpm for 30 min. The supernatant was filtered through a 0.45  $\mu\text{M}$  PES filter to remove residual debris followed by a three-step chromatographic purification consisting of a HiTrap Heparin column, HiTrap Q sepharose column, and HiTrap SP sepharose column. The supernatant was loaded on each column at 1.5 mL/min. The column was washed with buffer A until the absorbance at 280 nm was zero. The protein was eluted at 1.5 mL/min with a 300 mL linear gradient from zero to 0.5 M NaCl in buffer A. After each column, aliquots of each fraction were taken to assess the progress of the purification by SDS-PAGE and pNPP activity (**Figure 2-2, 2-3, 2-4**). Enzyme-containing fractions were concentrated and stored at  $-80^{\circ}\text{C}$ . Protein concentrations were monitored by NanoDrop 2000 micro-volume spectrophotometer (Thermo Scientific). The extinction coefficient ( $\epsilon_{280\text{nm}} = 0.88 \text{ mg/mL}^{-1} \text{ cm}^{-1}$ ) was estimated by the literature method.<sup>9</sup> Typical yield of purified PP1 $\gamma$  was 15 mg per liter of culture.

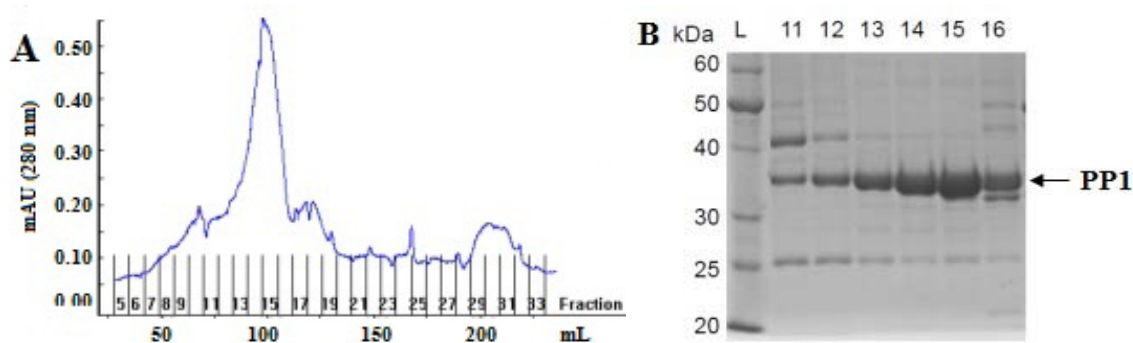


**Figure 2-3.** (A) Chromatogram of the purification of PP1 $\gamma$  on HiTrap Q sepharose column at 280 nm. (B) SDS-PAGE of fractions 11-16 from Q sepharose column. L: Ladder. Lanes 11-16 correspond to the indicated fractions in the chromatogram. These fractions were combined and purified further.

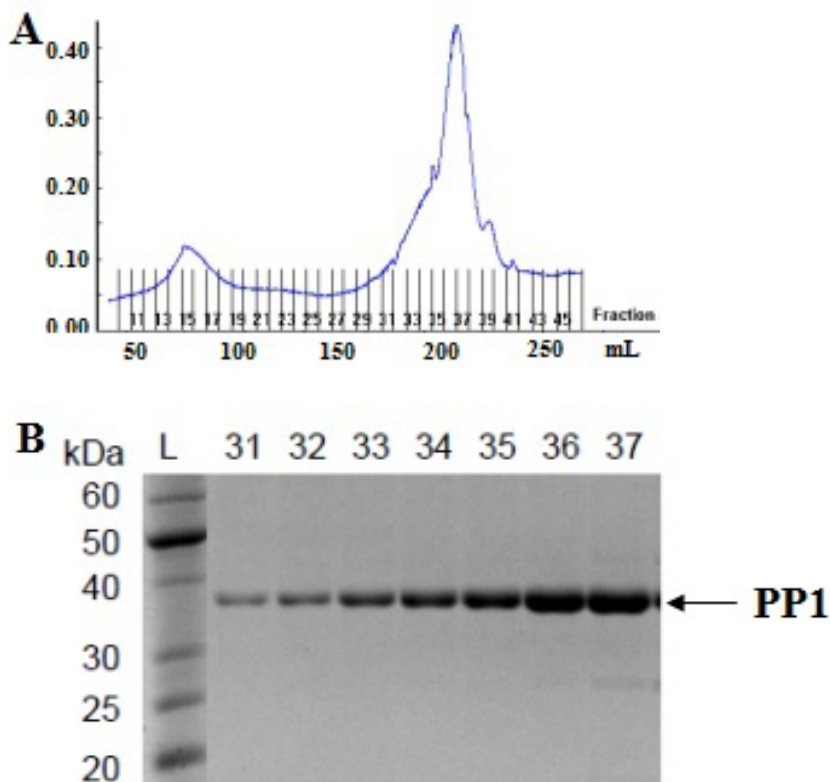


**Figure 2-4.** (A) Chromatogram of the purification of PP1 $\gamma$  on HiTrap SP sepharose column at 280 nm. (B) SDS-PAGE of fractions 31-37 from SP sepharose column. L: Ladder. Lanes 31-37 correspond to the indicated fractions in the chromatogram. These fractions were combined and concentrated, then stored at  $-80^{\circ}\text{C}$  freezer.

### 2.2.3 Generation of mutant proteins

PP1 $\gamma$  mutant proteins were generated using a two-step extension overlap PCR method<sup>10</sup> with sets of complementary oligonucleotide primers spanning the desired site of mutation (**Table 2-2**). For each PCR, the human wild type PP1 $\gamma$  plasmid was used as a template.

The first PCR amplification using the PP1F primer and 3' mutant primer created the DNA fragment running from the beginning of the PP1 $\gamma$  cDNA to the mutated sequence of interest. For example, the solution for the first PCR amplification of R96K

mutant contains 0.2  $\mu\text{M}$  PP1F, 0.2  $\mu\text{M}$  R96K 3'→5', 3 ng/ $\mu\text{L}$  PP1 $\gamma$  template, 1  $\mu\text{L}$  dNTP, 5  $\mu\text{L}$  buffer, 34  $\mu\text{L}$  DD water (double distilled water) and 1 unit of *deep vent polymerase*. The PCR conditions used were 95°C for 1 min for 1 cycle, then 95°C for 30 seconds, 50°C for 30 seconds, 72°C for 1 min for 30 cycles, followed by 72°C for 3 min for 1 cycle. This procedure was also performed with the PP1R primer and 5' mutant primer to give the other section running from the beginning of the mutated sequence to the end of PP1 $\gamma$  cDNA. For example, the solution contains 0.2  $\mu\text{M}$  PP1R, 0.2  $\mu\text{M}$  R96K 5'→3', 3 ng/ $\mu\text{L}$  PP1 $\gamma$  template, 1  $\mu\text{L}$  dNTP, 5  $\mu\text{L}$  buffer, 34  $\mu\text{L}$  DD water and 1 unit of *deep vent polymerase*. The PCR products were purified on a 1% agarose gel (**Figure 2-5 A**) and then extracted with QIAquick gel extraction kit.

**Table 2-2.** Primers used for each specific mutation. The underline bases indicate the changes in sequence from the wild type PP1 $\gamma$ . Bases shown in bold and italic indicate the restriction sites *NdeI* (PP1F) and *HindIII* (PP1R).

Primer	Sequence 5'→3'
PP1F	5'-GGAGGTCATATGGCGGATTTAG-3'
PP1R	5'-CATCGATAAGCTTGCATGCCTGCAGCTCGAC-3'
R96K	5'-GGGGACTATGTGGAC <b><i>AAG</i></b> GGGAAAGCAG-3'
R221K	5'-GGCTGGGGTGAAAATGAC <b><i>AAAG</i></b> GGAGTG-3'

The resulting PCR products were then applied to the second PCR amplification with the PP1F primer and PP1R primer to anneal two short mutated sections and give the full length mutated PP1 $\gamma$  cDNA. For example, the solution contains 0.2  $\mu\text{M}$  PP1F, 0.2  $\mu\text{M}$  PP1R, 2 ng/ $\mu\text{L}$  two PCR products of R96K from first step, 1  $\mu\text{L}$  dNTP, 5  $\mu\text{L}$  buffer, 27  $\mu\text{L}$  DD water and 1 unit of *deep vent polymerase*. The PCR conditions for the second

round amplification was for the first 5 cycles, 95°C for 30 seconds; 45°C for 40 seconds; 72°C for 90 seconds; and in the remaining 35 cycles, 95°C for 30 seconds, 58°C for 30 seconds, 72°C for 1 min. The PCR product was purified on a 1% agarose gel (**Figure 2-5 B**) and extracted using QIAquick gel extraction kit.

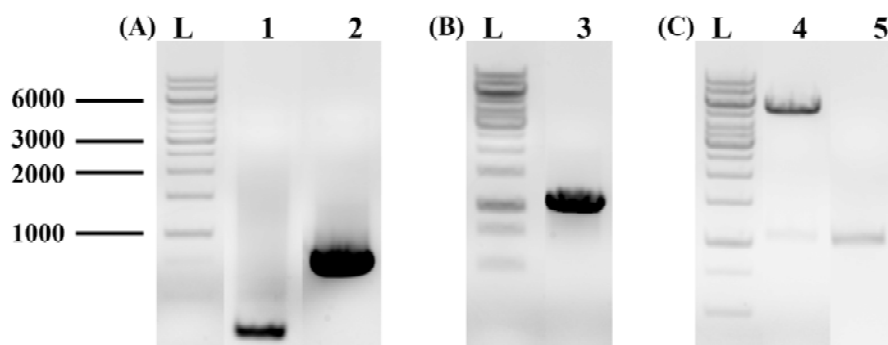


**Figure 2-5.** Analytical 1% agarose gel stained with ethidium bromide showing the overlap extension PCR of wild type PP1 $\gamma$  to produce the R96K mutant. (A) L: Ladder; Lane 1: first step PCR product obtained by using primers PP1F and R96K 3'→5'; Lane 2: first step PCR product obtained by using the primers PP1R and R96K 5'→3'. (B) L: Ladder; Lane 3: second step PCR product (full length R96K). (C) L: Ladder; Lane 4: PP1 $\gamma$  cDNA fragment after restriction digestion; Lane 5: R96K DNA fragment after restriction digestion.

The resulting full length mutated DNA and the PP1 $\gamma$  plasmid were both subjected to digestion with *NdeI* and *HindIII*. 1  $\mu$ g of vector (PP1 $\gamma$  plasmid) and 0.26  $\mu$ g of insert (full length mutated DNA, R96K) were placed into separate tube. To each tube, 1.5 units of *NdeI*, 1.5 units of *HindIII*, and 2  $\mu$ L buffer were added. The total volume was made up to 20  $\mu$ L with DD water. The tubes were incubated at 37°C for 1 h. 1  $\mu$ L shrimp alkaline phosphatase (SAP) was only added to vector sample tube. Both sample tubes were

incubated at 37 °C for another 30 min. The SAP was inactivated by incubation at 65 °C for 15 min. The resulted DNA samples were purified on an agarose gel (**Figure 2-5 C**) and applied to ligation.

The restriction digested vector and insert were ligated together by T4 DNA ligase. The quantity of vector was kept constant at 81 ng. Reactions were carried out at three different ratios of vector to insert from 1:2 until 1:5. Each reaction contained 1 µL 10 x T4 DNA ligase reaction buffer and 1 unit of T4 DNA ligase. The total volume was made up to 20 µL with pure water. The ligation reactions were incubated at room temperature for 10 mins.

Ten microliters of ligation mixture was used to transform competent DH5α cells. The mutant plasmid DNA was isolated from the culture using Qiagen Miniprep DNA purification kit. Desired mutations (R96K, R221K, R96KR221K double) were confirmed through DNA sequencing (**Appendix A44-A46**). Mutant proteins were expressed and purified using the same methods used to express and purify wild type PP1γ. Purified proteins were 95% pure estimated by SDS-PAGE.

#### **2.2.4 Generation of different metal forms of PP1γ**

Expression and purification of different metal forms of PP1γ were accomplished by the same method as PP1γ wild type (Mn<sup>2+</sup> form) except using other metal ions instead of MnCl<sub>2</sub> in the growth media and purification buffer. Protein concentrations were monitored by NanoDrop 2000 micro-volume spectrophotometer using the same extinction coefficient ( $\epsilon_{280\text{nm}} = 0.88 \text{ mg/mL}^{-1} \text{ cm}^{-1}$ ) as wild type. Typical yield of purified different metal forms of PP1γ was about 3-fold lower than wild type.

## 2.3 Kinetic measurements

### 2.3.1 UV-vis spectroscopy analysis of PP1 $\gamma$ -catalyzed hydrolysis of substrate classes

For the hydrolysis reactions producing the product 4-nitrophenol, reactions were followed by measuring the absorbance of the 4-nitrophenolate at 400 nm in a Spectramax plate reader at 25 °C. All of the reactions were performed in buffered solutions (50 mM Tris, 50 mM Bis-Tris, 100 mM NaOAc, 0.05 mM MnCl<sub>2</sub>). Enzymatic reactions were initiated with adding PP1 $\gamma$  at a concentration that varied between 25 and 250 nM depending upon the substrate classes. Enzymatic reactions were quenched by adding 1.5 M sodium carbonate bringing the final pH to  $\geq 10$ . The literature value of the extinction coefficient for the 4-nitrophenolate anion of 18300 cm<sup>-1</sup> M<sup>-1</sup> was used.<sup>11</sup> Initial rates (less than 5% of the reaction) were determined at a range of substrate concentrations and calculated from the absorbance change. The resulting initial rates and substrate concentrations were used to construct Michaelis-Menten plots (**Equation 2-1**). Values for  $V_{\max}$  and  $K_M$  were obtained by fitting the data to the Michaelis-Menten equation using a nonlinear least-squares fit (Kaleidagraph, Synergy Software). Values of  $k_{\text{cat}}$  were obtained by dividing  $V_{\max}$  by the corresponding enzyme concentration.

$$\frac{v}{[E_o]} = \frac{k_{\text{cat}}[S]}{K_M + [S]} \quad \text{Equation 2-1}$$

### 2.3.2 Reverse phase-HPLC analysis of PP1 $\gamma$ -catalyzed hydrolysis of substrate classes

For the reactions involving formation of other than 4-nitrophenols, reactions were monitored by the appearance of the product phenol using reverse phase HPLC. Substituent phenol (5 ~ 300  $\mu\text{M}$ ) was mixed well with buffered solution (50 mM Tris, 50

mM Bis-Tris, 100 mM NaOAc, 0.05 mM MnCl<sub>2</sub>, pH 7.0) and equilibrated at 25 °C for 10 min. Each vial was titrated to pH 4 with 1 M HCl before the injection. The calibration curve for each substituent phenol at certain wavelength was built by plotting concentrations vs. peak area. Each calibration curve contained at least ten points. The pK<sub>a</sub> for each substituted phenol was obtained from literature data<sup>1</sup> (**Table 2-3**).

**Table 2-3.** Conditions for HPLC used for product analysis of enzymatic assay and substrates for the PP1 $\gamma$ -catalyzed hydrolysis reaction with their leaving group pK<sub>a</sub> values.

Leaving group	Mobile phase (Methanol:Water)	Detection wavelength (nm)	Retention time (min)	pK <sub>a</sub>
3-NO <sub>2</sub> phenol	40:60	220	8.5	8.35
3-CN phenol	30:70	210	5.3	8.61
3-Cl phenol	50:50	220	9.1	9.02
4-Cl phenol	40:60	220	9.0	9.38
phenol	30:70	210	8.7	9.95

Hydrolysis of phosphorothioate and fluorophosphate substrates by PP1 $\gamma$  were carried out at 25°C in the same buffer as mentioned above. The substrate concentrations were varied from 0.1-10 mM. Enzymatic assays containing substrates and buffer were equilibrated at 25 °C for 5 min. Reactions were initiated with adding PP1 $\gamma$  at a concentration that varied between 25 and 250 nM depended upon the leaving group. Reactions were terminated with adding 1 M HCl to bring the pH down to 4. The reaction solution was filtered through a 0.45  $\mu$ m membrane filter before the injection. Hydrolyzed substituent phenols from wild type PP1 $\gamma$ -catalyzed reactions were separated with an Eclipse XDB-C18 column, 4.6  $\times$  150 mm, 5  $\mu$ m (Agilent). The mobile phase consisted of

water and methanol. The isocratic elute conditions, detection wavelength and retention times are shown in **Table 2-3**. The composition of the mobile phase and detection wavelength were altered for each phenol to reach the optimum separation and retention time. The relative concentrations of phenol product from enzymatic assay at this wavelength were then determined by peak area corresponding to the calibration curve.

### **2.3.3 Test for sulfatase activity**

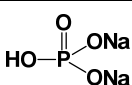
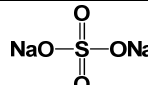
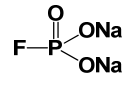
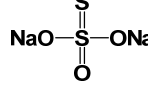
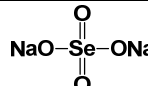
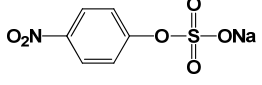
Both control and enzymatic reactions were followed by measuring the absorbance of the 4-nitrophenolate product at 400 nm at 25 °C. Buffered solutions (50 mM Tris, 50 mM Bis-Tris, 100 mM NaOAc, 0.05 mM MnCl<sub>2</sub>, 3 mM DTT, pH 7.0) were used. The concentrations of *para*-nitrophenyl sulfate potassium salt and PP1 $\gamma$  were 9.3 mM and 134.6  $\mu$ M, respectively. The control reaction was set up identically but without PP1 $\gamma$ . After 15 h, the changes in absorbance at 400 nm for both reactions were less than 0.003 absorbance units. The test for the PP1 $\gamma$  R96K and R221K mutants led to the same observation and the conclusion that *para*-nitrophenyl sulfate is not a substrate for PP1 $\gamma$  wild type or these mutants.

### **2.3.4 Inhibition measurement**

The rate of PP1 $\gamma$ -catalyzed pNPP hydrolysis in the presence of varying amounts of the inhibitors (**Table 2-4**) was determined by measuring the formation of the 4-nitrophenolate product at 400 nm as described above. Inhibitor concentrations used were in the range 3-fold to 1/5-fold of the  $K_i$ . The initial rates and pNPP concentrations were fitted to Lineweaver–Burk plots to determine the type of inhibition. A replot of the slope

of each reciprocal plot versus the corresponding inhibitor concentration ( $[I]$ ) at which it was obtained will give the inhibition constant ( $K_i$ ).

**Table 2-4.** Various inhibitors used in the PP1 $\gamma$ -catalyzed hydrolysis of **1a** (pNPP) at pH 7.0.

Inhibitor	Geometry	Inhibitor	Geometry
	Tetrahedral		Tetrahedral
	Tetrahedral		Tetrahedral
$\text{NH}_4\text{PF}_6$	Octahedral		Tetrahedral
$\text{NaBF}_4$	Tetrahedral		
$\text{MgF}_x$ <sup>[a]</sup>	Planar		Tetrahedral
$\text{AlF}_x$ <sup>[b]</sup>	Planar		

[a] Magnesium fluoride complexes can adopt either trigonal bipyramidal or octahedral geometry in active sites of proteins.<sup>12,13</sup> In trigonal bipyramidal geometry, three fluoride atoms coordinate to the magnesium ( $\text{MgF}_3$ ,  $x=3$ ) and adopt planar geometry during the transition state.<sup>12</sup> In octahedral geometry, four fluoride atoms coordinate to the magnesium ( $\text{MgF}_4$ ,  $x=4$ ). The phosphorus atom still shares a plane with four fluoride atoms [b] Aluminofluorides can adopt tetrahedral, trigonal bipyramidal, and octahedral geometries in a protein active site depending upon the number of fluoride atoms coordinating to the aluminum.<sup>14,15</sup>

All inhibitors were commercial products and were used as received except magnesium and aluminum fluorides ( $\text{AlF}_x$  and  $\text{MgF}_x$ ). The inhibition experiments for magnesium and aluminum fluorides ( $\text{AlF}_x$  and  $\text{MgF}_x$ ) contained aluminum or

magnesium chloride and from 2- to 6-fold excess sodium fluoride assuming that the concentration of inhibitory species equaled the concentration of Mg or Al. Since not all of the metal will be in the correct inhibitory complex state with fluoride, these fits give an underestimation of the inhibition constants of the putative  $\text{MF}_3$  species.

## 2.4 Isotope effect measurements

The  $^{18}\text{O}$  kinetic isotope effects were measured by the remote label method, using the nitrogen atom in the nitro group as a reporter for isotopic fractionation in the labeled oxygen positions. **Figure 2-6** shows the mixtures of isotopically labeled compounds needed for these experiments. The experimental procedures used to measure these isotope effects were similar to those used to measure KIEs in phosphoryl transfer reactions in which the leaving group is 4-nitrophenol.<sup>16</sup> The details of the data for the hydrolysis reactions of the pNPPT monoester dianions are given in the **Appendix A47**.

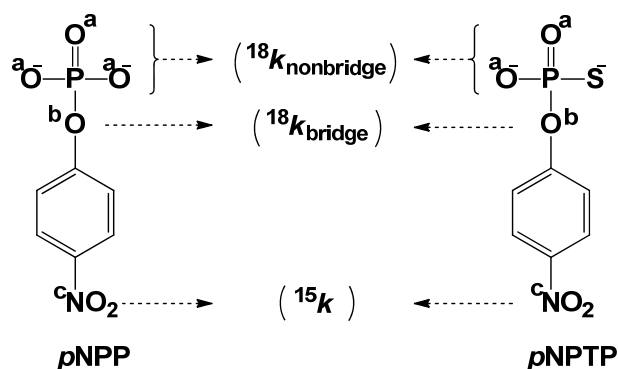


**Figure 2-6.** Substrates pNPP and pNPPT with the positions indicated at which isotope effects were measured. pNPPT has two, and pNPP has three non-bridging oxygen atoms (marked a). The scissile (leaving group) oxygen atoms are indicated by b, and the nitrogen atoms for  $^{15}\text{N}$  KIEs are marked c.

## 2.5 Summary

In summary, a total of eighteen substrates belonging to six different substrate classes were successfully synthesized and characterized by NMR. Two substrates (**3b** and **3c**) were newly reported compounds. PP1 $\gamma$  wild type was successfully expressed and purified as a soluble protein with full catalytic activity. Three new mutants of two arginine residues in the active site of PP1 $\gamma$  have been generated, expressed in *E. coli* DH5 $\alpha$  cells and purified as soluble protein. PP1 $\gamma$  activation by magnesium divalent cation was expressed and purified. Proper buffer solutions for running enzymatic reactions were developed. UV-vis spectroscopy and reverse phase-HPLC were applied to obtain the kinetic parameters of PP1 $\gamma$ -catalyzed hydrolysis of different substrate classes, and the inhibition constant of various inhibitors. Kinetic isotope effects of PP1 $\gamma$ -catalyzed hydrolysis of substrate **3a** were measured by the remote label method, using the nitrogen atom in the nitro group as a reporter for isotopic fractionation in the labeled oxygen positions.

## 2.6 References

- (1) Fasman, G. D. *Handbook of Biochemistry and Molecular Biology*; Wiley, 1975.
- (2) Catrina, I. E.; Hengge, A. C. *J. Am. Chem. Soc.* **1999**, *121*, 2156-2163.
- (3) Bourne, N.; Williams, A. *J. Org. Chem.* **1984**, *49*, 1200-1204.
- (4) Hartke, K.; Bartulín, Q. F. *J. Angewandte Chemie* **1962**, *74*, 214-216.
- (5) Wittmann, R. *Chemische Berichte* **1963**, *96*, 771-780.
- (6) McWhirter, C.; Lund, E. A.; Tanifum, E. A.; Feng, G.; Sheikh, Q. I.; Hengge, A. C.; Williams, N. H. *J. Am. Chem. Soc.* **2008**, *130*, 13673-13682.
- (7) Zalatan, J. G.; Herschlag, D. *J. Am. Chem. Soc.* **2006**, *128*, 1293-1303.

- (8) Zhang, A. J.; Bai, G.; Deans-Zirattu, S.; Browner, M. F.; Lee, E. Y. *J. Biol. Chem.* **1992**, *267*, 1484-1490.
- (9) Gill, S. C.; von Hippel, P. H. *Anal. Biochem.* **1989**, *182*, 319-326.
- (10) Zhang, Z.; Zhao, S.; Long, F.; Zhang, L.; Bai, G.; Shima, H.; Nagao, M.; Lee, E. *Y. J. Biol. Chem.* **1994**, *269*, 16997-17000.
- (11) Kirby, A. J.; Varvoglis, A. G. *J. Am. Chem. Soc.* **1967**, *89*, 415-423.
- (12) Toyoshima, C.; Nomura, H.; Tsuda, T. *Nature* **2004**, *432*, 361-368.
- (13) Baxter, N. J.; Olguin, L. F.; Golicnik, M.; Feng, G.; Hounslow, A. M.; Bermel, W.; Blackburn, G. M.; Hollfelder, F.; Waltho, J. P.; Williams, N. H. *Proc Natl Acad Sci U S A* **2006**, *103*, 14732-14737.
- (14) Li, L. *Crit. Rev. Oral Biol. Med.* **2003**, *14*, 100-114.
- (15) Schlichting, I.; Reinstein, J. *Nat. Struct. Biol.* **1999**, *6*, 721-723.
- (16) Hengge, A. C. *Acc. Chem. Res.* **2002**, *35*, 105-112.

## CHAPTER 3

### PP1 $\gamma$ EXHIBITS CATALYTIC PROMISCUITY AND HIGH CATALYTIC EFFICIENCY TOWARDS FIVE SUBSTRATE CLASSES

#### 3.1 Introduction

Phosphate monoester dianions and phosphodiester with aryl leaving groups are two substrates that normally react by different transition states in phosphoryl transfer reactions. The reactions of phosphate monoester dianions are concerted, with loose transition states.<sup>1-3</sup> Phosphodiester with aryl leaving groups have been shown by linear free energy relationships<sup>4,5</sup> (LFER) and kinetic isotope effects<sup>6,7</sup> (KIE) to also react by a concerted pathway, although the transition state is tighter (see **Chapter 1.2.3**). Aryl methylphosphonates, which are diester analogues, have been proved to undergo hydroxide-promoted hydrolysis by a mechanism and transition state similar to that of phosphate diesters though with slightly greater P–O bond fission.<sup>8</sup>

It has been discovered that the catalytic subunit of PP1 exhibits catalytic promiscuity towards phosphate monoesters and aryl methylphosphonates.<sup>8</sup> The reactions catalyzed by PP1 $\gamma$  have been examined by linear free energy relationships and kinetic isotope effects. The PP1 $\gamma$ -catalyzed hydrolysis of a series of aryl phosphate monoester substrates yields a Brønsted  $\beta_{lg}$  of  $-0.32$ , considerably less negative than that of the uncatalyzed hydrolysis of phosphate monoester dianions ( $-1.23$ ).<sup>9</sup> The reduction in magnitude of the Brønsted  $\beta_{lg}$  most likely reflects partial charge neutralization in the transition state by a general acid. For the monoester substrate pNPP, the transition states implied by the KIEs in the enzymatic and the uncatalyzed reactions are similar, with both characterized by a loose transition state with partial neutralization of the leaving group.

The PP1 $\gamma$ -catalyzed hydrolysis of a series of aryl methylphosphonate substrates yields a Brønsted  $\beta_{lg}$  of  $-0.30$ , which is smaller than the alkaline hydrolysis ( $-0.76$ ),<sup>10</sup> but similar to the  $\beta_{lg}$  measured for monoester substrates. A reduced  $\beta_{lg}$  most likely reflects general acid catalysis, as in the monoester reaction. The PP1 $\gamma$ -catalyzed hydrolysis of para-nitrophenyl phosphonate monoester (pNPMP) shows modest differences in the KIEs that indicate a larger extent of bond fission, closer to that of the monoester reaction. These data imply that the transition states of the PP1 $\gamma$ -catalyzed reactions of the two substrates are much more similar to one another than are the transition states of the respective uncatalyzed reactions. The modest inverse nonbridge KIEs on the PP1 $\gamma$ -catalyzed hydrolysis of both substrates most likely result from binding interactions with the metal center. This interpretation suggests that catalysis of pNPMP hydrolysis in the active site of PP1 $\gamma$  is achieved by a transition-state structure different from the one in solution, but with minimal energetic penalty as the catalytic proficiency for hydrolyzing both processes is rather similar.

Beside these remarkable results, very few kinetic studies have been performed on the catalytic promiscuity of PP1 $\gamma$ . This chapter focuses on the characterisation of the kinetic activity of the catalytic subunit of PP1 $\gamma$  towards five substrate classes, including dianions (phosphate monoester and phosphorothioate monoester) and monoanions (fluorophosphate, aryl methylphosphonate and phosphate diester). The specific aim of this chapter is to answer these fundamental questions:

- 1). To what degree, and with what result, do differences in the electronic and geometric nature of the transferring group affect catalysis?

2). What is the nature of the transition state for different substrates in enzymatic reactions?

How does catalysis affect the nature of transition states? Is distortion in transition state structure an element of catalysis in these systems?

3). What is the major factor that might affect catalytic promiscuity, and how might it assist in the evolution of new catalytic abilities from one group transfer to another?

## 3.2 Results and discussion

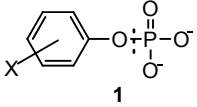
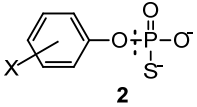
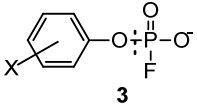
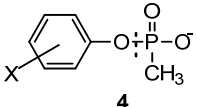
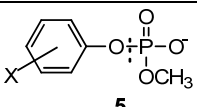
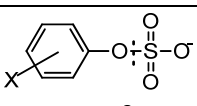
### 3.2.1 Design principles of substrate classes

To assess questions about promiscuity, specificity and catalytic mechanism of PP1 $\gamma$ -catalyzed reactions requires a systematic evaluation of the energy contributions to the transition state stabilization in the given active site by different substrates. In this work, a set of functional group modifications were made in the transferring group of the hydrolysis reactions. In addition to charge, the substrates vary in their reactivity, the center atom and the size of the transferring group, and in their mechanism and transition states for uncatalyzed hydrolysis.

The substrate classes may be grouped into two types by their charge in the pH range that was examined, the dianionic **1** and **2**, and the monoanionic **3-6** (**Table 3-1**). These esters also differ in the size of the group undergoing transfer from the ester group to water, and also have pronounced differences in the mechanism and transition state of their uncatalyzed hydrolysis reactions. Bacterially expressed PP1 can efficiently dephosphorylate small organic molecules such as phosphate monoester **1a**.<sup>11</sup> A sulfur substitution (**2**) for a non-bridging oxygen atom maintains charge, but perturbs the transferring group size and charge distribution. Experimental<sup>12</sup> and theoretical<sup>13</sup> evidence

regarding the charge distribution and bonding in phosphorothioates indicates that the sulfur atom holds greater negative charge and less double bond character than each of the two non-bridging oxygens. Phosphorothioates (**2**) typically react via an  $S_N1$  ( $D_N+A_N$ ) mechanism in which a (thio)metaphosphate intermediate is formed in the rate-determining step.<sup>14-16</sup> This highly reactive species is then attacked by a nucleophile in a subsequent rapid step.<sup>16-18</sup>

**Table 3-1.** Structures and molecular properties of the examined substrate classes. Dashed lines indicate the bonds that are broken during hydrolysis.

Substrate	Substrate charge	Reaction center	Electro-negativity of atoms in transferring group <sup>19,20</sup>	Uncatalyzed hydrolysis	
				Mechanism	Transition state
 <b>1</b>	-2	P	O 3.44	concerted	loose
 <b>2</b>	-2	P	O 3.44 S 2.58	$S_N1$	loose
 <b>3</b>	-1	P	O 3.44 F 3.98	concerted	tight
 <b>4</b>	-1	P	O 3.44 Me 2.27	concerted	tight
 <b>5</b>	-1	P	O 3.44 MeO 2.68	concerted	tight
 <b>6</b>	-1	S	O 3.44	concerted	loose

A fluorine substitution (**3**) will eliminate a negative charge compared to the phosphate monoesters. The intention of this design is to change the nature of the

transition state, while retaining the size and hydrogen bond donor/acceptor properties of the monoester. A methyl substitution (**4**) and a methoxyl substitution (**5**) on a non-bridging oxygen atom eliminates a negative charge at neutral pH, minimizes the steric changes incurred, and also makes the charge on the bridging oxygen atom more electropositive than that in a phosphate monoester. This effect arises because of the increased electrophilicity of the phosphorus atom that in turn increases the P-O bridging bond order. The reaction mechanism of substrates **3-5** are concerted, with tighter transition state.<sup>8,21-23</sup> Sulfate (**6**) and phosphate monoesters (**1**) share tetrahedral geometry with comparable bond angles and lengths, yet the amount and distribution of charge is different. The uncatalyzed hydrolysis of sulfate and phosphate monoesters occurs with similar rate constants and proceeds through loose transition states.<sup>24</sup> This similarity between phosphoryl and sulfuryl transfer reactions is also reflected in the ability of a few enzymes like *E. coli* AP that have evolved to catalyze one activity to also carry out the other.<sup>25</sup> Of interest is whether the transition states of the PP1-catalyzed reactions retain these differences.

### **3.2.2 Determination of optimal conditions for kinetic studies**

The three-component buffer system of Bis-Tris ( $pK_a$  6.50 at 25 °C), Tris ( $pK_a$  8.06 at 25 °C) and sodium acetate ( $pK_a$  4.76 at 25 °C) was chosen because the buffer is non-inhibitory towards PP1 $\gamma$ , is weakly metal-coordinating, and maintains ionic strength without the need for added salts as the pH is varied. Meanwhile, the buffer range spans the pH range in which PP1 $\gamma$  is active. The buffer concentration used for kinetic measurements was 50 mM Tris, 50 mM Bis-Tris, and 100 mM NaOAc.

It has been reported that among three isoforms of mammalian PP1 (PP1 $\alpha$ , PP1 $\beta$  and PP1 $\gamma$ ) expressed in *E. coli*, PP1 $\alpha$  and PP1 $\beta$  were completely dependent on external Mn<sup>2+</sup> for catalytic activity, while only PP1 $\gamma$  maintained activity in the buffer without added Mn<sup>2+</sup> (like PP1C which is the native PP1 catalytic subunit isolated from vertebrate tissues).<sup>11</sup> For this reason the dependence of recombinant PP1 $\gamma$  activity on the presence of Mn<sup>2+</sup> in buffer solution was quantitatively measured. **Table 3-2** shows the kinetic parameters of pNPP hydrolysis reactions in the absence and presence of increasing amounts of added MnCl<sub>2</sub>.

**Table 3-2.** Effect of external manganese on PP1 $\gamma$ -catalyzed hydrolysis. Kinetic parameters of pNPP hydrolysis by PP1 $\gamma$  were measured under 25°C at pH 7.0 in buffer solution (50 mM Tris, 50 mM Bis-Tris, and 100 mM NaOAc) with variable MgCl<sub>2</sub> concentration.

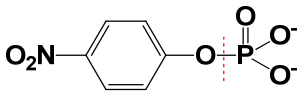
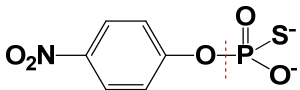
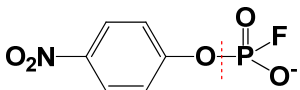
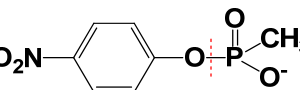
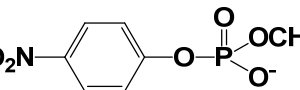
[MnCl <sub>2</sub> ] (mM)	$k_{\text{cat}}$ (s <sup>-1</sup> )	$K_M$ (mM)
0	2.9±0.1	3.4±0.2
0.05	3.4±0.1	3.6±0.2
0.10	3.3±0.1	3.4±0.1
0.20	2.9±0.1	3.4±0.1

In the presence of added Mn<sup>2+</sup>, the activity of PP1 $\gamma$  was not changed significantly. For instance, the addition of MnCl<sub>2</sub> provided a slight increase in rate at low concentration (<0.05 mM), then a slight decrease at high concentration (>0.05 mM). It has been noted previously<sup>26</sup> that very high concentrations of MnCl<sub>2</sub> (0.5 mM) were found to be inhibitory at pH 7.5. Therefore, a low concentration of Mn<sup>2+</sup> (0.05 mM) was used in all kinetic buffers for optimal PP1 $\gamma$  activity.

### 3.2.3 PP1 $\gamma$ exhibits catalytic promiscuity towards all of the substrate classes except substrate 6.

PP1 $\gamma$  performs multiple turnovers with each phosphate substrate examined, and saturation kinetics was observed for all substrates except *p*-nitrophenyl sulfate, **6**. (**Figure A48**) The initial data was fit to Michaelis-Menten equation (**Equation 3-1**) to get the kinetic parameters shown in **Table 3-3**.

**Table 3-3.** Kinetic parameters for the hydrolysis of substrates **1a-5a** at pH 7.0 by PP1 $\gamma$  wild type.

substrates	$k_{\text{cat}}$ (s <sup>-1</sup> )	$K_{\text{M}}$ (mM)	$k_{\text{cat}}/K_{\text{M}}$ , (M <sup>-1</sup> s <sup>-1</sup> )
 <b>1a (pNPP)</b>	3.2±0.1	3.6±0.3	869±3
 <b>2a (pNPPT)</b>	(2.9±0.1) ×10 <sup>-2</sup>	1.5±0.1	20±3
 <b>3a (pNPFP)</b>	0.8±0.1	9.2±0.4	83±7
 <b>4a. (pNPMP)</b>	1.1±0.2	13.0±1.4	86±8
 <b>5a (pNP diester)</b>	(1.6±0.1) ×10 <sup>-2</sup>	9.2±0.9	1.7±0.3

One important kinetic parameter is  $k_{\text{cat}}$ , which is also called the turnover number. It is equivalent to the number of substrate molecules converted to product in a given unit of time on a single enzyme molecule when the enzyme is saturated with substrate.<sup>27</sup> Another way of thinking of  $k_{\text{cat}}$  is as the first order rate constant for reaction of the enzyme-substrate complex (ES). The Michaelis constant  $K_M$  is another important parameter, which is described as the substrate concentration at which an enzyme-catalyzed reaction proceeds at one-half its maximum velocity. The parameters  $k_{\text{cat}}$  and  $K_M$  are useful in comparing catalytic efficiencies of different enzymes by taking the ratio  $k_{\text{cat}}/K_M$ . Basically, it is the rate constant for the conversion of free enzyme and free substrate to free enzyme and free product.

$$\frac{v}{[E_o]} = \frac{k_{\text{cat}}[S]}{K_M + [S]}$$

**Equation 3-1**

PP1 $\gamma$  is a less efficient catalyst for the hydrolysis of phosphorothioate esters **2** than for phosphate esters **1** with a reduction in turnover number of 2 orders of magnitude. A reduced catalytic effectiveness for phosphorothioates has also been reported in alkaline phosphatase<sup>14,28-30</sup> and in protein-tyrosine phosphatases.<sup>31-33</sup> This is opposite to the effect of sulfur substitution on the uncatalyzed reaction; phosphorothioate monoesters undergo hydrolysis faster than their phosphate ester counterparts. The reduced enzymatic rates have been attributed to reduction in transition state stabilization, resulting from poorer affinity of the transition state for the phosphorothioate substrate. Sulfur substitution has several consequences on charge distribution and geometry; compared to oxygens in the non-bridging positions, sulfur has greater negative charge and less double bond character<sup>12,13</sup> as well as a larger Van der Waals radius and longer bond length (1.94 Å

versus 1.57Å). The turnover number at pH 7.0 for the PP1 $\gamma$ -catalyzed hydrolysis of **3a** is only ~4-fold lower than **1a**; the higher  $K_M$  results in an overall catalytic efficiency that is about an order of magnitude lower than **1a**. The methyl substitution (**4a**) for a non-bridging oxygen atom maintains a similar bond length around the reaction center but removes hydrogen bond donor-acceptor properties and reduces the negative charge. The turnover number for the PP1 $\gamma$ -catalyzed hydrolysis of **4a** is only 3-fold lower than **1a** at pH 7.0, while the overall catalytic efficiency is about an order of magnitude lower. For the fluorophosphate and methylphosphonate substrates the  $k_{cat}$  and  $K_M$  values are similar. The methoxyl substitution (**5a**) on a nonbridging oxygen atom converts the substrate into a diester, which will have the largest steric requirement of all of the substrates tested. The turnover number is most strongly affected by this substitution, decreased by ~200-fold compared to **1a** and  $k_{cat}/K_M$  more than 400-fold reduced.

The values for  $K_M$  at pH 7.0 for the substrates **1a-5a** shown in **Table 3-3** indicate that the dianionic substrates **1a** and **2a** have the best affinity for the enzyme. The lower  $K_M$  of the phosphorothioate compared to the phosphate may reflect the preference of  $Mn^{2+}$  to coordinate sulfur ligands, an effect that has been previously noted.<sup>34,35</sup> The  $K_M$  values for monoanionic substrates **3a**, **4a** and **5a** are higher. This, and the similarity of  $K_M$  for **3a** and **5a**, indicates that loss of a negative charge has a larger effect on reducing binding than the addition of steric bulk by addition of a methyl or methoxy in place of a non-bridging oxygen atom.

The overall kinetic data obtained at pH 7 show that variations in the molecular properties of the substrates affect the turnover number ( $k_{cat}$ ) more than the Michaelis constant ( $K_M$ ).

### 3.2.4 The PP1 $\gamma$ -catalyzed hydrolysis of substrate classes 1-5 follows the same catalytic mechanism.

The pH dependencies of  $k_{\text{cat}}/K_{\text{M}}$  for substrates **2a**, **3a**, and **5a** were measured and showed a bell-shaped profile indicative of catalysis by both acidic and basic residues (**Figure 3-1**). For the pH range sampled the protonation states of the substrates do not change. The data were fitted to **Equation 3-2**, derived on the assumption that the active ionic form requires one acidic (defined by  $K_{\text{a}}^1$ ) and one basic residue (defined by  $K_{\text{a}}^2$ ). The derived  $\text{p}K_{\text{a}}$  values and values of  $(k_{\text{cat}}/K_{\text{M}})^{\text{lim}}$  obtained are shown in first three columns in **Table 3-4**. The previously reported pH profiles for substrates **1a** and **4a** are also shown in **Figure 3-1**.

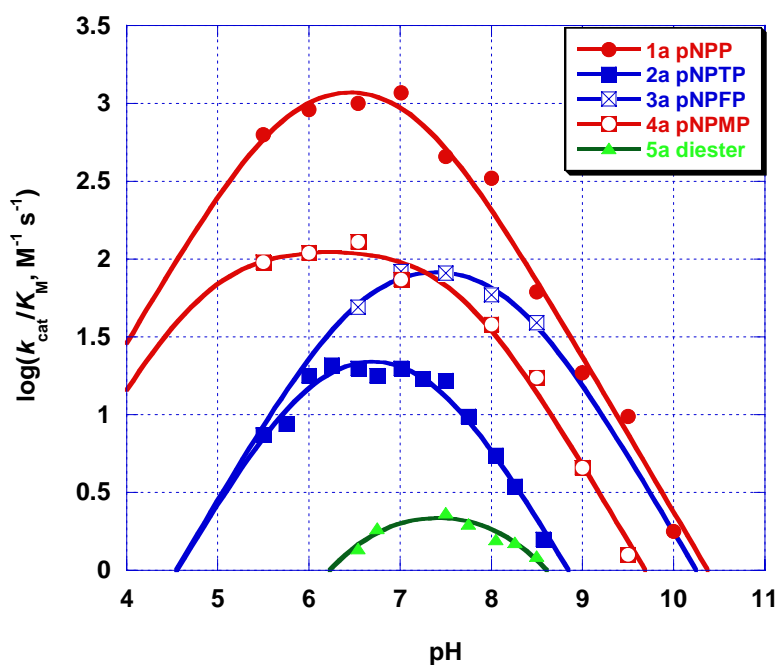


**Figure 3-1.** pH-rate profiles of  $k_{\text{cat}}/K_{\text{M}}$  for the hydrolysis of five different substrate classes catalyzed by PP1 $\gamma$ : **2a** (■), **3a** (⊠) and **5a** (▲) are from this work; **1a** (●) and **4a** (◻) have been previously reported.<sup>8</sup> Solid lines are fitted to **Equation 3-2**.

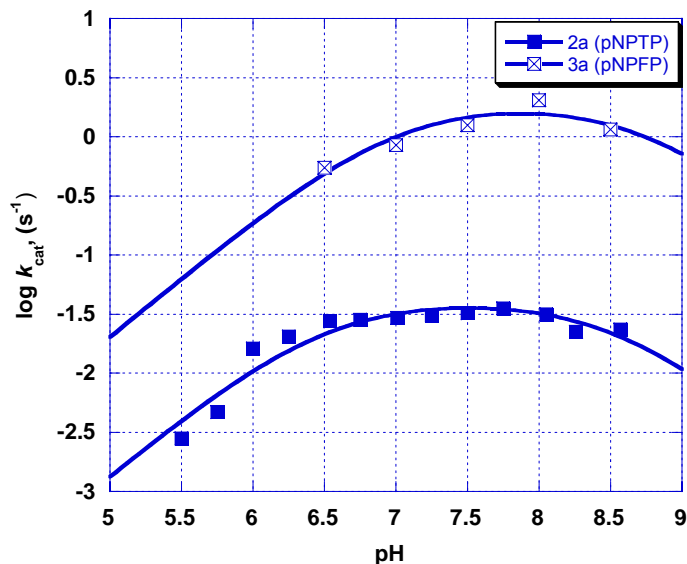


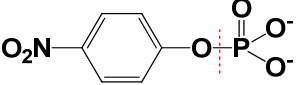
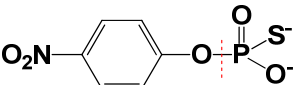
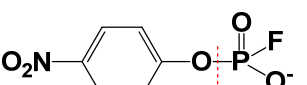
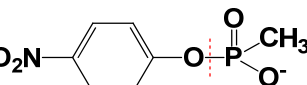
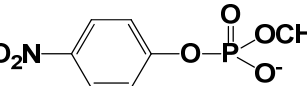
**Figure 3-2.** pH-rate profiles of  $k_{\text{cat}}$  for the hydrolysis of two different substrate classes catalyzed by PP1 $\gamma$ : **2a** (■) and **3a** (⊠). Solid lines are fitted to **Equation 3-2**.

$$\frac{k_{\text{cat}}}{K_{\text{M}}} = \left( \frac{k_{\text{cat}}}{K_{\text{M}}} \right)^{\text{lim}} \left( \frac{K_{\text{a}}^1 [\text{H}^+]}{K_{\text{a}}^1 K_{\text{a}}^2 + K_{\text{a}}^1 [\text{H}^+] + [\text{H}^+] [\text{H}^+]} \right) \quad \text{Equation 3-2}$$

The pH-rate profiles for the substrates (**1a–5a**) are bell-shaped and largely coincide; indicating the same active site and enzymatic mechanism is followed, with catalysis by both acidic and basic residues. Based on the crystal structure of PP1 and related Ser/Thr phosphatases, a metal-coordinated water molecule has been proposed to be the nucleophile and the deprotonation of this species is likely represented by  $\text{p}K_{\text{a}1}$ .<sup>36</sup> Although the values for  $\text{p}K_{\text{a}1}$  obtained from fits of  $\log k_{\text{cat}}/K_{\text{M}}$  for esters **2a** and **3a** differ slightly (6.0 and 6.5, respectively), plotting  $k_{\text{cat}}$  for these substrates yields identical values for  $\text{p}K_{\text{a}1}$  ( $\text{p}K_{\text{a}1} = 6.5 \pm 0.1$ ) of the ES complex. (**Figure 3-2**) These  $\text{p}K_{\text{a}}$  values are consistent with the assignment of the lower  $\text{p}K_{\text{a}}$  to a metal-bound water.<sup>37</sup> The fitted kinetic  $\text{p}K_{\text{a}1}$  value for substrate **5a** is about 1  $\text{p}K_{\text{a}}$  unit higher than the other substrate

classes. Since  $pK_{a1}$  is presumed to represent the nucleophilic metal-coordinated water, this perturbation may be due to alterations in the geometry or the solvation sphere of the nucleophile in the free enzyme, which is the most sterically demanding of the five substrate classes. The residue H125 is plausibly assigned to act as a general acid, responsible for the basic limb of the pH-rate profile.

**Table 3-4.** The kinetic  $pK_a$  values for PP1 $\gamma$ -catalyzed hydrolysis of substrates **1a-5a** at 25 °C derived from fits to **Equation 3-2**. Substrates **2a**, **3a** and **5a** are from this work. Data for substrates **1a** and **4a** have been previously reported.<sup>8</sup>

substrates	$pK_{a1}$	$pK_{a2}$	$k_{cat}/K_M^{lim}$ ( $M^{-1} s^{-1}$ )	$k_w$ ( $M^{-1} s^{-1}$ )	$(k_{cat}/K_M^{lim})/k_w$
 <b>1a</b> (pNPP)	6.0±0.2	7.2±0.2	1850±500	$2.3 \times 10^{-11}$	$8.0 \times 10^{13}$
 <b>2a</b> (pNPTP)	6.0±0.1	7.4±0.1	31±4	$1.8 \times 10^{-10}$	$1.7 \times 10^{11}$
 <b>3a</b> (pNPFP)	6.5±0.1	8.2±0.1	105±15	$\leq 2 \times 10^{-10}$	$\geq 5 \times 10^{11}$
 <b>4a</b> . (pNPMP)	6.0±0.2	7.2±0.2	240±30	$1.8 \times 10^{-11}$	$1.3 \times 10^{13}$
 <b>5a</b> (pNP diester)	7.2±0.2	7.5±0.2	0.98±0.39	$1.2 \times 10^{-13}$	$8.2 \times 10^{12}$

The values for  $k_{cat}/K_M^{lim}$  obtained from the pH profiles allow a comparison to be made of the catalytic efficiencies for each substrate. For PP1 $\gamma$ , catalytic efficiency

decreases in the order **1a**>**4a** ~ **3a**>**2a**>**5a**. The pH 7.0 specific data for substrates **1a-5a** show the same trends. The  $k_{\text{cat}}/K_{\text{M}}^{\text{lim}}$  values vary from a high of 1850  $\text{M}^{-1}\text{s}^{-1}$  for the phosphate monoester **1a** to a low of 0.98  $\text{M}^{-1}\text{s}^{-1}$  for the diester **5a**. However, the differences in  $k_{\text{cat}}/K_{\text{M}}^{\text{lim}}$  from the fastest to the slowest substrates are only ~2000-fold. Catalytic efficiencies for the monoanionic substrates **3a** and **4a** are superior to that for **2a**, although **2a** shares the dianionic charge of phosphate monoesters that are the natural substrates for PP1 $\gamma$ .

### **3.2.5 The PP1 $\gamma$ -catalyzed reactions exhibit remarkable rate accelerations compared with the corresponding uncatalyzed hydrolysis reactions.**

The fourth column ( $k_{\text{w}}$ ) of **Table 3-4** lists the second-order rate constants for the uncatalyzed reactions with water of substrates **1a-5a**. These were obtained from literature information as follows. For **1a**, the pseudo-first order rate constant of  $1.3 \times 10^{-9} \text{ s}^{-1}$  for the water reaction at 25 °C was calculated from the reported activation parameters<sup>38</sup> and divided by 55 M to obtain the second order rate constant. Similarly, for **2a**, the pseudo first order rate constant of  $9.8 \times 10^{-9} \text{ s}^{-1}$  at 25 °C was calculated from reported activation parameters<sup>15</sup> and divided by 55 M. The rate constant for the water reaction of fluorophosphate ester **3a** has been measured at 80 °C ( $4 \times 10^{-7} \text{ s}^{-1}$ ), but without activation parameters. However, this reaction can be compared with the second rate constants for reaction with hydroxide at this temperature ( $0.058 \text{ M}^{-1} \text{ s}^{-1}$ ), to give a ratio of  $7 \times 10^{-6}$ :1. If the enthalpy of activation is at least as large as for the specific base catalyzed reaction, then the ratio at 25 °C will be at least as small. As the second order rate constant for reaction with hydroxide has also been measured at 42 °C, it can be estimated as  $3 \times 10^{-5} \text{ M}^{-1} \text{ s}^{-1}$  at 25 °C. Data shown in **Table 3-4** is as an upper limit estimated from the above

describe. The second order rate constant shown for **4a** has been reported previously at 30 °C and 60 °C,<sup>39</sup> and the Eyring equation was used to predict the rate constant at 25 °C. For **5a**, an estimate of  $1.3 \times 10^{-11} \text{ s}^{-1}$  was obtained for the reaction of bis-4-nitrophenyl diester with water by using the reported temperature dependence of the spontaneous hydrolysis of the bis-2,4-dinitrophenyl diester and LFER data for symmetrical diaryl phosphate diesters at 100 °C. An Eyring plot for the bis-2,4-dinitrophenyl diester hydrolysis was constructed, and the assumption made that the bis-4-nitrophenyl diester will have the same intercept (effectively assuming that the entropy of activation is the same for the two compounds). The LFER data at 100 °C were used to generate a second point for this compound, and the two points used to estimate the rate of hydrolysis at 25 °C. This number is statistically corrected for the two leaving groups (the effect of the non-leaving group on phosphate diester hydrolysis is small, unlike the effect in phosphate triesters) and for the concentration of water to give the value in **Table 3-4**.

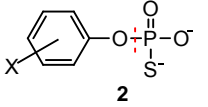
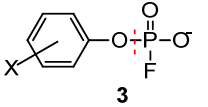
The second order rate constants for the reactions of **1a-5a** with water are all very low, reflecting the fact that these hydrolysis reactions have high kinetic barriers. The very low rates for the uncatalyzed reactions with water for these substrates also imply that PP1 $\gamma$  is an efficient catalyst for all of them. The ratio of the enzymatic catalytic efficiency ( $k_{\text{cat}}/K_{\text{M}}^{\text{lim}}$ ) to the second-order rate constant for the reaction with water ( $k_{\text{w}}$ ) gives the second-order rate enhancement (shown in the fifth column of **Table 3-4**), a measure of the degree to which PP1 $\gamma$  reduces the activation barrier for the hydrolysis reactions. These vary from  $1.7 \times 10^{11}$  to  $8.0 \times 10^{13}$  which are in the range of values observed for other catalytically promiscuous enzymes, such as *BcPMH*.<sup>40</sup> These values are all very high and vary over a narrow range of only  $\sim 2$  orders of magnitude, and correspond to reductions in

activation energy of from 16 to 19 kcal/mol. This demonstrates that PP1 $\gamma$  is an effective catalyst for all of these substrates, despite the variations in size and charge of the transferring group. For comparison, the promiscuous *BcPMH*, assigned as a member of the alkaline phosphatase superfamily, exhibits second-order rate accelerations ranging from  $10^7$  to as high as  $10^{19}$  for a range of phosphate monoester, diester, and triester substrates, as well as sulfate monoesters, corresponding to decreases in the energy of activation between 14.4 and 27.2 kcal/mol.<sup>40</sup> The larger and more variable rate accelerations of *BcPMH* suggest that its active site provides the potential for additional effects that synergize with the reactivity of the metal ion. The different active site of PP1 provides less, and similar, stabilization of catalysis toward different substrate classes.

### **3.2.6 LFER and KIE measurements indicate that the mechanism of PP1 $\gamma$ -catalyzed reactions and transition states are similar for all substrate classes.**

By using the series of aryl leaving groups in **Table 3-5**, a Brønsted plot ( $\beta_{lg}$ ) was obtained with catalytic efficiencies [ $\log(k_{cat}/K_M)$ ] of PP1 $\gamma$ -catalyzed hydrolysis reactions as a function of the  $pK_a$  of the conjugate acid the leaving group at pH 7.0 for phosphorothioate (**2**) and fluorophosphate (**3**) esters. The diester substrate (**5**) reacted too slowly to obtain LFER data. **Figure 3-3** shows the Brønsted plots for the substrate classes **1-4**, which includes previous data for the PP1 $\gamma$ -catalyzed hydrolysis of substrate types **1** and **4** for comparison. The slopes are collected in **Table 3-6** and shown with the values for the corresponding uncatalyzed hydrolysis reactions.

**Table 3-5.** Substrates for the PP1 $\gamma$ -catalyzed hydrolysis reaction with their leaving group  $pK_a$  values.<sup>41</sup>

Phenyl substituent (X)	$pK_a$		
		<b>2</b>	<b>3</b>
4-NO <sub>2</sub>	7.14	<b>a</b>	<b>a</b>
4-CN	7.95	<b>b</b>	<b>b</b>
3-CN	8.61	<b>c</b>	<b>c</b>
4-Cl	9.38	<b>d</b>	<b>d</b>
3-Cl	9.02	<b>e</b>	<b>e</b>
H-	9.95	<b>f</b>	<b>f</b>
3-NO <sub>2</sub>	8.35	<b>g</b>	
4-Cl, 3-NO <sub>2</sub>	7.78	<b>h</b>	

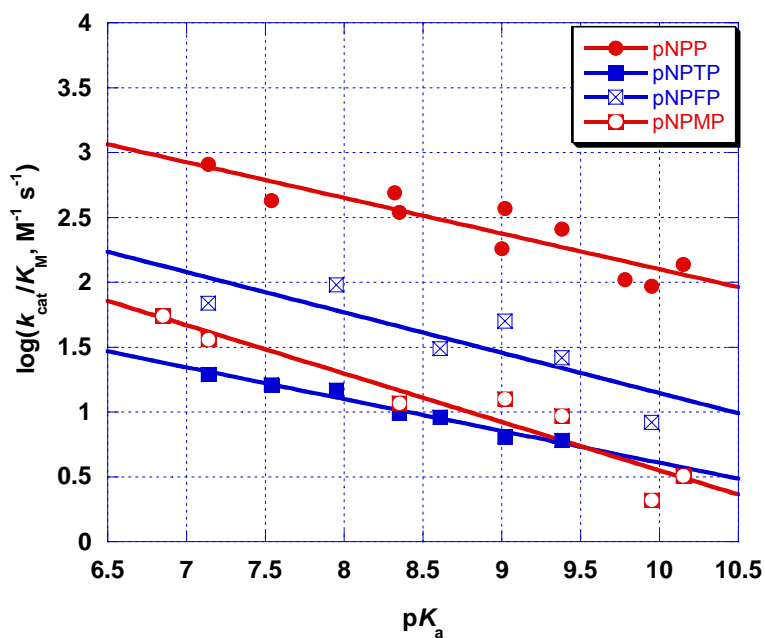


**Figure 3-3.** Brønsted plot for the PP1 $\gamma$ -catalyzed hydrolysis of four substrate classes: **2** aryl phosphorothioate monoester (■) and **3** aryl fluorophosphate monoester (⊠) are from this work; **1** aryl phosphate monoester dianion (●) and **4** aryl methylphosphonate monoester (◻) are from literature.<sup>8</sup>

**Table 3-6.** Brønsted  $\beta_{lg}$  values for the PP1 $\gamma$ -catalyzed and for the uncatalyzed hydrolysis reactions of substrate classes 1-4.

Substrate class	Brønsted $\beta_{lg}$ for PP1 $\gamma$ -catalyzed reaction	Brønsted $\beta_{LG}$ for uncatalyzed hydrolysis
1	-0.32 <sup>8</sup>	-1.23 <sup>38</sup>
2	-0.25 $\pm$ 0.02	-1.1 <sup>14</sup>
3	-0.40 $\pm$ 0.07	-0.63 <sup>21</sup>
4	-0.30 <sup>8</sup>	-0.69 <sup>8</sup>

The Brønsted slopes for all of the PP1 $\gamma$ -catalyzed reactions fall within a much narrower range from -0.25 to -0.40, while those for the uncatalyzed reactions range from -0.63 to -1.23. The similar  $\beta_{lg}$  data suggest that in contrast to the uncatalyzed reactions, the PP1 $\gamma$ -catalyzed reactions share more similar transition states. Small  $\beta_{lg}$  values shown by all four substrates classes indicate that enzyme-catalyzed hydrolysis has low sensitivity to the  $pK_a$  of the leaving group. The first possible explanation is that the positively charged environment of the active site has decreased the extent of the P-O bond cleavage during the transition state, and therefore there is less accumulation of negative charge on the leaving group oxygen during the transition state. The most plausible explanation for a decrease in P-O bond cleavage would be a change to a more associative transition state. The other possible reason is that the transition states are still highly dissociative in character but there is neutralization of the leaving group oxygen either through hydrogen bonding from the conserved residues (R96 and R221) or from the conserved histidine residue acting as a general acid.

To complement the LFER data and further investigate the potential bond cleavage and charge changes at the transition state, heavy atom kinetic isotope effects (KIEs) for

aryl phosphorothioate monoesters were measured (**Table 3-7**). KIEs have been reported for a number of enzymatic and uncatalyzed hydrolysis reactions of phosphate and phosphonate esters, and those for the PP1 $\gamma$  reaction with substrates **1a** and **4a** have been previously measured.<sup>8</sup> In this work, the KIEs for the PP1 $\gamma$  reaction with substrate **2a** were reported. Syntheses for the needed double-labeled forms of the fluorophosphate ester could not be carried out with sufficient isotopic purity, precluding KIE determinations with **4a**.

**Table 3-7.** KIE data for uncatalyzed and PP1 $\gamma$ -catalyzed reactions. Numbers shown in bold are from this work. Numbers in parentheses are the standard errors in the last decimal place.

	Results for <b>2a</b> ( <i>p</i> NPTP)		Results for <b>1a</b> ( <i>p</i> NPP)		Results for <b>4a</b> ( <i>p</i> NPMP)	
	Dianion H <sub>2</sub> O attack, 50°C <sup>14,42</sup>	PP1 $\gamma$ -catalyzed	Dianion H <sub>2</sub> O attack, 95°C <sup>38,43</sup>	PP1 $\gamma$ -catalyzed <sup>8</sup>	Monoanion OH attack, 25°C <sup>8</sup>	PP1 $\gamma$ -catalyzed <sup>8</sup>
<sup>18</sup> <i>k</i> <sub>nonbridge</sub>	<b>1.0135 (13)</b>	<b>0.9717 (18)</b>	0.9994 (5)	0.9959 (4)	1.0015 (4)	0.9973 (4)
<sup>18</sup> <i>k</i> <sub>bridge</sub>	<b>1.0237 (7)</b>	<b>1.0161 (5)</b>	1.0189 (5)	1.0170 (3)	1.0098 (4)	1.0129 (3)
<sup>15</sup> <i>k</i>	<b>1.0027 (1)</b>	<b>1.0001 (1)</b>	1.0028 (2)	1.0010 (2)	1.0006 (3)	1.0010 (1)

All KIEs were measured by the competitive method, in which a mixture of the isotopic isomers is present in solution and the isotope effects are obtained using isotope ratio mass spectrometry to monitor isotope ratios as a function of the fraction of reaction. Measurement of KIEs using the competitive method for enzyme-catalyzed reactions yields the isotope effect on (V/K), or, the isotope effect on the rate-limiting step for the part of the overall reaction sequence up to and including the first irreversible step. For PP1 $\gamma$ -catalyzed reactions this will be P-O bond fission, and thus the isotope effects will

reflect this chemical step, even if a subsequent step such as product release is rate-limiting in the overall kinetic mechanism.

Like the Brønsted  $\beta_{lg}$  value, the KIE in the leaving group for the PP1 $\gamma$ -catalyzed reaction of **2a** are diminished from their values in the uncatalyzed hydrolysis. The magnitude of  $^{15}(V/K)$  reflects the negative charge developed on the leaving group in the TS. The  $^{15}(V/K)$  KIE of unity indicates that leaving group neutralization is complete, and is more effective than with substrates **1a** and **4a**. Why general acid catalysis should be more effective with this substrate is not clear, but the magnitude of the Brønsted  $\beta_{lg}$  slope for phosphorothioates is also slightly smaller than the other substrate types, also suggestive of a smaller degree of change in effective charge at the transition state than with the other substrates. The leaving group  $^{18}(V/K)_{bridge}$  is affected by P-O bond fission and by protonation. With the *para*-nitrophenyl leaving group, this KIE may be as large as 1.035 when there is no inverse contribution from protonation. The primary  $^{18}(V/K)_{bridge}$  in the PP1 $\gamma$ -catalyzed hydrolysis of **2a** is similar to previously obtained values for phosphatase reactions in which the TS is characterized by extensive P-O bond fission and concurrent protonation of the leaving group. In the uncatalyzed hydrolysis of **2a**, the magnitude for  $^{18}k_{bridge}$  implies a large degree of P-O bond fission in the transition state, and  $^{15}k$  clearly demonstrates that the leaving group departs as the charged anion. In the PP1 $\gamma$ -catalyzed hydrolysis reaction of **2a** the magnitude of  $^{18}(V/K)_{bridge}$  is reduced, consistent with general acid protonation of the leaving group in the transition state that is hypothesized to be carried out by histidine 125. This  $^{18}(V/K)_{bridge}$  value is similar to those measured in other phosphoryl transfer reactions in which extensive P-O bond fission is accompanied by leaving group protonation.<sup>44</sup> This value is also similar to those of

substrates **1a** and **4a**, supporting the notion from the Brønsted  $\beta_{lg}$  data that bond fission to the leaving group is similar in each substrate reaction on the enzyme. The other oxygen KIE,  $^{18}(V/K)_{nonbridge}$ , is significantly inverse, in contrast to the normal KIE for the solution hydrolysis. This same switch to an inverse  $^{18}(V/K)_{nonbridge}$  in a metallophosphatase-catalyzed reaction of **2a** has been noted previously, and ascribed to an inverse effect arising from coordination of the thiophosphoryl group to the metal center.<sup>14,29</sup>

The overall picture supported by the LFER and KIE data is a transition state with extensive P-O bond fission involving general acid protonation of the leaving group. The mechanism of PP1 $\gamma$ -catalyzed reactions and transition states are similar for all substrate types, with slightly better neutralization of the leaving group in the reactions of phosphorothioates.

### **3.2.7 The binding of inhibitors is affected primarily by charge rather than size.**

To further investigate the relative influences of size, geometry, and charge on affinity for the active site of PP1 $\gamma$ , a series of small molecule ionic inhibitors with various geometries were tested as inhibitors (**Table 3-8**).

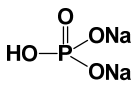
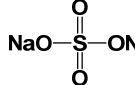
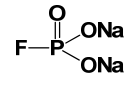
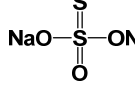
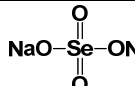
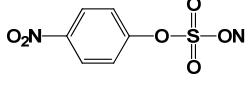
The left side of the Table compares the affinity of inorganic phosphate with a series of fluoride-based inhibitors. Phosphate monoesters undergo reaction by a concerted mechanism with trigonal bipyramidal transition state. Of the tested inhibitors, only the metal fluorides are able to assume this geometry. As phosphate analogues, the metallic fluorides  $AlF_x$  and  $MgF_x$  have been shown to be useful chemical probes for structural and mechanistic studies in phosphoryl transfer reaction because they mimic the transition state for phosphoryl transfer when  $x = 3$ . The Al-F bond has a similar length as the P-O bond in phosphate esters (1.5-1.6Å). It is believed that aluminofluorides can adopt

tetrahedral, trigonal bipyramidal, and octahedral geometries in a protein active site.<sup>45,46</sup> Magnesium fluoride complexes with trigonal bipyramidal and octahedral geometries have been found in active sites of proteins.<sup>47,48</sup> Here, while neither magnesium, aluminum, or fluoride ion alone are effective inhibitors, strong inhibition is observed in combination. This indicates that the inhibitory species are magnesium fluoride and aluminum fluoride complexes formed *in situ*. It is not certain what geometry these metallic fluoride inhibitors adopt when bound to the active site of PP1 $\gamma$ , but based on precedents with other phosphoryl transfer enzymes, a trigonal bipyramidal geometry with three fluorides in equatorial positions is most likely. <sup>19</sup>F NMR has been used to successfully characterize MgF<sub>3</sub> complexes at an enzymatic active site<sup>48</sup> but was unsuccessful here due to the presence of paramagnetic Mn<sup>2+</sup> ions.

Sodium fluoride and magnesium chloride alone were very weak inhibitors, with estimated inhibition constants of 150 mM (NaF) and 70 mM (MgCl<sub>2</sub>). The simple fluoride salt NaF shows negligible inhibition of PP1 $\gamma$ . In contrast, fluoride has been found to significantly inhibit the activity of bovine spleen purple acid phosphatase (PAP), a member of a related class of metallophosphatases with a dinuclear metal center, with  $K_i$  ranging between 2 mM to 3  $\mu$ M depending upon the pH and metal in the active site.<sup>49</sup> Crystal structures show fluoride displaces the hydroxide bridging the two metal ions in PAP.<sup>50</sup> The tetrahedral fluorophosphate dianion and tetrafluoroborate monoanion are both competitive inhibitors with similar inhibition constants; the difference implies a difference in equilibrium binding ( $\Delta\Delta G$ ) of only 1.1 kcal. Unexpectedly, the octahedral hexafluoroborate anion is also a competitive inhibitor with  $K_i = 5.56$  mM, lower than that

for tetrafluoroborate. To the best of our knowledge, this is the first example of an octahedral anion inhibitor of a phosphatase.

**Table 3-8.** Inhibition of the PP1 $\gamma$ -catalyzed hydrolysis of **1a** (pNPP) by various inhibitors at pH 7.0. The inhibition was found to be competitive in all cases.

Inhibitor	Geometry	$K_i$ (mM)	Inhibitor	Geometry	$K_i$ (mM)
	Tetrahedral	1.2 $\pm$ 0.2		Tetrahedral	35.5 $\pm$ 1.8
	Tetrahedral	3.0 $\pm$ 0.2		Tetrahedral	21.7 $\pm$ 1.9
$\text{NH}_4\text{PF}_6$	Octahedral	5.6 $\pm$ 0.8		Tetrahedral	30.1 $\pm$ 1.6
$\text{NaBF}_4$	Tetrahedral	8.2 $\pm$ 2.1			
$\text{MgF}_x$ [a]	Planar	0.8 $\pm$ 0.1		Tetrahedral	39.9 $\pm$ 9.5
$\text{AlF}_x$ [a]	Planar	(3.2 $\pm$ 0.3) $\times 10^{-2}$			

[a] Inhibition constants for  $\text{MgF}_x$  and  $\text{AlF}_x$  were calculated as described in **Chapter 2.3.4**.

Magnesium fluoride complexes can adopt either trigonal bipyramidal or octahedral geometry in active sites of proteins.<sup>47,48</sup> In trigonal bipyramidal geometry, three fluoride atoms coordinate to the magnesium ( $\text{MgF}_3$ ,  $x=3$ ) and adopt planar geometry during the transition state.<sup>47</sup> In octahedral geometry, four fluoride atoms coordinate to the magnesium ( $\text{MgF}_4$ ,  $x=4$ ). The phosphorus atom still shares a plane with four fluoride atoms [b] Aluminofluorides can adopt tetrahedral, trigonal bipyramidal, and octahedral geometries in a protein active site depending upon the number of fluoride atoms coordinating to the aluminum.<sup>45,46</sup>

The results indicate that the binding of anions to the active site of PP1 $\gamma$  is more affected by charge while changes in geometry are well tolerated.

The right side of the table compares the affinity of inorganic sulfate and analogues and will be discussed in the next section.

### 3.2.8 *para*-Nitrophenyl sulfate is not a substrate for PP1 $\gamma$

The fact that *para*-nitrophenyl sulfate (pNPS) is not a substrate for PP1 $\gamma$  is surprising in light of its promiscuity for monoanionic phosphorus-based substrates. Sulfate and phosphate monoesters share tetrahedral geometry with comparable bond angles and lengths. The uncatalyzed hydrolysis reactions of sulfate and phosphate monoesters both occur with similar rate constants and with similar loose transition states. This similarity between phosphoryl and sulfuryl transfer reactions is reflected in the ability of several other promiscuous enzymes, including *E. coli* alkaline phosphatase, the sulfatase PAS, and the hydrolase BcPMH that carry out both activities.<sup>25</sup> The inability of PP1 $\gamma$  to catalyze pNPS hydrolysis is not due to an inability to bind to the active site. Inhibition experiments demonstrate that **6a** binds to the active site, albeit weakly, as it is a competitive inhibitor ( $K_i = 39.9$  mM). The significantly higher  $K_i$  compared to the monoanionic phosphoester substrates is in keeping with the weaker affinity of sulfate as a metal ligand compared with phosphate. However, even at high substrate concentrations and long reaction times, no activity with pNPS was observed. The reason for this discrimination is not clear.

Inhibition experiments show that sulfate and sulfate analogues are weak competitive inhibitors of the phosphate monoesterase activity of PP1 $\gamma$ , with inhibition constants ( $K_i$ ) ranging 22 mM to 40 mM (**Table 3-8**). Even with the same molecular geometry, changing the center atom from phosphorus to sulfur or selenium dramatically decreases binding affinity. The oxygen atoms of the sulfate group have a lower charge

density compared to phosphate anions, which accounts for their weaker Lewis basicity and evidently results in a loss of the ability for active site interactions to effectively stabilize the transition state for sulfuryl transfer relative to phosphoryl transfer.

### 3.3 Summary

In summary, the results shown in this chapter provide evidences to the original questions on the beginning:

- 1) PP1 $\gamma$  is an effective catalyst for the hydrolysis of both monoanionic and dianionic phosphate-ester based substrates **1-5**, with second-order rate accelerations that fall within the narrow range of  $10^{11}$  to  $10^{13}$ , which suggest that the PP1 active site is tolerant of variations in the electronic and geometric nature of the transferring group.
- 2) The transition states of PP1 $\gamma$ -catalyzed reactions for four substrate classes (**1-4**) are similar even though these substrates have differing mechanisms in their uncatalyzed hydrolysis reactions. Thus, the enzyme catalyzes the hydrolysis of these substrates by transition states that are controlled by the active site environment more than by the intrinsic nature of the substrates.
- 3) Inhibition experiments suggest that the PP1 $\gamma$  active site is tolerant of variations in the geometry of bound ligands. This characteristic may permit the effective catalysis even of substrates whose steric requirements may result in perturbations to the positioning of the transferring group both in the initial enzyme-substrate complex, and in the transition state. The reason for the inability of PP1 $\gamma$  to catalyze the hydrolysis of a sulfate ester is unclear, and unexpected, since the charge and transition state of this substrate are well within the range of those of the phosphorus-based substrates that are effectively catalyzed.

### 3.4 References

- (1) Herschlag, D.; Jencks, W. P. *J. Am. Chem. Soc.* **1989**, *111*, 7579-7586.
- (2) Thatcher, G. R. J.; Kluger, R. *Advances in Physical Organic Chemistry* **1989**, *25*, 99-265.
- (3) Herschlag, D.; Jencks, W. P. *J. Am. Chem. Soc.* **1989**, *111*, 7587-7596.
- (4) Basaif, S. A.; Davis, A. M.; Williams, A. *J. Org. Chem.* **1989**, *54*, 5483-5486.
- (5) Kirby, A. J.; Younas, M. *J. Chem. Soc. B* **1970**, 1165-1172.
- (6) Cassano, A. G.; Anderson, V. E.; Harris, M. E. *J. Am. Chem. Soc.* **2002**, *124*, 10964-10965.
- (7) Hengge, A. C.; Tobin, A. E.; Cleland, W. W. *J. Am. Chem. Soc.* **1995**, *117*, 5919-5926.
- (8) McWhirter, C.; Lund, E. A.; Tanifum, E. A.; Feng, G.; Sheikh, Q. I.; Hengge, A. C.; Williams, N. H. *J. Am. Chem. Soc.* **2008**, *130*, 13673-13682.
- (9) Kirby, A. J.; Varvoglis, A. G. *J. Am. Chem. Soc.* **1967**, *89*, 415-423.
- (10) Chin, J.; Banaszczyk, M.; Jubian, V.; Zou, X. *J. Am. Chem. Soc.* **1989**, *111*, 186-190.
- (11) Zhang, A. J.; Bai, G.; Deans-Zirattu, S.; Browner, M. F.; Lee, E. Y. *J. Biol. Chem.* **1992**, *267*, 1484-1490.
- (12) Iyengar, R.; Eckstein, F.; Frey, P. A. *J. Am. Chem. Soc.* **1984**, *106*, 8309-8310.
- (13) Allen, L. C.; Liang, C. X. *J. Am. Chem. Soc.* **1987**, *109*, 6449-6453.
- (14) Hollfelder, F.; Herschlag, D. *Biochemistry* **1995**, *34*, 12255-12264.
- (15) Catrina, I. E.; Hengge, A. C. *J. Am. Chem. Soc.* **1999**, *121*, 2156-2163.

- (16) Burgess, J.; Blundell, N.; Cullis, P. M.; Hubbard, C. D.; Misra, R. *J. Am. Chem. Soc.* **1988**, *110*, 7900-7901.
- (17) Cullis, P. M.; Iagrossi, A. *J. Am. Chem. Soc.* **1986**, *108*, 7870-7871.
- (18) Cullis, P. M.; Misra, R.; Wilkins, D. J. *J. Chem. Soc., Chem. Commun.* **1987**, 1594-1596.
- (19) Pauling, L. *J. Am. Chem. Soc.* **1932**, *54*, 3570-3582.
- (20) Huheey, J. E. *J. Phys. Chem.* **1965**, *69*, 3284-3291.
- (21) Alkherraz, A.; Kamerlin, S. C. L.; Feng, G. Q.; Sheikh, Q. I.; Warshel, A.; Williams, N. H. *Faraday Discussions* **2010**, *145*, 281-299.
- (22) Hengge, A. C.; Onyido, I. *Curr. Org. Chem.* **2005**, *9*, 61-74.
- (23) Zalatan, J. G.; Herschlag, D. *J. Am. Chem. Soc.* **2006**, *128*, 1293-1303.
- (24) Catrina, I.; O'Brien, P. J.; Purcell, J.; Nikolic-Hughes, I.; Zalatan, J. G.; Hengge, A. C.; Herschlag, D. *J. Am. Chem. Soc.* **2007**, *129*, 5760-5765.
- (25) O'Brien, P. J.; Herschlag, D. *J. Am. Chem. Soc.* **1998**, *120*, 12369-12370.
- (26) Alessi, D. R.; Street, A. J.; Cohen, P.; Cohen, P. T. W. *Euro. J. Biochem.* **1993**, *213*, 1055-1066.
- (27) Wang, X.; Randall, C. R.; True, A. E.; Que, L., Jr. *Biochemistry* **1996**, *35*, 13946-13954.
- (28) Zalatan, J. G.; Catrina, I.; Mitchell, R.; Grzyska, P. K.; O'Brien P, J.; Herschlag, D.; Hengge, A. C. *J. Am. Chem. Soc.* **2007**, *129*, 9789-9798.
- (29) Holtz, K. M.; Catrina, I. E.; Hengge, A. C.; Kantrowitz, E. R. *Biochemistry* **2000**, *39*, 9451-9458.

- (30) Nikolic-Hughes, I.; Rees, D. C.; Herschlag, D. *J. Am. Chem. Soc.* **2004**, *126*, 11814-11819.
- (31) Zhang, Y. L.; Hollfelder, F.; Gordon, S. J.; Chen, L.; Keng, Y. F.; Wu, L.; Herschlag, D.; Zhang, Z. Y. *Biochemistry* **1999**, *38*, 12111-12123.
- (32) Cassel, D.; Glaser, L. *Proc Natl Acad Sci U S A* **1982**, *79*, 2231-2235.
- (33) Zhang, Z. Y.; Maclean, D.; McNamara, D. J.; Sawyer, T. K.; Dixon, J. E. *Biochemistry* **1994**, *33*, 2285-2290.
- (34) Sigel, R. K. O.; Song, B.; Sigel, H. *J. Am. Chem. Soc.* **1997**, *119*, 744-755.
- (35) Wang, S. L.; Karbstein, K.; Peracchi, A.; Beigelman, L.; Herschlag, D. *Biochemistry* **1999**, *38*, 14363-14378.
- (36) Goldberg, J.; Huang, H. B.; Kwon, Y. G.; Greengard, P.; Nairn, A. C.; Kuriyan, J. *Nature* **1995**, *376*, 745-753.
- (37) Coleman, J. E. *Annu. Rev. Biophys. Biomol. Struct.* **1992**, *21*, 441-483.
- (38) Kirby, A. J.; Jencks, W. P. *J. Am. Chem. Soc.* **1965**, *87*, 3209-3216.
- (39) Behrman, E. J.; Biallas, M. J.; Brass, H. J.; Edwards, J. O.; Isaks, M. *J. Org. Chem.* **1970**, *35*, 3063-3070.
- (40) van Loo, B.; Jonas, S.; Babtie, A. C.; Benjdia, A.; Berteau, O.; Hyvonen, M.; Hollfelder, F. *Proc Natl Acad Sci U S A* **2010**, *107*, 2740-2745.
- (41) Fasman, G. D. *Handbook of Biochemistry and Molecular Biology*, Wiley, 1975.
- (42) Catrina, I. E.; Hengge, A. C. *J. Am. Chem. Soc.* **2003**, *125*, 7546-7552.
- (43) Hengge, A. C.; Edens, W. A.; Elsing, H. *J. Am. Chem. Soc.* **1994**, *116*, 5045-5049.
- (44) Hengge, A. C. *Acc. Chem. Res.* **2002**, *35*, 105-112.
- (45) Li, L. *Crit. Rev. Oral Biol. Med.* **2003**, *14*, 100-114.

- (46) Schlichting, I.; Reinstein, J. *Nat. Struct. Biol.* **1999**, *6*, 721-723.
- (47) Toyoshima, C.; Nomura, H.; Tsuda, T. *Nature* **2004**, *432*, 361-368.
- (48) Baxter, N. J.; Olguin, L. F.; Golicnik, M.; Feng, G.; Hounslow, A. M.; Bermel, W.; Blackburn, G. M.; Hollfelder, F.; Waltho, J. P.; Williams, N. H. *Proc Natl Acad Sci U S A* **2006**, *103*, 14732-14737.
- (49) Pinkse, M. W.; Merkx, M.; Averill, B. A. *Biochemistry* **1999**, *38*, 9926-9936.
- (50) Schenk, G.; Elliott, T. W.; Leung, E.; Carrington, L. E.; Mitic, N.; Gahan, L. R.; Guddat, L. W. *Bmc Structural Biology* **2008**, *8*, 6-12.

**CHAPTER 4**  
**MUTAGENESIS AND METAL ACTIVATION STUDIES**  
**ON RECOMBINANT PP1 $\gamma$**

#### 4.1 Introduction

##### 4.1.1 Mutagenesis studies on recombinant PP1 $\gamma$

Mutagenesis studies provide another pathway for the identification of functionally important residues within a protein. Many insights into the roles of particular amino acids in the catalytic mechanism of PP1 have been collected by mutagenesis studies.<sup>1-4</sup>

(Figure 4-1)

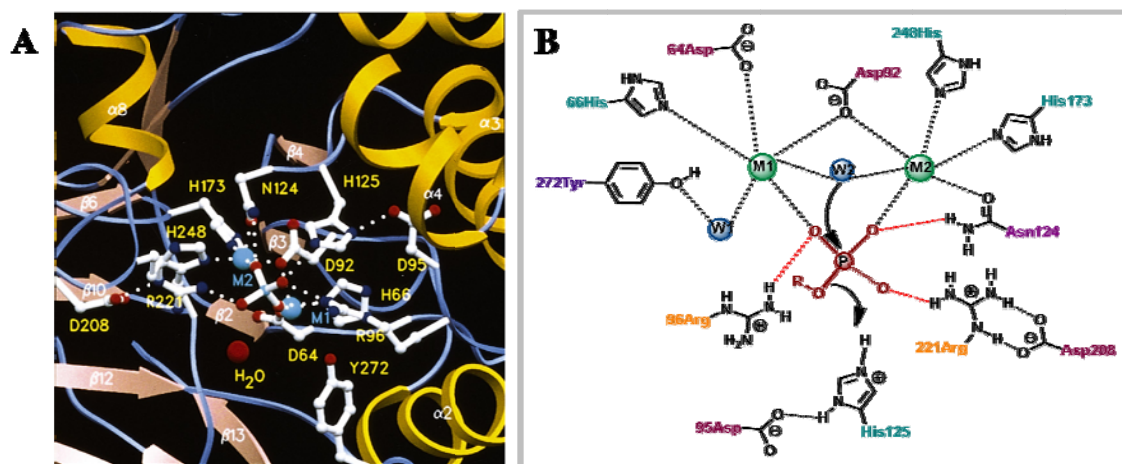


**Figure 4-1.** (A) Crystal structure of the catalytic site showing metal ions (cyan spheres) and tungstate binding site.<sup>5</sup> (B) Schematic diagram of the active site of PP1 $\gamma$  and proposed reaction mechanism involving nucleophilic attack by bridging hydroxide. The modeled phosphate monoester substrate is shown in a hypothetical binding mode. The hydrogen bonds of the phosphorus oxygens to N124, R96 and R221 are shown as red dashed lines.<sup>6</sup>

In contrast to the extensive study of six conserved residues (D64, H66, D92, N124, H173 and H248) which are believed to serve as ligands for the metal ions in the active site of PP1 $\gamma$ , the R96 and R221 residues in the active site of PP1 $\gamma$  which are suggested to bind to the substrate oxygens and may contribute to stabilization of a penta-coordinate transition state, have been given much less study (**Figure 4-1**). In previously published work, the R96 residue has been mutated into alanine (A) and glutamic acid (E) (**Table 1-6**). The replacement of arginine with alanine results in the loss of a hydrogen bond donor to the transferring group. The R96A mutant exhibited a large decrease in  $k_{\text{cat}}$  (>400-fold), but no significant change in  $K_{\text{M}}$  for the physiological substrate phosphorylated phosphorylase  $\alpha$ .<sup>4</sup> The replacement of arginine with glutamic acid seems an odd choice because it will result in conversion of a hydrogen bond donor to a hydrogen bond acceptor to the transferring group. The R96E mutant resulted in a 700-fold loss in catalytic efficiency with a small effect on  $K_{\text{M}}$  for phosphorylase  $\alpha$  as the substrate.<sup>2</sup> These results are consistent a role in which R96 donates a hydrogen bond to the phosphorus oxygens and functions in stabilizing a penta-coordinate transition state. The lesser effect on  $K_{\text{M}}$  indicates that this hydrogen bonding is more critical for catalysis than substrate recognition. The R221 residue has been only mutated into serine (S) (**Table 1-6**). The R221S mutant exhibited a large reduction in  $k_{\text{cat}}$  ( $\approx$ 200-fold), but in contrast to the R96A mutant, showed a significant reduction in affinity for substrate ( $\approx$ 10-fold increase in  $K_{\text{M}}$ ).<sup>4</sup> This is suggestive of a more important role for R221 in binding of substrate.

The Arg96 residue is part of a characteristic sequence motif (GDxVDRG) that is contained in all PPP superfamily members. In this respect, the Arg53 residue in bacteriophage  $\lambda$  PPase ( $\lambda$ PP) is equivalent to Arg96 in PP1.<sup>7</sup> Mutation of R53 of  $\lambda$ PP to

alanine significantly decreased the affinity for pNPP.<sup>8</sup> The apparent  $K_M$  for pNPP increases 21-fold. The  $V_{max}$  for the R53A mutant is also decreased, indicating that Arg53 is also important for catalysis.

#### 4.1.2 Metal ions at the active site

One difference between bacterially expressed PP1 and the native enzyme is that bacterially expressed PP1, especially PP1 $\alpha$  and PP1 $\beta$ , requires addition of  $Mn^{2+}$  to the buffer solution to maintain catalytic activity (**Chapter 1.4.2.4**). This phenomenon brings up a critical question: what are the effects of the divalent metal centers on the activity of recombinant catalytic subunit of PP1?

It has been shown that by using ion-exchange chromatography on a Mono-Q FPLC column to remove  $Mn^{2+}$  from the enzyme storage solution, wild type PP1 retained ~20% of the original activity.<sup>4</sup> This result suggested that the active site of PP1 held divalent metal ions tightly so that some bound metal retained. Addition of 1 mM  $Mn^{2+}$ , but not other metals, fully restored enzyme activity (**Figure 4-2A**). Of the metals tested,  $Mg^{2+}$  and  $Zn^{2+}$  are the best two which exhibit approximately 20% activity compared to  $Mn^{2+}$ . Other metal ions tested including  $Co^{2+}$ ,  $Ca^{2+}$ ,  $Fe^{2+}$ ,  $Ni^{2+}$ ,  $Cd^{2+}$ , or  $Cu^{2+}$  were not as effective or were only weakly effective in activating the enzyme.<sup>4</sup>

The alternative method for removing endogenous  $Mn^{2+}$  from PP1 active site is the use of a high concentration of EDTA to chelate the metal ions, followed by dialysis of the enzyme solution against MOPS buffer.<sup>9</sup> Addition of  $Co^{2+}$  or  $Mn^{2+}$  efficiently reactivate PP1. Treatment of enzyme with 1 mM  $Ca^{2+}$ ,  $Cu^{2+}$ ,  $Fe^{2+}$ ,  $Ni^{2+}$ , or 5 mM  $Mg^{2+}$  did not reactivate the PP1, while 1 mM  $Zn^{2+}$  had only a slightly stimulating effect. Interestingly,

treatment of the enzyme with a combination of  $\text{Fe}^{2+}$  and  $\text{Zn}^{2+}$  (but not the individual metal ions) significantly activated PP1 (**Figure 4-2B**).

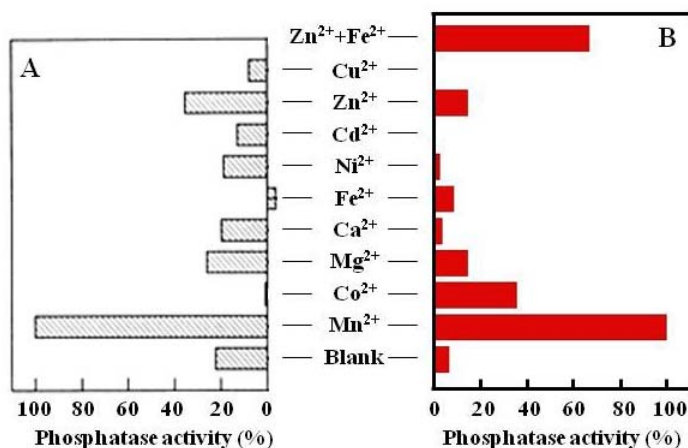


**Figure 4-2.** Phosphatase activity of reactivation PP1 by different metal ion. (A) Metals in PP1 were removed by Mono-Q chromatography before assay. Enzyme activity was measured as 100% in presence (+) of 1 mM  $\text{Mn}^{2+}$  chloride as indicated in text. In the presence of other metal chloride, enzyme activities were normalized. (B) The endogenous  $\text{Mn}^{2+}$  in PP1 active site is removed by using high concentration of EDTA to chelate the metal ions, then dialyzed enzyme solution against MOPS buffer.<sup>9</sup>

#### 4.1.3 Specific aims

In the present study, we have used site-directed mutagenesis to further evaluate the roles played by Arg96 and Arg221 amino acid residues and metal centers in the active site of PP1, in catalysis and in recognizing different substrate classes. The results will help to answer these fundamental questions:

- 1) What are functions of Arg96 and Arg221?
- 2) Which residues chosen for mutation interact with the transferring group and control the substrate preference?

- 3) Can a single mutation change catalytic promiscuity and provide evidence for protein evolution?
- 4) What are the effects of the identity of the divalent metal ions on the activity of recombinant catalytic subunit of PP1 $\gamma$ ?

## 4.2 Results and discussion

### 4.2.1 Design principle of Arg $\rightarrow$ Lys mutants

In the previous study, the R96 and R221 residues in the active site of PP1 $\gamma$  were suggested to bind to the substrate oxygens and may contribute to stabilization of a penta-coordinate transition state. The X-ray structure of PP1 indicates these two residues might have different functions. The guanidinium group of Arg96 forms a salt bridge with a phosphorus oxygen atom bound to metal ion 1. The guanidinium group of Arg221 forms a salt bridge with a phosphorus oxygen atom that is accessible to solvent but not bound to metal ions (**Figure 4-1 A**).

Arginine and lysine are positively charged, polar amino acids, and can be considered to be somewhat amphipathic, as the part of the side chain nearest to the backbone is long, carbon containing, and hydrophobic, whereas the end of the side chain is positively charged. The basicity of arginine ( $pK_a=12.48$ ) is greater than lysine ( $pK_a=10.53$ ), and the side chain of arginine is longer. Mutation of Arg96 to lysine could weaken the hydrogen bond interaction with metal-bound phosphorus oxygen by decreasing nucleophilicity and extending the interaction distance, and consequently decrease the transition state stabilization. In addition to catalytic effects the mutation of Arg221 to lysine could mainly affect substrate binding since this change would provide

additional space for active site to tolerate a more sterically demanding substrate. The double mutations of R96 and R221 to lysine could test a combination of the above hypothesis.

#### 4.2.2 Kinetic properties of Arg→Lys mutants

**Table 4-1.** Catalytic parameters of pNPP hydrolysis by PP1 $\gamma$  R96K and R221K mutants at varying pH. Uncertainties are shown in the parentheses.

pH	$k_{\text{cat}}$ ( $\text{s}^{-1}$ )		$K_{\text{M}}$ (mM)		$k_{\text{cat}}/K_{\text{M}}$ ( $\text{s}^{-1} \text{M}^{-1}$ )	
	R96K	R221K	R96K	R221K	R96K	R221K
5.50	0.0090 (0.0002)		0.40 (0.05)		22 (4)	
5.75	0.0140 (0.0005)	0.0070 (0.0001)	0.42 (0.06)	0.14 (0.02)	34 (8)	54 (5)
6.00	0.030 (0.001)	0.016 (0.001)	0.83 (0.08)	0.20 (0.04)	36 (5)	77 (11)
6.25	0.063 (0.002)	0.057 (0.001)	1.3 (0.1)	0.32 (0.03)	47 (7)	179 (10)
6.50	0.068 (0.002)	0.072 (0.002)	1.3 (0.1)	0.34 (0.05)	53 (9)	213 (22)
6.75	0.149 (0.005)	0.25 (0.01)	2.7 (0.2)	0.8 (0.1)	55 (6)	315 (33)
7.00	0.206 (0.008)	0.54 (0.01)	3.4 (0.3)	1.7 (0.1)	60 (8)	315 (16)
7.50	0.215 (0.009)	1.23 (0.08)	4.3 (0.4)	4.2 (0.5)	50 (7)	293 (31)
8.00	0.24 (0.01)		9.5 (0.9)		25 (4)	
8.26	0.16 (0.01)	0.47 (0.06)	11 (1)	5 (1)	16 (4)	100 (23)
8.50	0.19 (0.05)	0.9 (0.4)	22 (7)	22 (11)	9 (2)	41 (8)
8.75	0.24 (0.06)	0.53 (0.05)	29 (8)	12 (2)	8 (1)	44 (6)
9.05	0.10 (0.02)	0.56 (0.06)	19 (4)	25 (3)	5.3 (0.7)	22 (6)

The pH dependence of pNPP hydrolysis by two mutants, R96K and R221K, was determined at 25 °C in a three-component buffer (50 mM Tris, 50 mM Bis-Tris, 100 mM NaOAc, and 0.05 mM MnCl<sub>2</sub>). The kinetic measurements were carried out between pH 5.5–9.0 in the presence of 0.2–10.0 mM pNPP and reactions were initiated by adding the mutant proteins (see Chapter 2.3.1 for details). The catalytic parameters for pNPP hydrolysis by PP1 $\gamma$  R96K and R221K mutants as a function of pH are shown in **Table 4-1**. These data were used to construct pH-rate profiles to assist in the interpretation of the effect these mutations have on the chemical mechanisms of PP1 $\gamma$ -catalyzed hydrolysis.

#### pH dependence of $k_{\text{cat}}/K_M$

The pH profiles that will be of the most value will be  $\log(k_{\text{cat}}/K_M)$  for each of the substrates. The pH dependence of  $\log(k_{\text{cat}}/K_M)$  follows the conversion of free enzyme and free substrate (E+S) until the first irreversible step and therefore reports on ionisations in the free enzyme and free substrate. The pH dependence of  $k_{\text{cat}}/K_M$  for the substrate pNPP with the two mutants showed similar bell-shaped profiles as for the wild type enzyme, indicative of catalysis by both acidic and basic residues (**Figure 4-3**). The  $k_{\text{cat}}/K_M$  versus pH data were fit to **Equation 3-2** to obtain  $(k_{\text{cat}}/K_M)^{\text{lim}}$  and derived  $\text{p}K_a$  values. (**Table 4-2**)

**Table 4-2.** The derived kinetic  $\text{p}K_a$  values for mutants of PP1 $\gamma$ .

Protein	PP1 $\gamma$ WT	PP1 $\gamma$ R96K	PP1 $\gamma$ R221K
$\text{p}K_{a1}$	6.0 $\pm$ 0.2	5.8 $\pm$ 0.1	6.8 $\pm$ 0.2
$\text{p}K_{a2}$	7.2 $\pm$ 0.2	7.9 $\pm$ 0.1	7.5 $\pm$ 0.1
<b>Maximal rate</b> ( $k_{\text{cat}}/K_M^{\text{lim}}, \text{M}^{-1} \text{s}^{-1}$ )	1850 $\pm$ 500	65 $\pm$ 7	654 $\pm$ 186

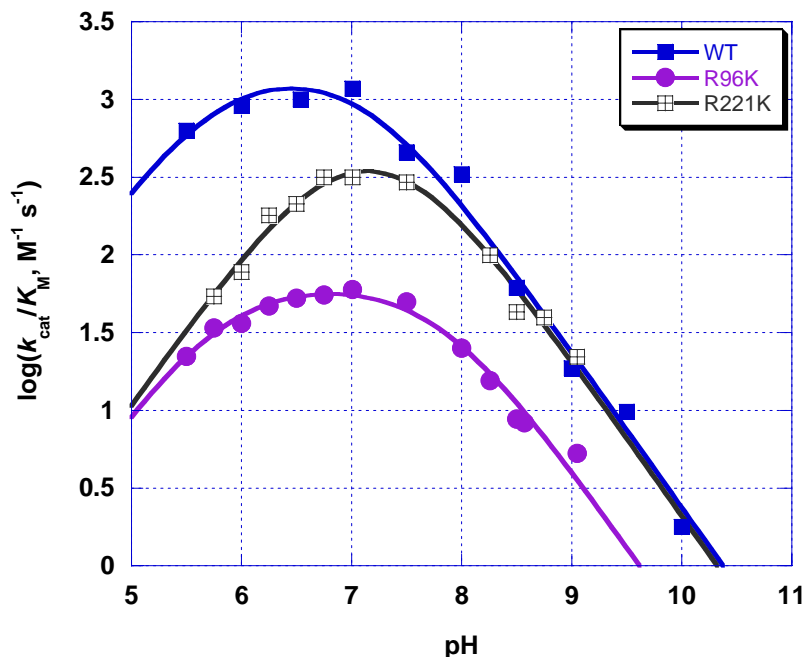


**Figure 4-3.** Comparison of the pH dependence of  $\log(k_{cat}/K_M)$  for pNPP hydrolysis by wild type PP1 $\gamma$  (■), the R96K (●), and the R221K (⊞) mutants.

The pH-rate profiles of  $k_{cat}/K_M$  values for wild type PP1 $\gamma$ , R96K and R221K mutants largely coincide, suggesting the same active site and enzymatic mechanism is followed, with catalysis by both acidic and basic residues. The deprotonated form of the metal-coordinated water molecule is proposed to be the nucleophile and represented by  $pK_{a1}$ . For R96K, the  $pK_{a1}$  value differs negligibly from wild type. The kinetic  $pK_{a1}$  value for R221K is  $\sim 1$  unit higher than for the wild type. The perturbation caused by R221K may not only weaken the salt bridge with one of the phosphoryl group oxygens, but also alter the geometry or the solvation sphere of the nucleophile, which may explain the higher  $pK_{a1}$  value. The H125 residue is plausibly assigned to act as a general acid and protonate the leaving group oxygen atom accelerating the dephosphorylation, and would

then be responsible for the  $pK_{a2}$  of the pH-rate profile. Compared to the variation of  $pK_{a1}$ , relative to the wild type, the R96K mutation alters  $pK_{a2}$  more than R221K.

### pH dependence of $k_{cat}$

The pH dependence of  $k_{cat}$  follows the conversion of the enzyme-substrate complex (ES) into free enzyme and product (E+P), and therefore reports on ionizations in the rate-determine step following formation of the enzyme-substrate complex (ES) rather than free enzyme and substrate (E + S). Comparison of the pH dependence of  $k_{cat}$  for pNPP hydrolysis by PP1 $\gamma$  R96K (●) and R221K (⊞) mutants is shown in **Figure 4-4**.

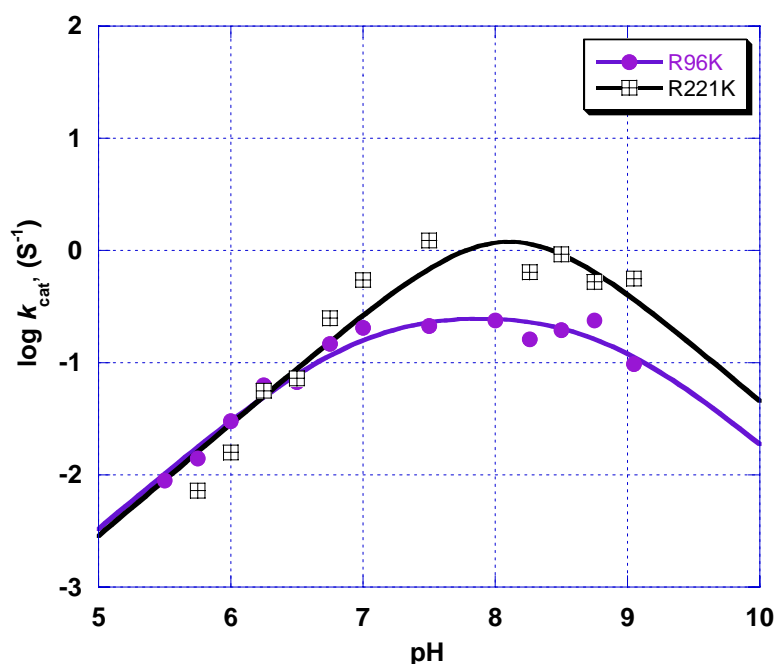


**Figure 4-4.** Comparison of the pH dependence of  $\log(k_{cat})$  for pNPP hydrolysis by PP1 $\gamma$  R96K (●) and R221K (⊞) mutants.

The pH dependence of  $k_{cat}$  which follows a bell shaped curve as same as the pH-rate profiles of  $k_{cat}/K_M$  indicates that two ionizations are critical for activity. Both

mutants exhibit maximal rate at  $\sim$  pH 8.0. Fitting the R96K data to **Equation 3-2** gives deduced  $pK_a'$  values of  $7.0\pm 0.1$  and  $8.8\pm 0.2$ , which shift about 1  $pK_a$  unit higher than the one obtained from fits of  $\log(k_{cat}/K_M)$  (**Table 4-3**).

**Table 4-3.** Kinetic parameters and values from the hydrolysis of pNPP by the R96K mutant.

	Free enzyme		Enzyme-substrate complex
$pK_{a1}$	$5.8\pm 0.1$	$pK_{a1}'$	$7.0\pm 0.1$
$pK_{a2}$	$7.9\pm 0.1$	$pK_{a2}'$	$8.8\pm 0.2$
$(k_{cat}/K_M)^{lim}, M^{-1} s^{-1}$	$65\pm 7$	$k_{cat}^{lim}, s^{-1}$	$0.3\pm 0.1$

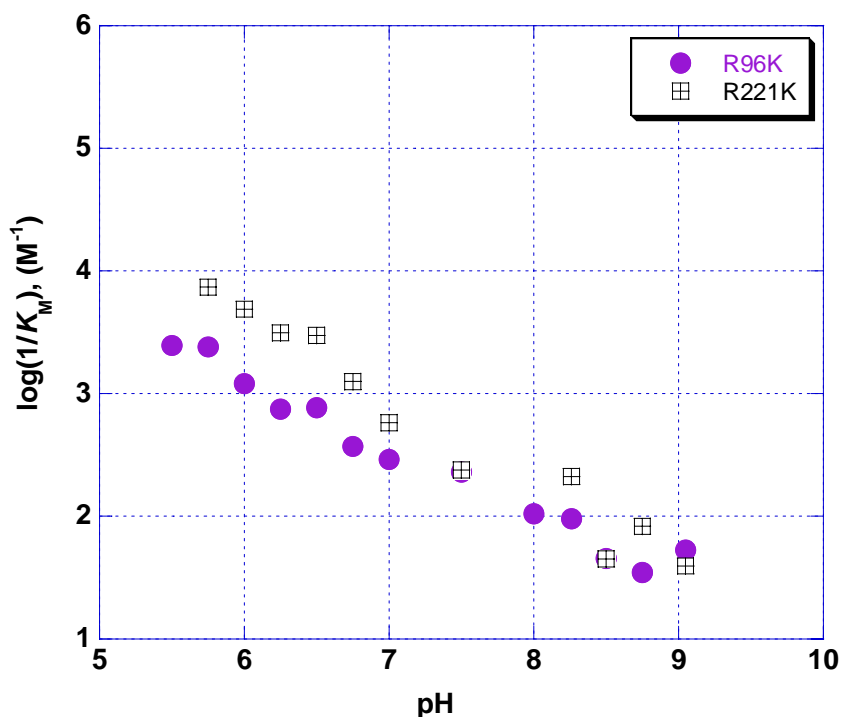
The higher  $pK_{a1}'$  value in the  $k_{cat}$  plot could be due to the deprotonation of the nucleophile. If the nucleophile is the metal bound hydroxide, then upon binding of substrate the  $pK_a$  of the nucleophile may increase as the substrate bound-metal sites will be less electron withdrawing than in the free enzyme. These  $pK_a$  values are consistent with the assignment of the lower  $pK_a$  to the metal-bound water. The higher  $pK_{a2}'$  value in  $k_{cat}$  plot could be due to His125 residue partially protonation the leaving group of bound substrate.

### pH dependence of $K_M$

The pH dependence of  $1/K_M$  follows the conversion of free enzyme and substrate (E + S) into enzyme-substrate complex (ES), and therefore reports on ionisations in the free enzyme and free substrate.

For both mutants, the slope from the plot of  $\log(1/K_M)$  versus pH is  $\sim 1$  which indicates the  $K_M$  value increases steadily up to  $\sim 3$  orders of magnitude from pH 5.5 to pH

9.0. (**Figure 4-5**) The steadily increasing  $K_M$  value with increasing pH for both mutants implies that an ionization affects binding within the active site, with a  $pK_a$  that is outside the range of the plot. A metal-bound hydroxide or an arginine residue are two possibilities for such deprotonation, which would reasonable be expected to decrease binding affinity by charge repulsion.

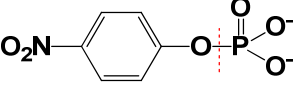
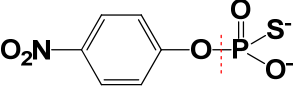
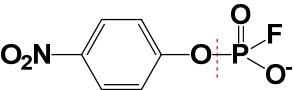
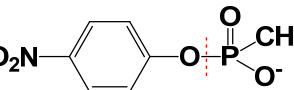
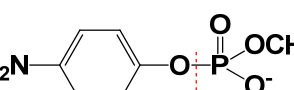


**Figure 4-5.** Comparison of the pH dependence of  $\log(1/K_M)$  for pNPP by PP1 $\gamma$  R96K (●) and R221K (⊞) mutants.

#### 4.2.3 Hydrolysis of substrates 1-5a by PP1 $\gamma$ mutants

The abilities of the R221K and R96K mutants, and the double mutant, of PP1 $\gamma$  to catalyze the hydrolysis of substrates **1-5a** were compared at pH 7.0. Michaelis-Menten plots were used to obtain the catalytic efficiency of each mutant compared with native PP1 $\gamma$  (**Table 4-4**).

**Table 4-4.** Catalytic efficiency ( $k_{\text{cat}}/K_{\text{M}}$ ,  $\text{M}^{-1}\text{s}^{-1}$ ) for the hydrolysis of substrates **1a-5a** at pH 7.0 by wild type and arginine mutants of PP1 $\gamma$ .

Substrate	Enzyme	$k_{\text{cat}}$ ( $\text{s}^{-1}$ )	$K_{\text{M}}$ (mM)	$k_{\text{cat}}/K_{\text{M}}$ ( $\text{M}^{-1}\text{s}^{-1}$ )
 <b>1a (pNPP)</b>	WT	3.2±0.1	3.6±0.3	869±3
	R96K	0.206±0.003	3.4±0.3	60±8
	R221K	0.544±0.004	1.7±0.1	315±31
	Double	(9.9±0.2)×10 <sup>-3</sup>	0.56±0.05	18±2
 <b>2a (pNPTP)</b>	WT	(2.9±0.1)×10 <sup>-2</sup>	1.5±0.1	20±3
	R96K	(3.0±0.2)×10 <sup>-3</sup>	3.8±0.4	0.8±0.1
	R221K	(4.0±0.1)×10 <sup>-3</sup>	2.1±0.2	1.9±0.2
 <b>3a (pNPFP)</b>	WT	0.76±0.03	9.2±0.4	83±7
	R96K	0.26±0.04	10.4±2.2	25±4
	R221K	2.05±0.05	13.1±0.4	157±8
	Double	0.081±0.009	4.9±1.2	16.5±5.8
 <b>4a. (pNPMP)</b>	WT	1.1±0.2	13±1	86±8
	R96K	0.18±0.03	15±4	11±2
	R221K	2.0±0.1	17±2	115±10
	Double	0.108±0.005	19±1	5.7±0.7
 <b>5a (diester)</b>	WT	0.016±0.001	9.2±0.9	1.7±0.3
	R96K	(5.2±0.5)×10 <sup>-3</sup>	14.8±1.8	0.35±0.08
	R221K	0.029±0.008	17±6	1.8±0.4

The R96K mutation primarily affects  $k_{\text{cat}}$  but has negligible effects on  $K_{\text{M}}$ . These data further confirm that the major function of Arg96 is stabilization of the transition state instead of substrate binding. Meanwhile, the R96K mutant exhibits a larger decrease

in  $k_{\text{cat}}$  for dianion substrates (**1a** and **2a**) than monoanion substrates (**3a**, **4a** and **5a**). It was anticipated that Arg96 would stabilize the transition states of dianion substrates more effectively.

The R221K mutation also primarily affects  $k_{\text{cat}}$ , but it was less impaired than the R96K mutant for all substrate classes. Most interestingly, for the monoanionic substrates **3a** and **4a**, the mutant R221K exhibits  $k_{\text{cat}}$  that is superior to the native enzyme, leading to catalytic efficiencies  $k_{\text{cat}}/K_M$  better than the wild type. For the monoanionic diester **5a** the values are similar. This is suggestive of a more important role for this residue in stabilization of the transition state than in binding of substrate.

#### 4.2.4 Preliminary study on $\text{Mg}^{2+}$ activation of PP1 $\gamma$

Recombinant PP1 has been depleted in  $\text{Mn}^{2+}$  either by using ion-exchange chromatography on a Mono-Q FPLC column or by using high concentration of EDTA to chelate the metal ions, followed by dialysis. In this work, the di- $\text{Mg}^{2+}$  form of PP1 $\gamma$  was generated by a different method than the literature. In place of  $\text{Mn}^{2+}$ ,  $\text{Mg}^{2+}$  was used as the only divalent metal source in transformations and in the growth media to express PP1 $\gamma$ . Subsequently, 1 mM  $\text{Mg}^{2+}$  was always included in buffer used in purification and kinetic measurements. The typical yield of purified  $\text{Mg}^{2+}$  form of PP1 $\gamma$  was about 3-fold lower than when  $\text{Mn}^{2+}$  was used.

Although the definitive identification of the metal ions present has not been done to directly prove the formation of the di-Mg form of PP1, previously studies have shown that  $\text{Mg}^{2+}$  can reactivate PP1 more than 20% activity comparison to  $\text{Mn}^{2+}$  form.<sup>4</sup>

The preliminary kinetic study for the hydrolysis of pNPP catalyzed by the PP1 $\gamma$   $\text{Mg}^{2+}$  form generated as described above is shown in **Figure 4-6**. The pH rate profile of

PP1 $\gamma$  wild type is aligned for comparison. The pH dependence of  $k_{\text{cat}}/K_{\text{M}}$  for the  $\text{Mg}^{2+}$  form of PP1 $\gamma$  shows a similar bell-shaped pH rate profile as the PP1 $\gamma$  wild type, although with the maximal rate at  $\sim$  pH 8.2. The  $(k_{\text{cat}}/K_{\text{M}})^{\text{lim}}$  value for the  $\text{Mg}^{2+}$  form of PP1 $\gamma$  is decreased about 3 orders of magnitude compared to the wild type. The effect of metal replacement on active site geometry is unknown. The reduced catalytic efficiency might be caused by weakening of the nucleophilicity of metal bridging water molecule, or reduced activation of the substrate. Additional experimentation is needed to follow up on these preliminary results.

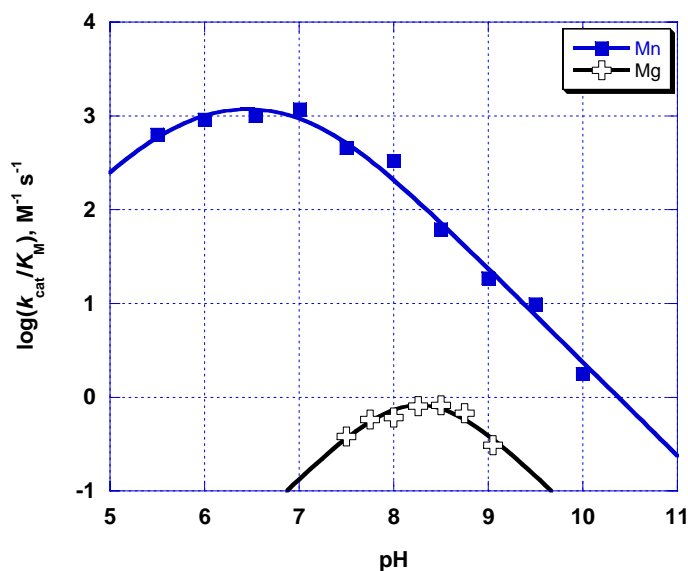


**Figure 4-6.** Dependence of  $k_{\text{cat}}/K_{\text{M}}$  on pH for the hydrolysis of *p*NPP by PP1 $\gamma$  Mn(II) form (■) and by PP1 Mg(II) form (⊠).

### 4.3 Summary

In summary, the results shown in this chapter provide evidence, pertinent to the original questions as follows:

- 1) The Arg96 and Arg221 residues in the active site of PP1 $\gamma$  are suggested to bind to the substrate oxygens and contribute to stabilization of a penta-coordinate transition state.
- 2) Mutation of these two arginine residues to lysine has been accomplished and identified. The catalytic efficiencies and substrate preferences were evaluated for two active site arginine mutants, R96K and R221K. Both the R96K and R221K mutations have minor effects on  $K_M$  but major effects on  $k_{cat}$ . The R96K mutant is more impaired than the R221K mutant for all substrate classes.
- 3) The conservative mutation of arginine 221 to lysine results in a mutant that more effectively catalyzes monoanionic substrates than the native enzyme. The surprising result in substrate preference from a single, conservative mutation lends support to the notion that mutations following gene duplication can result in an altered enzyme with different catalytic capabilities and preferences, and may, following subsequent mutations, provide a pathway for the evolution of new enzymes.
- 4) The effect of metal replacement on active site geometry is unknown.  $(k_{cat}/K_M)^{lim}$  value for Mg<sup>2+</sup> form of PP1 $\gamma$  decreased about 3 orders of magnitude compared to the wild type. The reduced catalytic efficiency might be caused by weakening the nucleophilicity of metal bridging water molecule or a reduction in polarizing the substrates.

#### 4.4 References

- (1) Zhang, Z.; Zhao, S.; Long, F.; Zhang, L.; Bai, G.; Shima, H.; Nagao, M.; Lee, E. Y. *J. Biol. Chem.* **1994**, *269*, 16997-17000.
- (2) Zhang, J.; Zhang, Z.; Brew, K.; Lee, E. Y. *Biochemistry* **1996**, *35*, 6276-6282.
- (3) Zhang, L.; Zhang, Z.; Long, F.; Lee, E. Y. *Biochemistry* **1996**, *35*, 1606-1611.

- (4) Huang, H. B.; Horiuchi, A.; Goldberg, J.; Greengard, P.; Nairn, A. C. *Proc Natl Acad Sci U S A* **1997**, *94*, 3530-3535.
- (5) Goldberg, J.; Huang, H. B.; Kwon, Y. G.; Greengard, P.; Nairn, A. C.; Kuriyan, J. *Nature* **1995**, *376*, 745-753.
- (6) McWhirter, C.; Lund, E. A.; Tanifum, E. A.; Feng, G.; Sheikh, Q. I.; Hengge, A. C.; Williams, N. H. *J. Am. Chem. Soc.* **2008**, *130*, 13673-13682.
- (7) Riordan, J. F.; McElvany, K. D.; Borders, C. L., Jr. *Science* **1977**, *195*, 884-886.
- (8) Zhuo, S.; Clemens, J. C.; Stone, R. L.; Dixon, J. E. *J. Biol. Chem.* **1994**, *269*, 26234-26238.
- (9) Chu, Y.; Lee, E. Y.; Schlender, K. K. *J. Biol. Chem.* **1996**, *271*, 2574-2577.

## CHAPTER 5

### CONCLUSIONS

The research presented in this dissertation is aimed at designing various substrates and protein phosphatase 1 (PP1) mutants to understand the hydrolysis mechanism and shed light on the origin of catalytic promiscuity of PP1.

Six different substrate classes were chosen that had variations in charge, reactivity, the center atom and the size of the transferring group, as well as in the mechanism and transition states for uncatalyzed hydrolysis: aryl phosphate monoesters (**1**), aryl phosphorothioate monoesters (**2**), aryl fluorophosphate monoesters (**3**), aryl methylphosphonate monoesters (**4**), aryl methyl phosphate diesters (**5**) and aryl sulfate monoesters (**6**). A total of eighteen substrates were successfully synthesized and identified. Two substrates (**3b** and **3c**) were newly reported compounds.

Enzyme kinetics studies, linear free energy relationships and kinetic isotope effect are the three major tools employed in this study to obtain the insight into the nature of transition state and reaction mechanisms.

PP1 $\gamma$  performs multiple turnovers with each substrate examined, and saturation kinetics is observed for all substrates except *p*-nitrophenyl sulfate, **6**. Largely coincident, bell-shaped pH-rate profiles of substrate **2a**, **3a** and **5a** in this work, and that of substrate **1a** and **4a** from the literature, indicate that the same active site and enzymatic mechanism is followed, with catalysis by both an acidic and basic residue. The metal-bridging water molecule is implicated to be the nucleophile and the deprotonation of this species is represented by  $pK_{a1}$  based on deduced  $pK_a$  from pH-rate profile and the crystal structure

of PP1. The residue H125 is plausibly assigned to act as a general acid, responsible for the basic limb of the pH-rate profile.

At pH 7, which is near the optimal pH for all five substrate classes, variations in the molecular properties of the substrates affect the turnover number ( $k_{\text{cat}}$ ) more than the Michaelis constant ( $K_{\text{M}}$ ) for PP1 $\gamma$ . The variation of  $k_{\text{cat}}$  values from the fastest which is phosphate monoester **1a**, to the slowest, which is phosphate diester **5a**, is  $\sim 200$ -fold. However, the variation of  $K_{\text{M}}$  is only  $\sim 4$ -fold. The catalytic efficiency of PP1 $\gamma$  decreases in the order **1a**>**4a**  $\sim$  **3a**>**2a**>**5a**. The  $(k_{\text{cat}}/K_{\text{M}})^{\text{lim}}$  values vary from a high of  $1850 \text{ M}^{-1}\text{s}^{-1}$  for the phosphate monoester **1a** to a low of  $0.98 \text{ M}^{-1}\text{s}^{-1}$  for the diester **5a**. Catalytic efficiencies for the monoanionic substrates **3a** and **4a** are superior to that for **2a**, although **2a** shares the dianionic charge of phosphate monoesters that are the natural substrates for PP1 $\gamma$ .

The second-order rate enhancements  $[(k_{\text{cat}}/K_{\text{M}})^{\text{lim}}/k_{\text{w}}]$  by PP1 $\gamma$ , which reflect the degree of reduction of the activation barrier by PP1 $\gamma$  for the hydrolysis reactions, vary from  $1.7 \times 10^{11}$  to  $8.0 \times 10^{13}$ , and correspond to reductions in activation energy of from 16 to 19 kcal/mol. The high second-order rate enhancement values but narrow changes demonstrate that PP1 $\gamma$  is an effective catalyst for all of these substrates, despite the variations in size and charge of the transferring group.

The linear free energy relationships have been measured for substrates **2** and **3**. The Brønsted slopes  $\beta_{\text{lg}}$  for all of the PP1 $\gamma$ -catalyzed reactions falling within a narrow range from -0.25 to -0.40 provide evidence that PP1 $\gamma$ -catalyzed reactions share more similar transition states, which is in contrast to those for the uncatalyzed reactions (which range from -0.63 to -1.23). Small  $\beta_{\text{lg}}$  values shown by all four substrates classes indicate

that enzyme-catalyzed hydrolysis has low sensitivity to the  $pK_a$  of the leaving group, which can either be caused by a more associative transition state, or by neutralization of the buildup of negative charge on the leaving group oxygen in a dissociative transition state.

Heavy atom kinetic isotope effects (KIEs) for aryl phosphorothioate monoesters (**2a**) catalyzed by PP1 $\gamma$  were measured by the competitive method and show diminish from their values in the uncatalyzed hydrolysis. The  $^{15}(V/K)$  KIE of unity indicates that leaving group neutralization is complete. The magnitude of the primary  $^{18}(V/K)_{\text{bridge}}$  is reduced compared to uncatalyzed reaction, consistent with general acid protonation of the leaving group in the transition state that is hypothesized to be carried out by histidine 125. The similarity between this value obtained with new substrates and previously reported values for substrates **1a** and **4a**, also supports the notion from the Brønsted  $\beta_{\text{lg}}$  data that bond fission to the leaving group is similar in each substrate reaction on the enzyme. The other oxygen KIE,  $^{18}(V/K)_{\text{nonbridge}}$ , is significantly inverse, in contrast to the normal KIE for the solution hydrolysis, which arises from coordination of the thiophosphoryl group to the metal center.

The overall picture supported by the LFER and KIE data is a transition state with extensive P-O bond fission involving general acid protonation of the leaving group. The mechanism of the PP1 $\gamma$ -catalyzed reactions and transition states are similar for all substrate types, with slightly better neutralization of the leaving group in the reactions of phosphorothioates.

The PP1 $\gamma$  active site has been proved to be tolerant of variations in the geometry of bound ligands by inhibition experiments. This characteristic may permit the effective

catalysis even of substrates whose steric requirements may result in perturbations to the positioning of the transferring group both in the initial enzyme-substrate complex, and in the transition state. Moreover, the active site of PP1 $\gamma$  is more affected by charge changes than the geometry.

The reason for the inability of PP1 $\gamma$  to catalyze the hydrolysis of the sulfate ester is unclear, and unexpected. The weaker Lewis basicity of the sulfate group compared to the phosphate group might cause the loss of the ability for active site interactions to effectively stabilize the transition state for sulfuryl transfer relative to phosphoryl transfer.

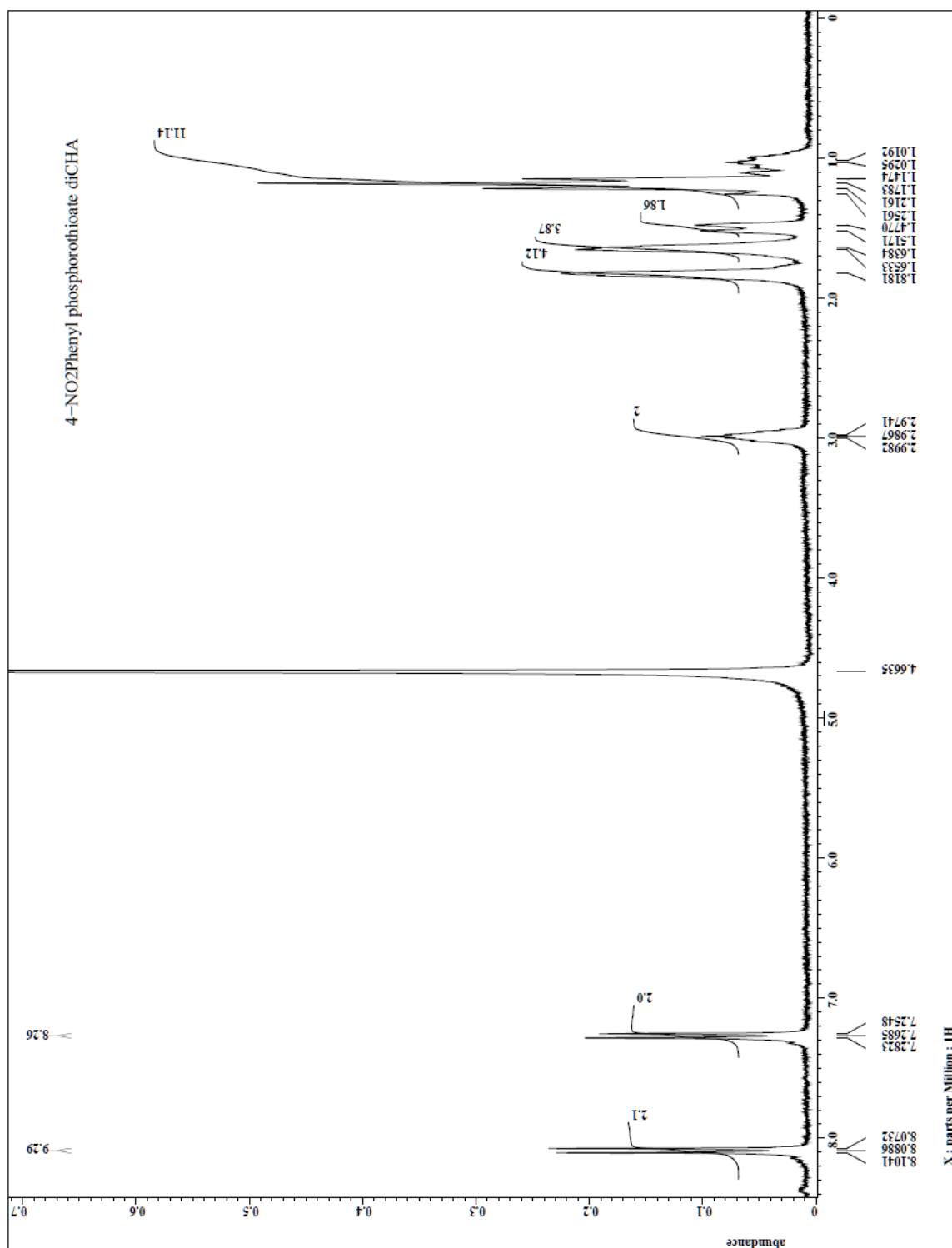
The R96 and R221 residues in the active site of PP1 $\gamma$  are suggested to bind to the substrate oxygens and may contribute to stabilization of a penta-coordinate transition state. Mutations of R96 and R221 to lysine maintain hydrogen bond donating ability, but provide additional space that might facilitate binding and catalysis of the more sterically demanding substrates. The pH dependence of pNPP hydrolysis by two mutants, R96K and R221K, has been determined at 25 °C in first time. The pH-rate profiles of  $k_{\text{cat}}/K_M$  values for wild type PP1 $\gamma$ , R96K and R221K mutants largely coincide suggesting the same active site and enzymatic mechanism is followed. The conservative mutation of arginine 221 to lysine results in a mutant that more effectively catalyzes monoanionic substrates than the native enzyme. The surprising result in substrate preference from a single, conservative mutation lends support to the notion that mutations following gene duplication can result in an altered enzyme with different catalytic capabilities and preferences, and may, following subsequent mutations, provide a pathway for the evolution of new enzymes.

The observations obtained from PP1 $\gamma$ -catalyzed reactions suggest that the promiscuous activity of PP1 can be explained by a number of possible general criteria, which could shed light on the key role of catalytic promiscuity in the natural history of enzymes, and creation families and superfamilies of potent and highly specialized enzymes.

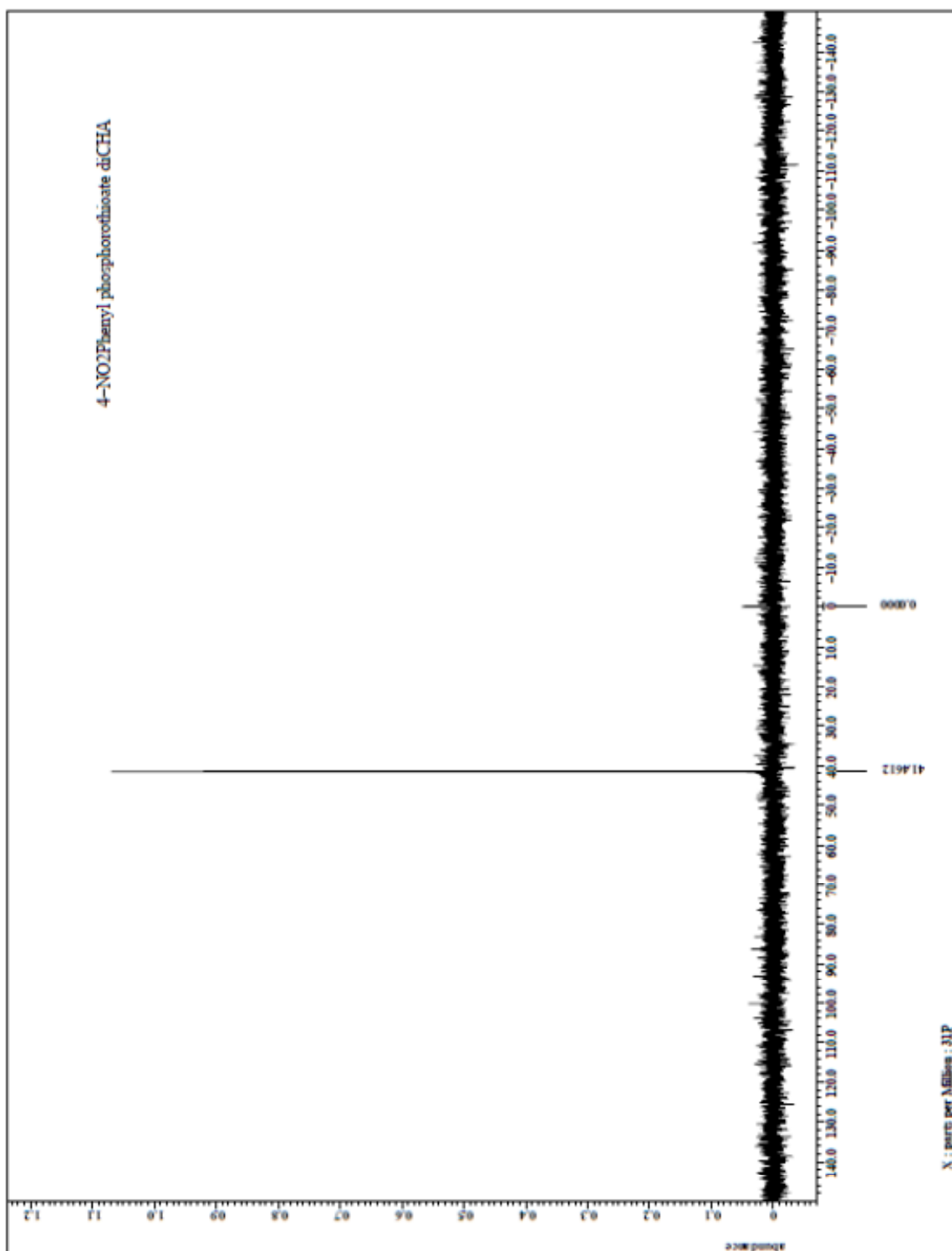
(1). *Native and promiscuous reactions share key features.* In this case, the PP1 $\gamma$ -catalyzed reactions involve the same general acid/base catalysis and require the similar transition states during the catalysis, regardless the nature of the transition states in uncatalyzed reactions. At the same time, some rather more subtle mechanistic features influence the degree of promiscuity very little, like substrate charges and geometries.

(2). *It is possible to alter the substrate preference by single, conservative mutations in the reactive active site.* In this case, the conservative mutation of arginine 221 to lysine results in a mutant that more effectively catalyzes monoanionic substrates than the native enzyme. More systematic research would be done to explore the origin of this unique preference. The catalytic motif of two metal ions has been shown to lower the  $pK_a$  of the nucleophile and thus increasing the reactivity of nucleophile for the reactions. More efforts would be donated to develop a technique to confirm the metal centers in PP1 $\gamma$  active site and further study the reactivation function of different metal ions.

APPENDIX



**A1.** <sup>1</sup>H NMR spectrum of **2a** [Chapter 2]



A2. <sup>31</sup>P NMR spectrum of **2a** [Chapter 2]

# ATLANTIC MICROLAB, INC.

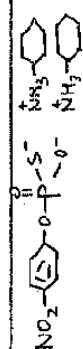
**SUBMITTER**

Sample No. 1      Company / School Utah State University      Address 0300 Old Main Hill      Logan, UT 84322

P.O. Box 2288      No. 10      P.O. Box 30091      (770) 242-0082

[www.atlanticmicrolab.com](http://www.atlanticmicrolab.com)      PROFESSOR/SUPERVISOR: Alvan C. Hengge      YUAN CHU      DATE 04/28/2010

P.O. #: 4246040016067235

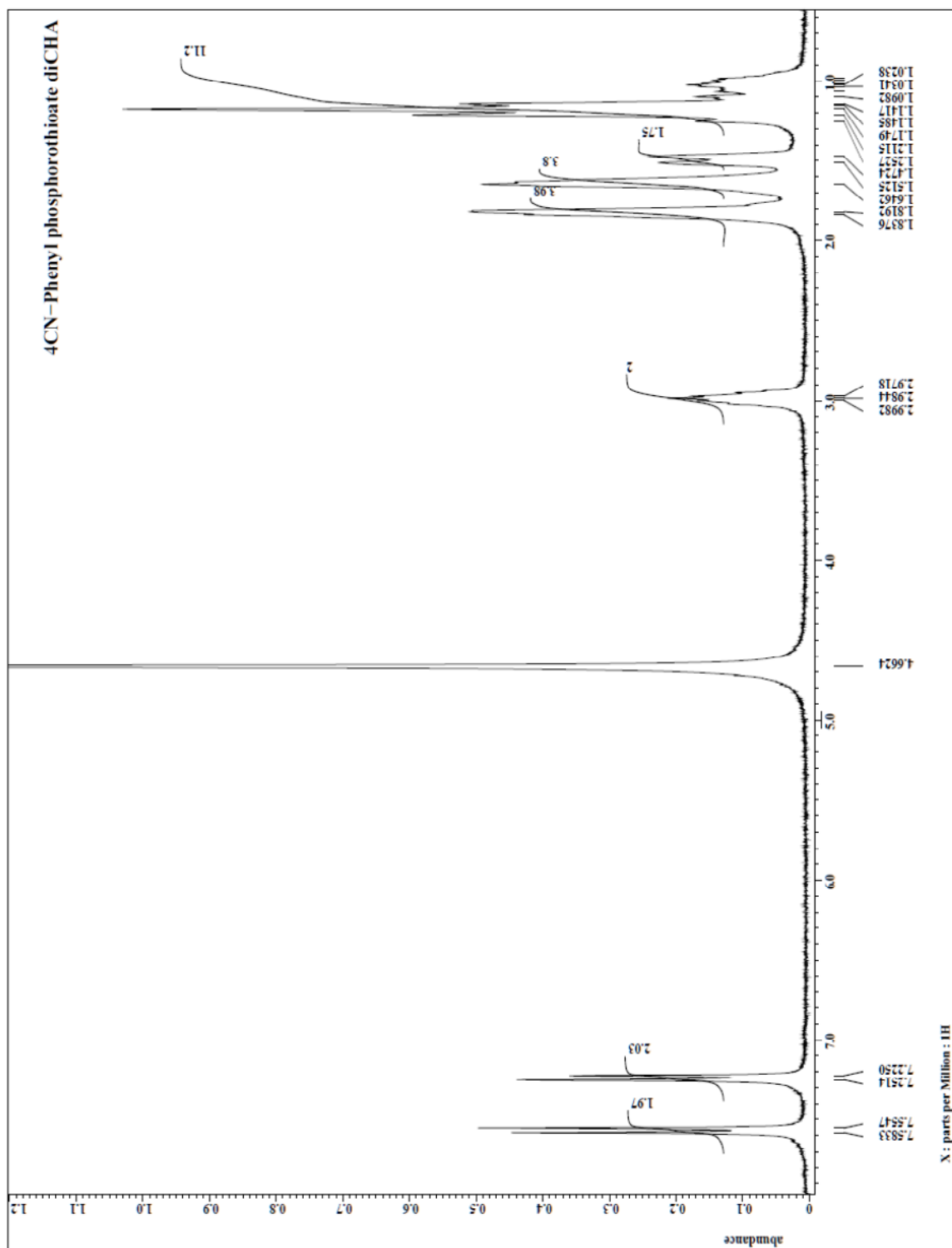


Element	Theory	Found	Single <input checked="" type="checkbox"/> Duplicate <input type="checkbox"/>
C	49.87	50.00	Elements Present: C, H, O, P, S, N
H	7.44	7.25	Analyze for: C, H, N
N	9.69	9.68	Hygroscopic <input type="checkbox"/> Explosive <input type="checkbox"/> M.P. _____ B.P. _____
To be dried: Yes <input type="checkbox"/> No <input checked="" type="checkbox"/>			
Temp. _____ Vac. _____ Time _____			
FAX Service <input type="checkbox"/> EMAIL Service <input checked="" type="checkbox"/>			
FAX # / EMAIL <u>yuan.chu@aggiemail.usu.edu</u>			
Rush Service <input type="checkbox"/> (SEE CURRENT PRICE LIST)			
Phone Service <input type="checkbox"/>			
Phone No. _____			

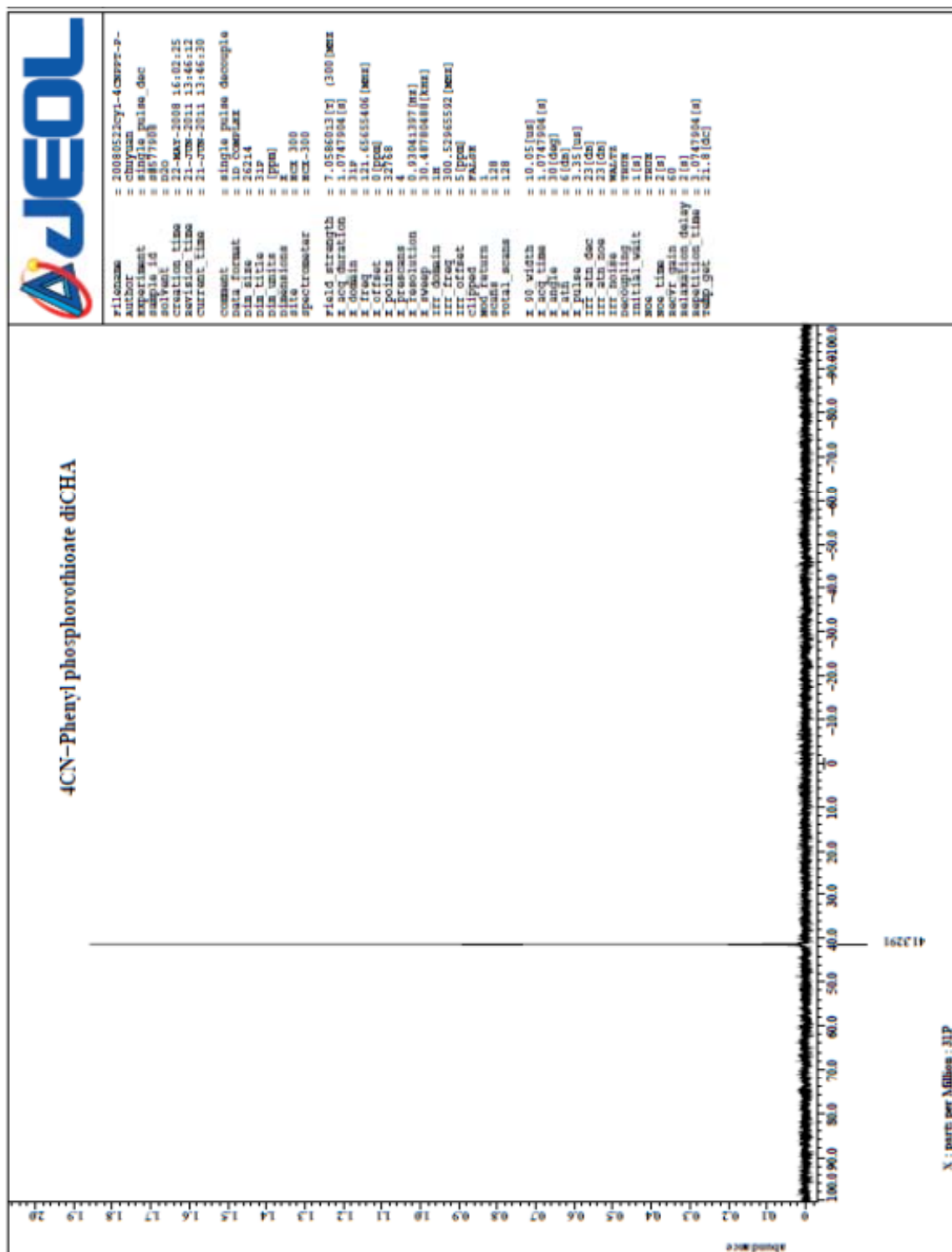
Date Received MAY 03 2010      Date Completed MAY 04 2010

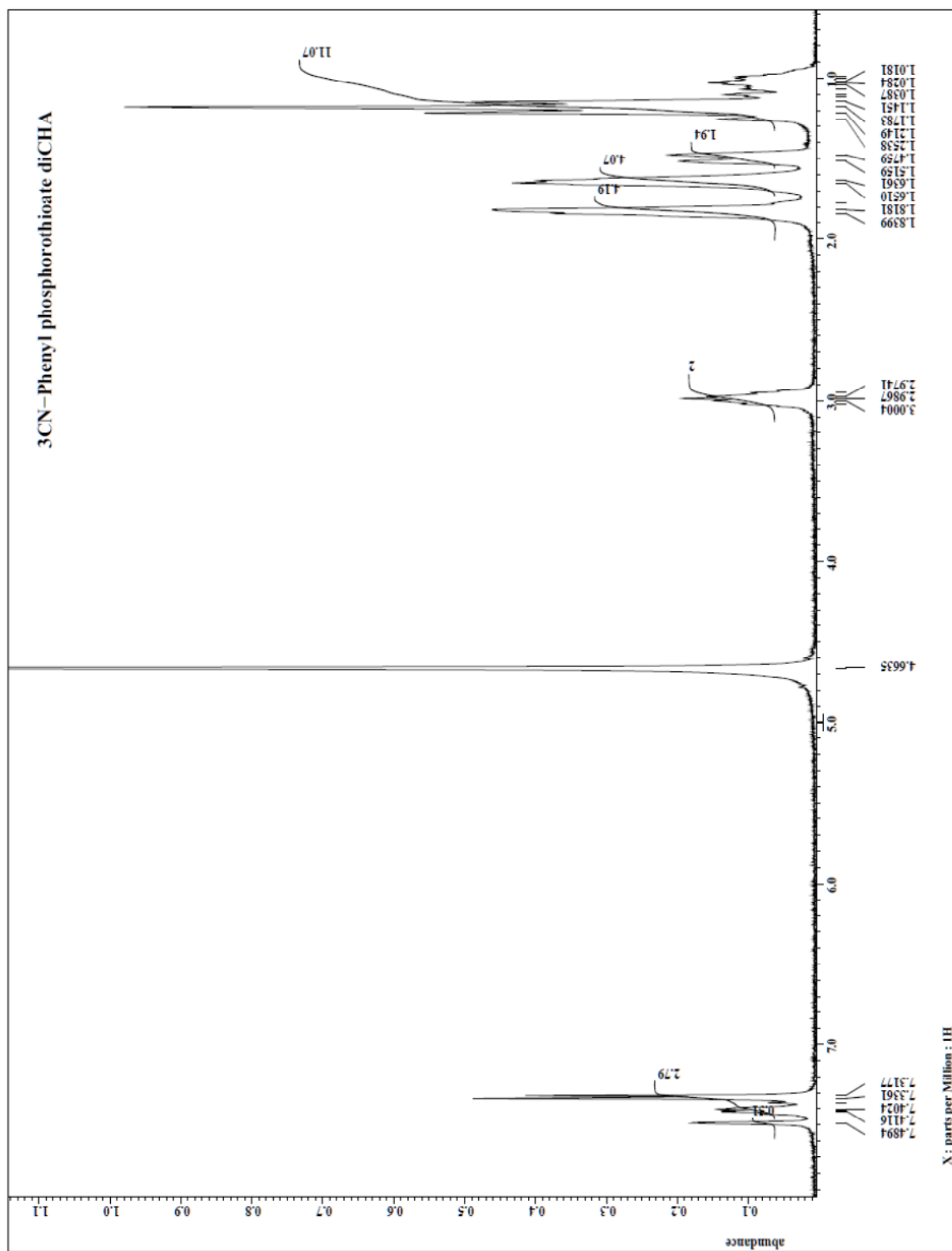
Remarks: \_\_\_\_\_

A3. Elemental analysis result of 2a [Chapter 2]

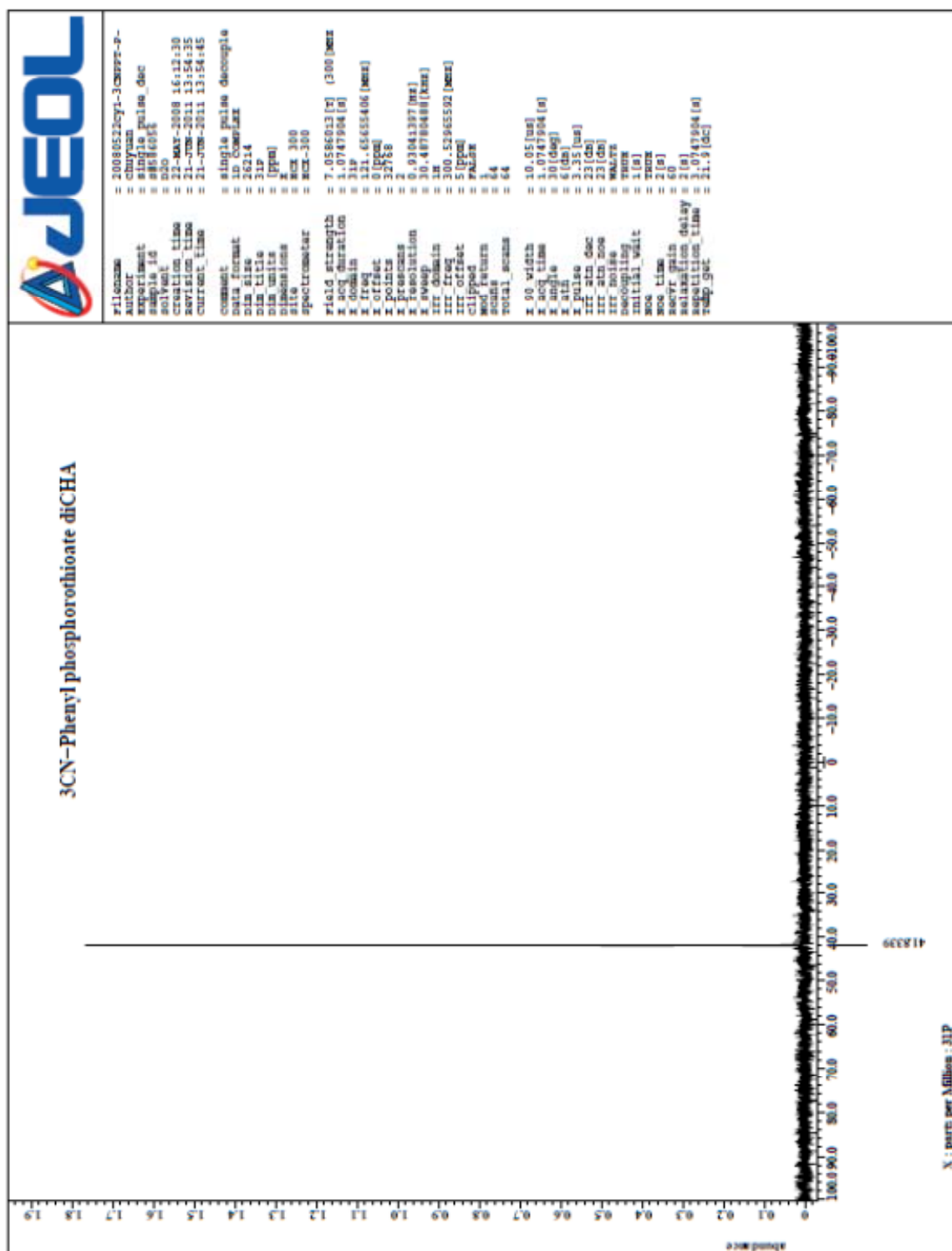


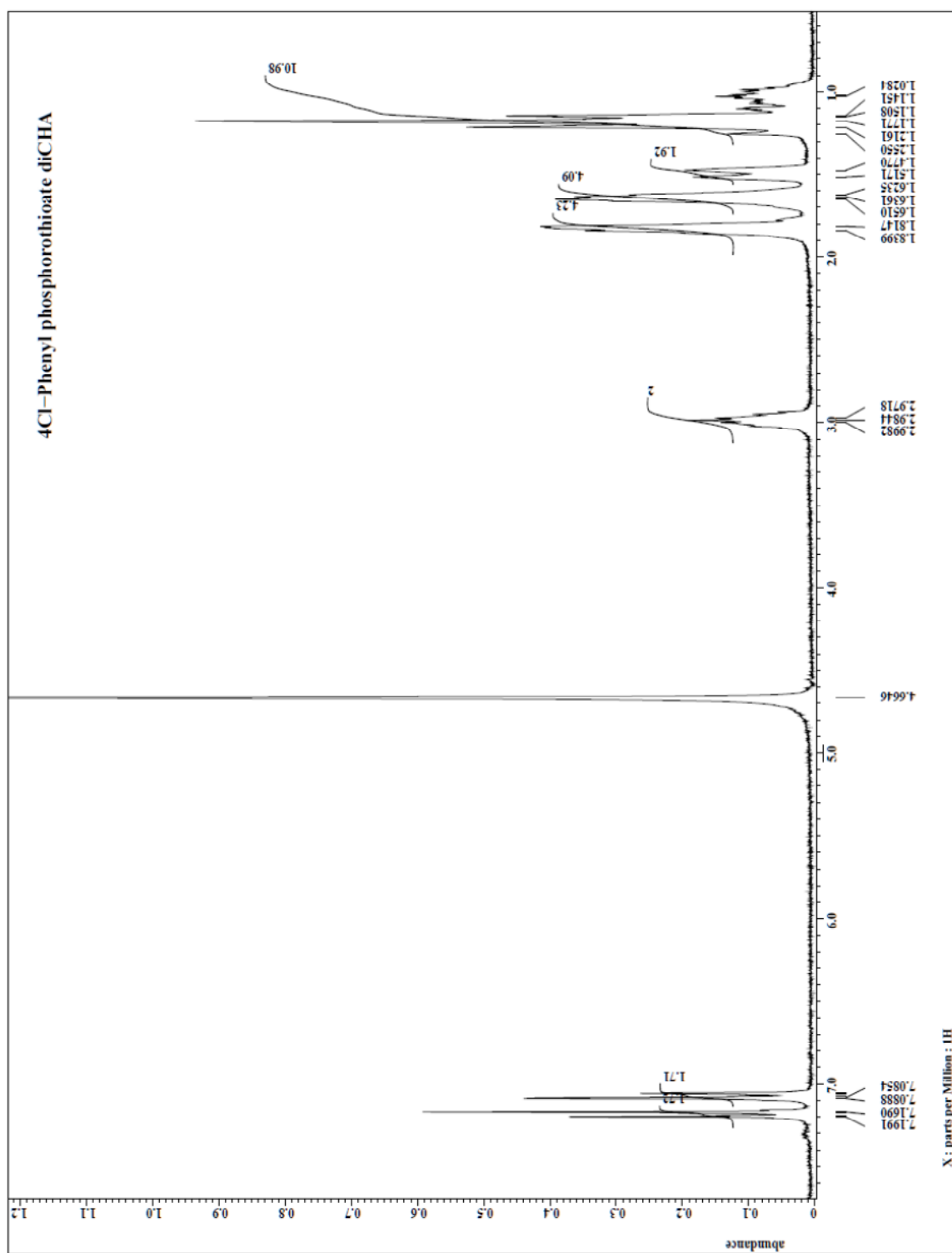
A4.  $^1\text{H}$  NMR spectrum of **2b** [Chapter 2]

A5.  $^{31}\text{P}$  NMR spectrum of **2b** [Chapter 2]

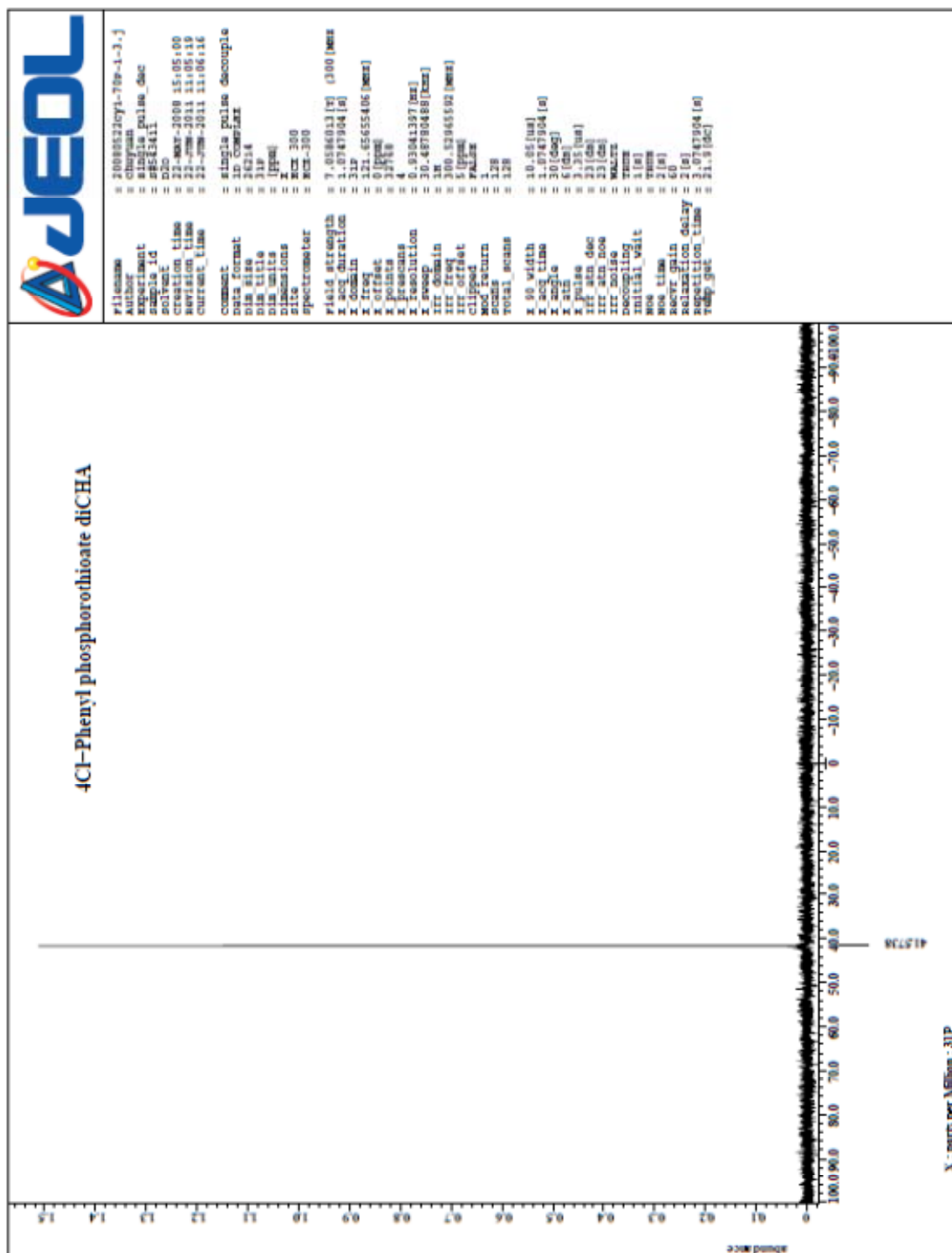


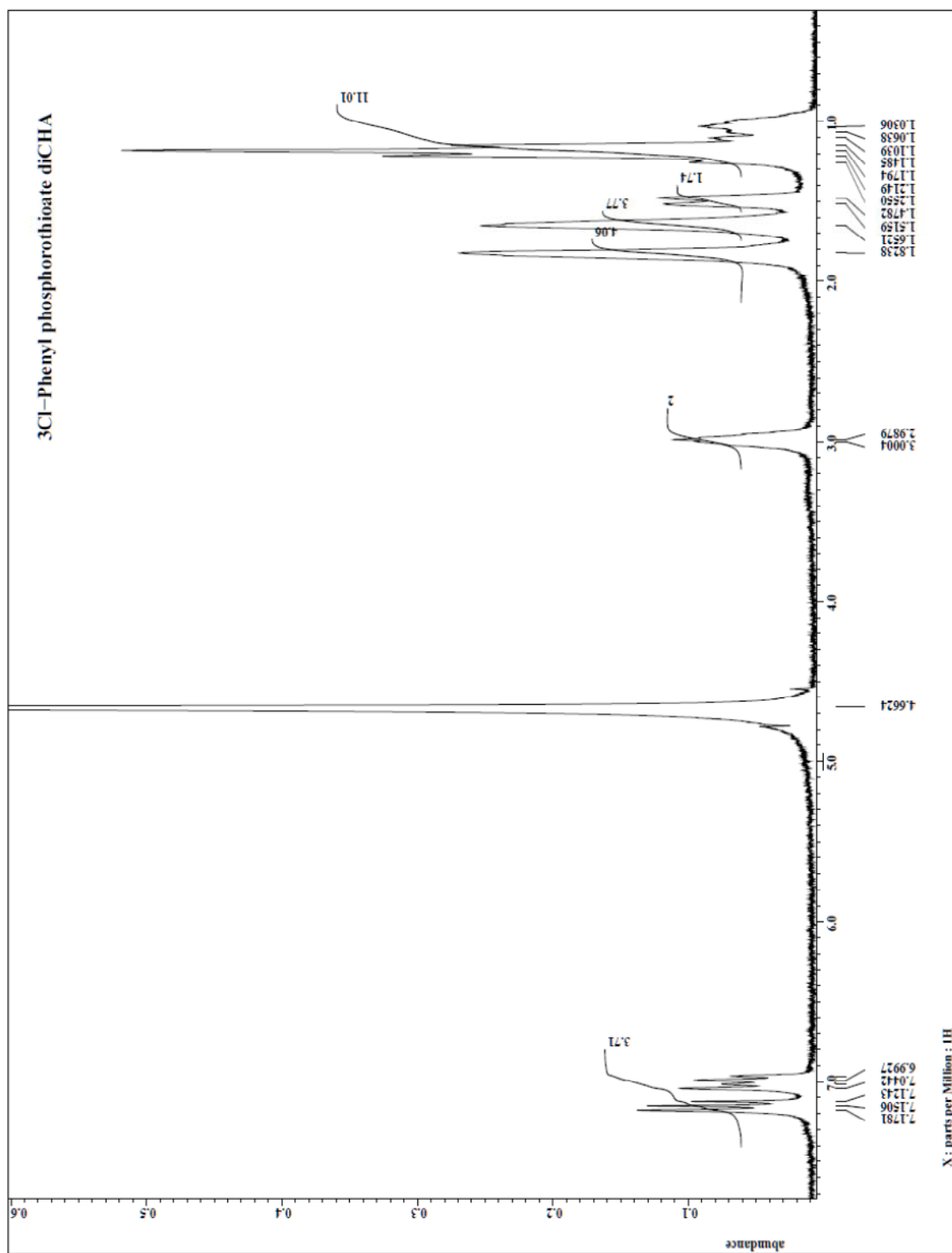
A6.  $^1\text{H}$  NMR spectrum of **2c** [Chapter 2]

A7.  $^{31}\text{P}$  NMR spectrum of **2c** [Chapter 2]

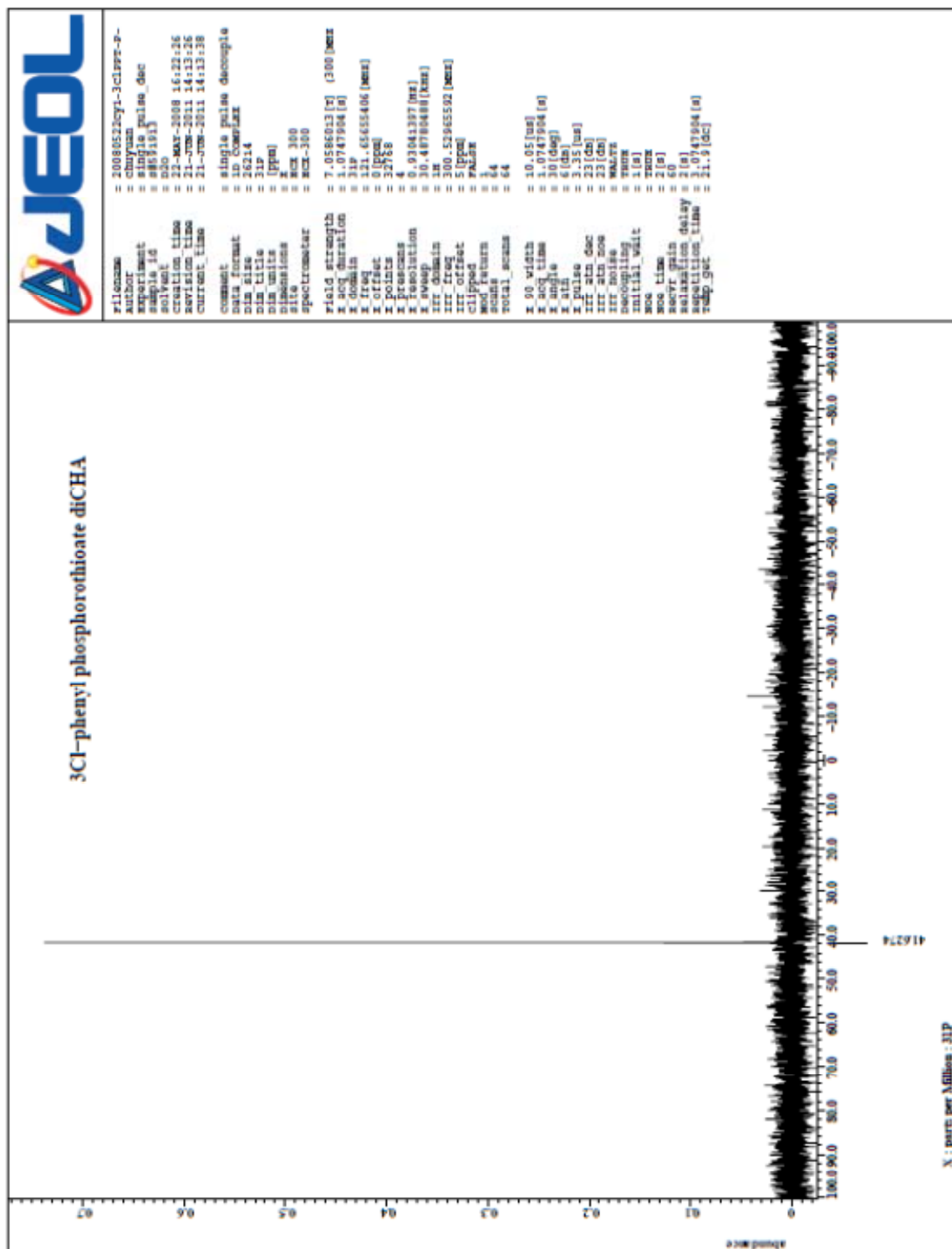


A8.  $^1\text{H}$  NMR spectrum of **2d** [Chapter 2]

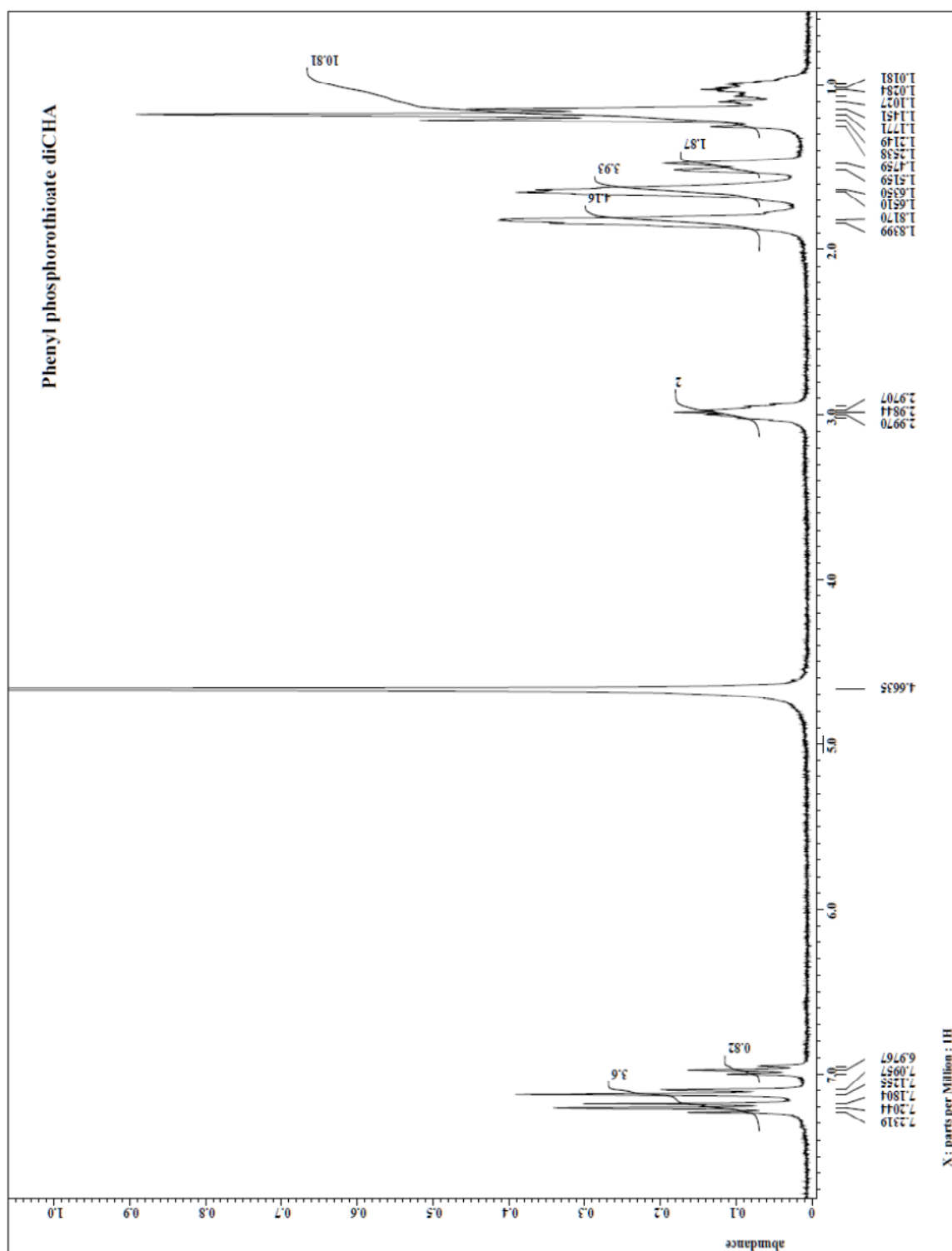
A9.  $^{31}\text{P}$  NMR spectrum of **2d** [Chapter 2]



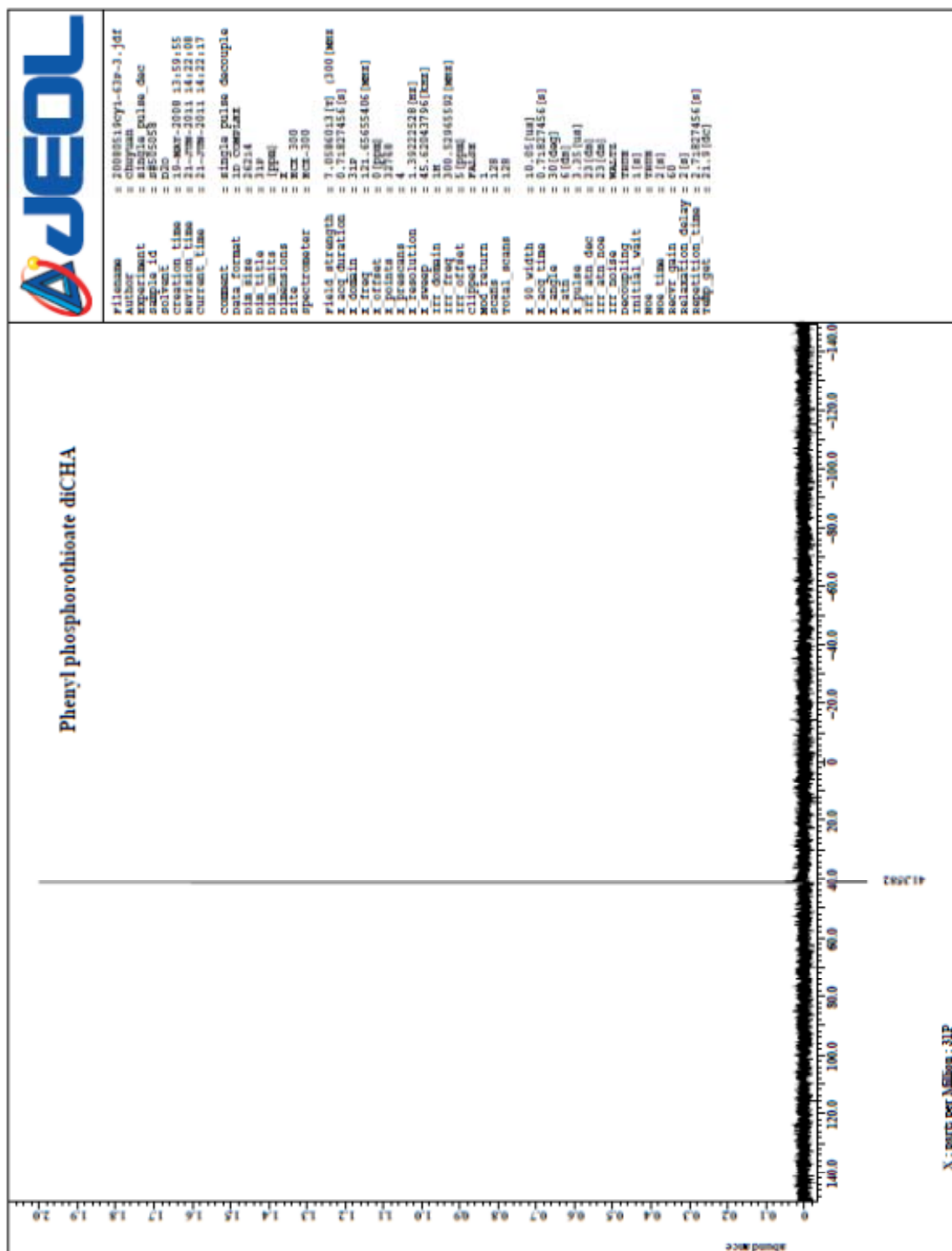
A10.  $^1\text{H}$  NMR spectrum of **2e** [Chapter 2]

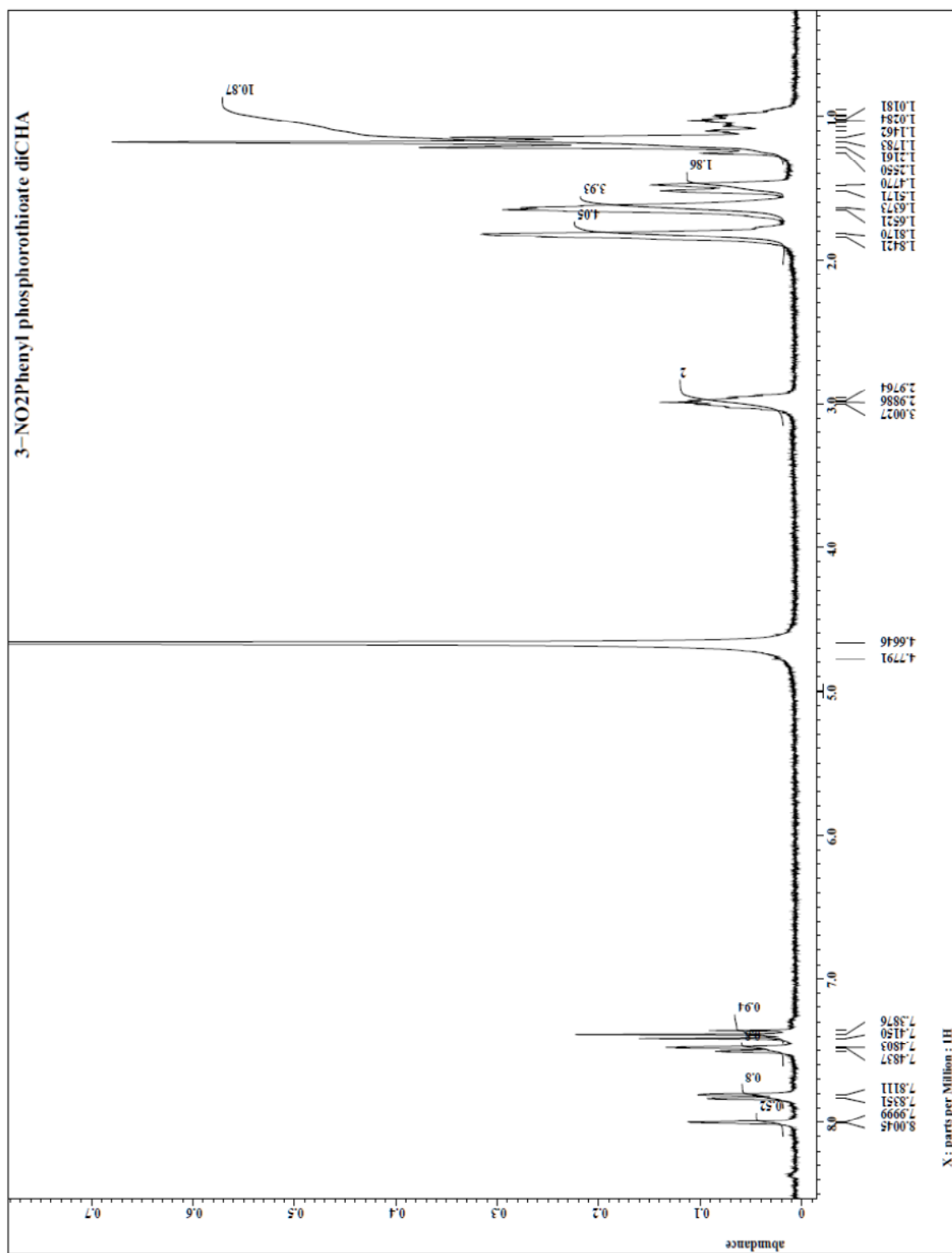


**A11.**  $^{31}\text{P}$  NMR spectrum of **2e** [Chapter 2]



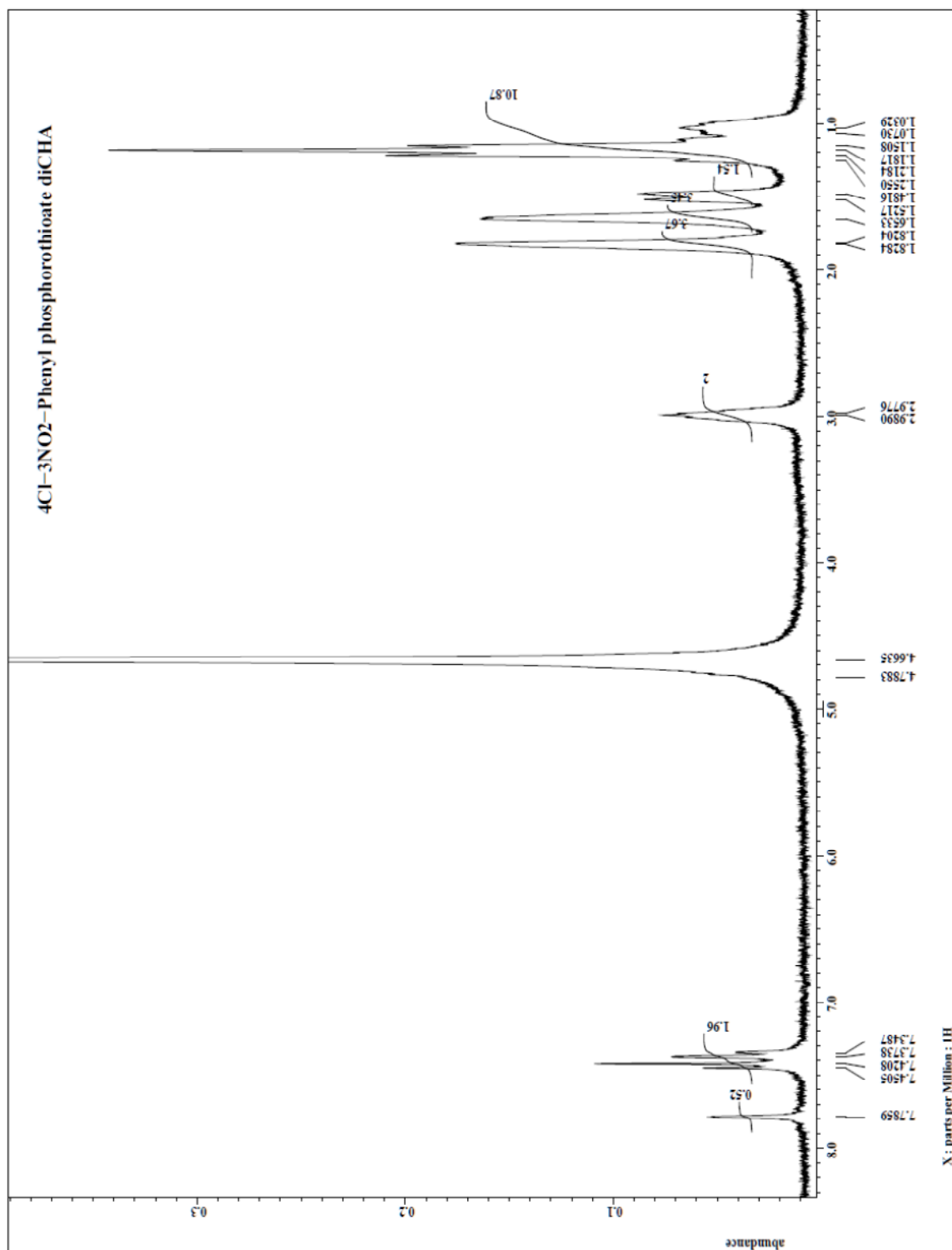
A12.  $^1\text{H}$  NMR spectrum of **2f** [Chapter 2]

A13.  $^{31}\text{P}$  NMR spectrum of **2f** [Chapter 2]

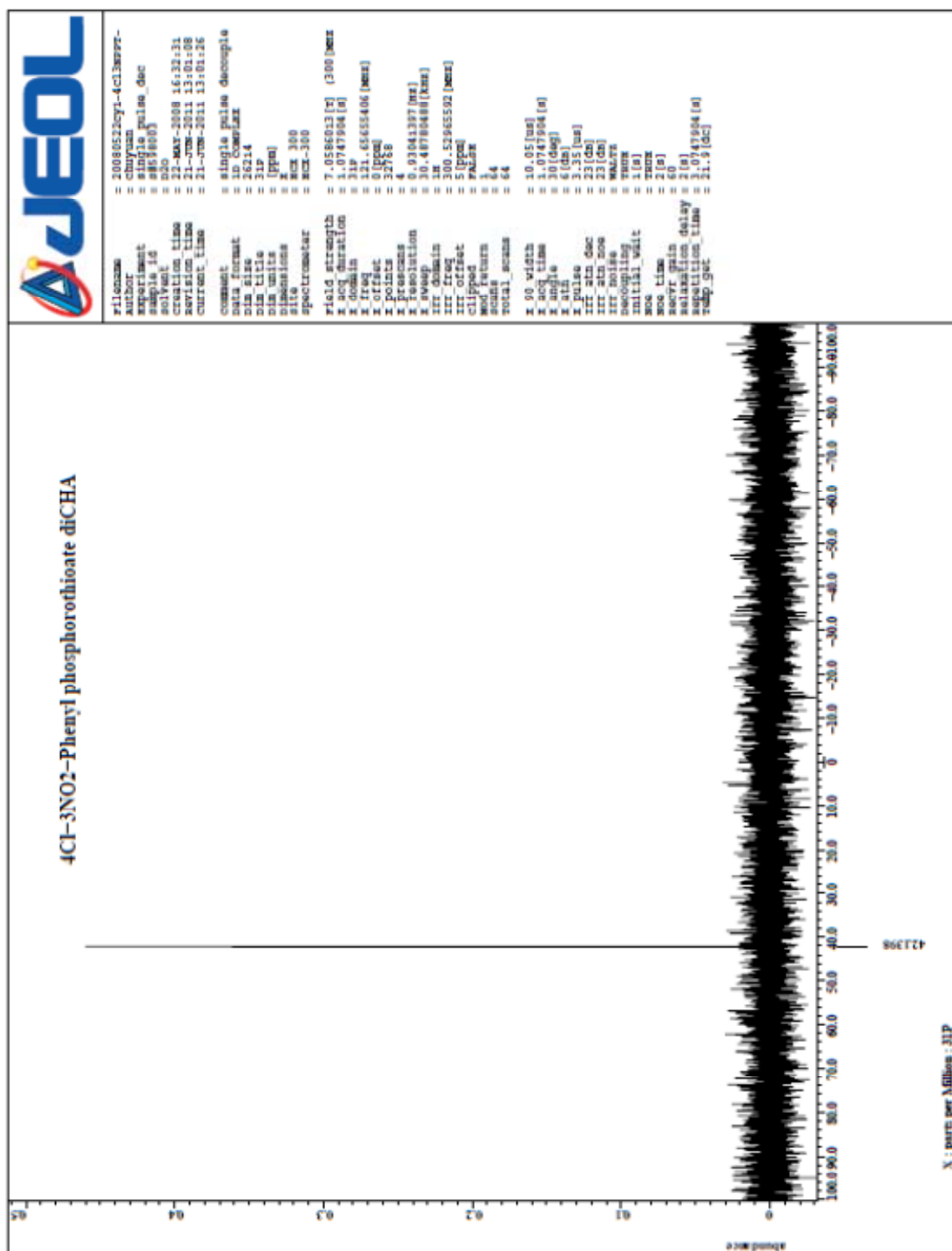


A14. <sup>1</sup>H NMR spectrum of **2g** [Chapter 2]

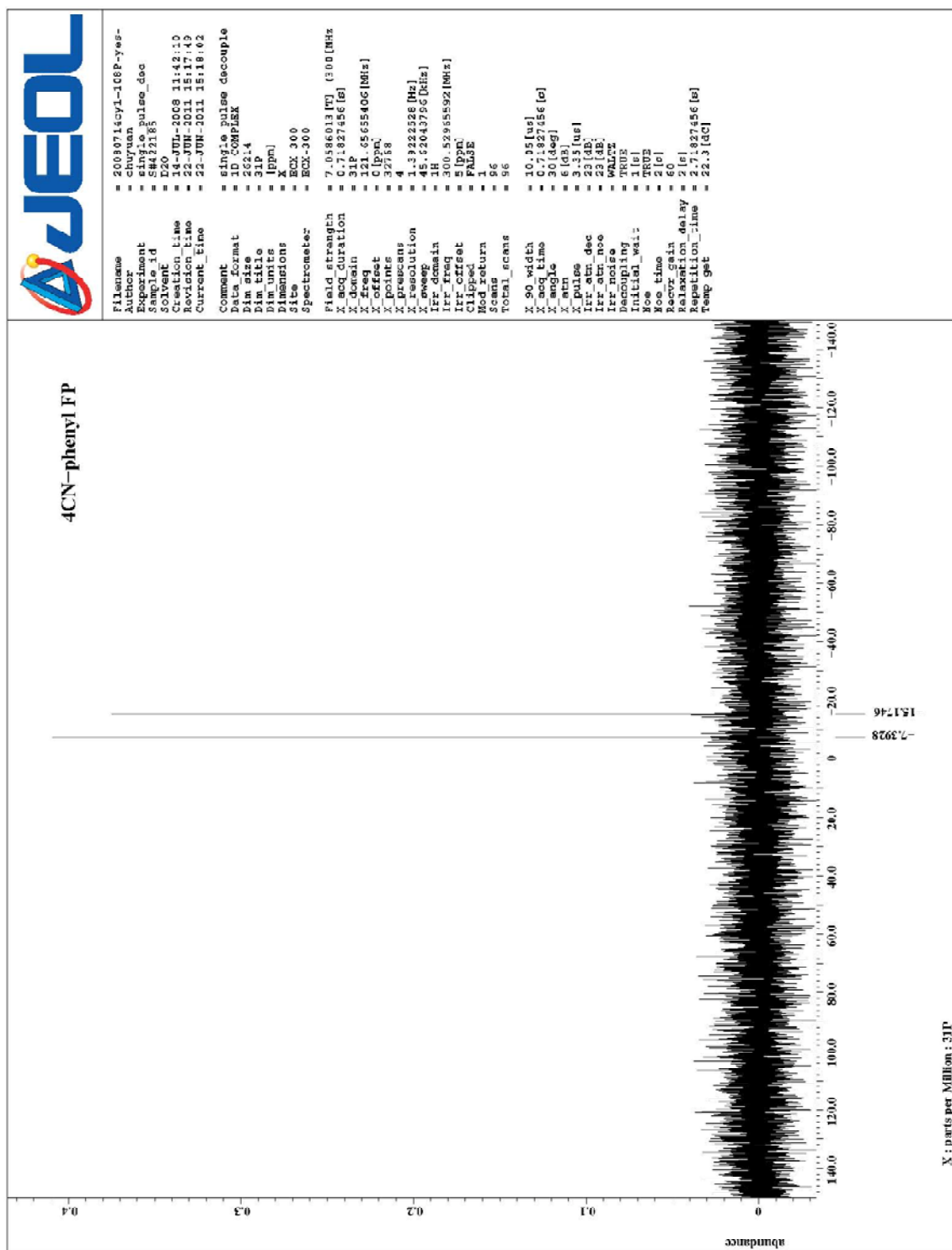




**A16.**  $^1\text{H}$  NMR spectrum of **2h** [Chapter 2]

A17. <sup>31</sup>P NMR spectrum of **2h** [Chapter 2]

A18.  $^1\text{H}$  NMR spectrum of **3b** [Chapter 2]

A19.  $^{31}\text{P}$  NMR spectrum of **3b** [Chapter 2]



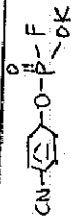
# ATLANTIC MICROLAB, INC.

Sample No. 2

P.O. Box 2288  
Norcross, Georgia 30091  
(770) 242-0082

[www.atlanticmicrolab.com](http://www.atlanticmicrolab.com)

PROFESSOR/SUPERVISOR: Alvan C. Hengge  
P.O. #: 4246040016067235



**SUBMITTER**

Company / School: Utah State University  
Address: 0300 Old Main Hill  
Logan, UT 84322

NAME: YUAN CHU      DATE: 04/28/2010

Element	Theory	Found	Single <input checked="" type="checkbox"/>	Duplicate <input type="checkbox"/>
C	35.15	34.87		
H	1.69	1.50		
N	5.86	5.75		
Elements Present: C, H, O, P, F, N, K Analyze for: C, H, N Hygroscopic <input type="checkbox"/> Explosive <input type="checkbox"/> M.P. _____ B.P. _____ To be dried: Yes <input type="checkbox"/> No <input checked="" type="checkbox"/> Temp. _____ Vac. _____ Time _____ FAX Service <input type="checkbox"/> EMAIL Service <input checked="" type="checkbox"/> FAX# /EMAIL: yuan.chu@aggilemail.usu.edu Rush Service <input type="checkbox"/> (SEE CURRENT PRICE LIST) Phone Service <input type="checkbox"/> PRICE LIST) Phone No. _____				

Date Received

MAY 03 2010

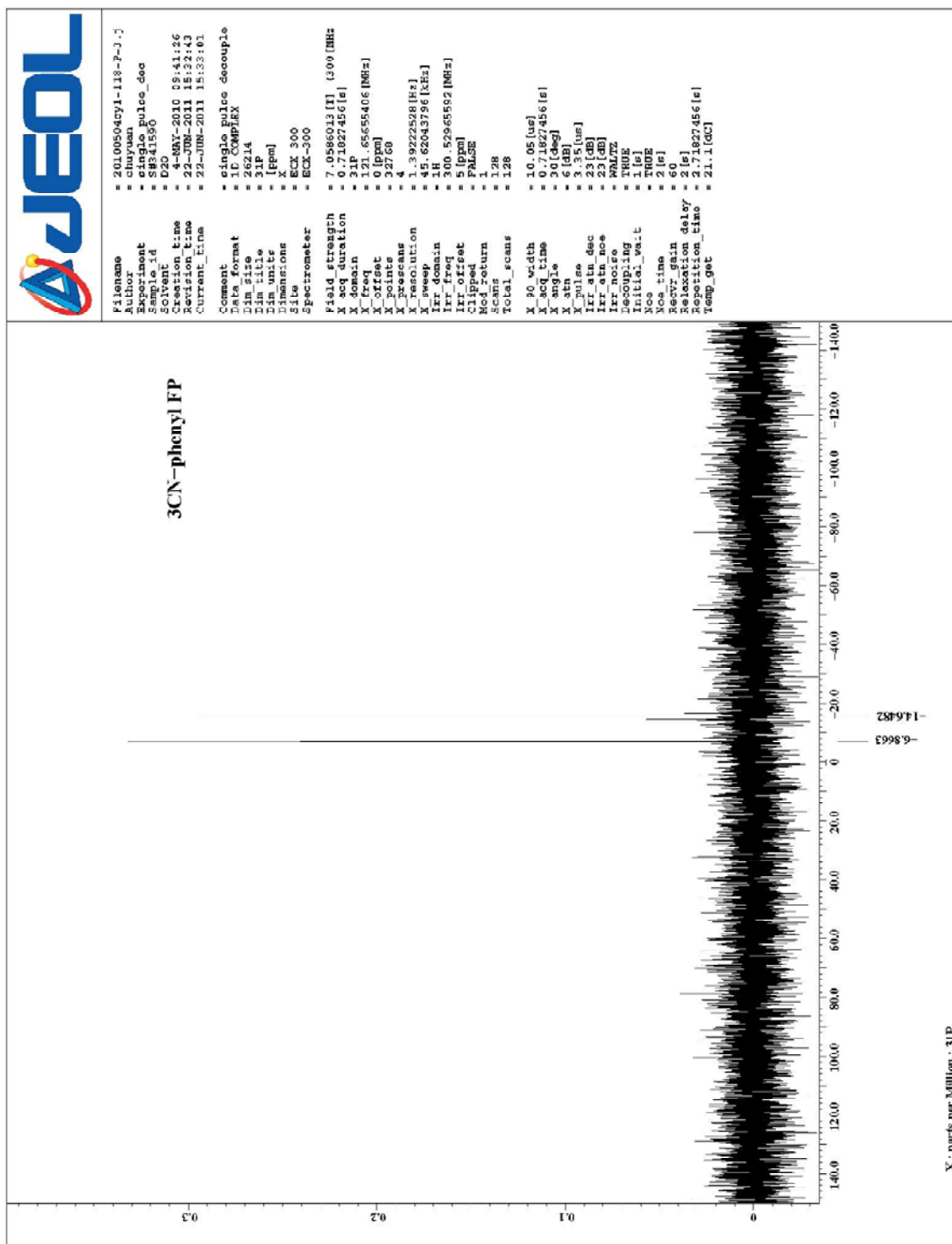
Remarks:

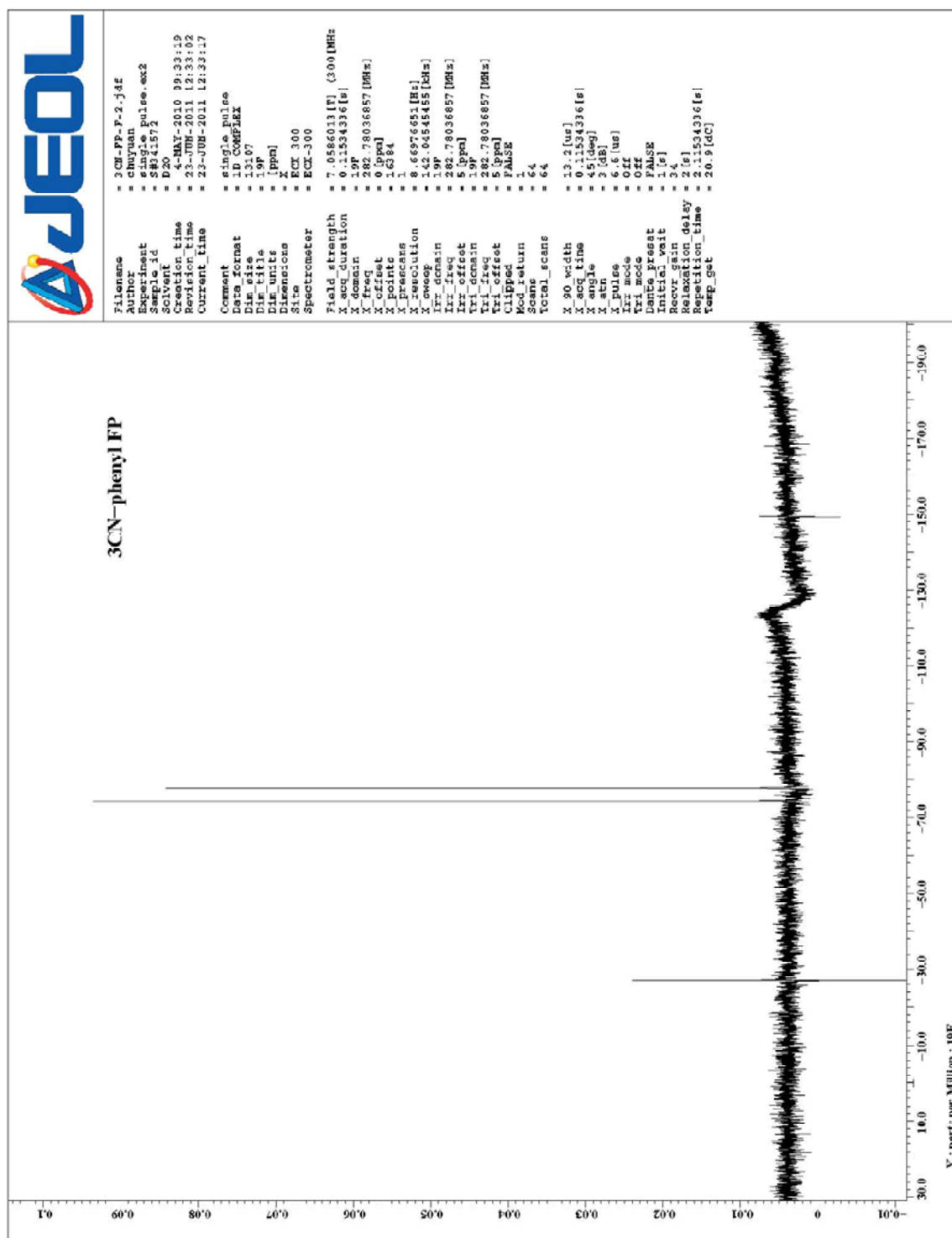
Date Completed

MAY 04 2010

A21. Elemental analysis result of 3b [Chapter 2]



A23.  $^{31}\text{P}$  NMR spectrum of **3c** [Chapter 2]

A24.  $^{19}\text{F}$  NMR spectrum of **3c** [Chapter 2]











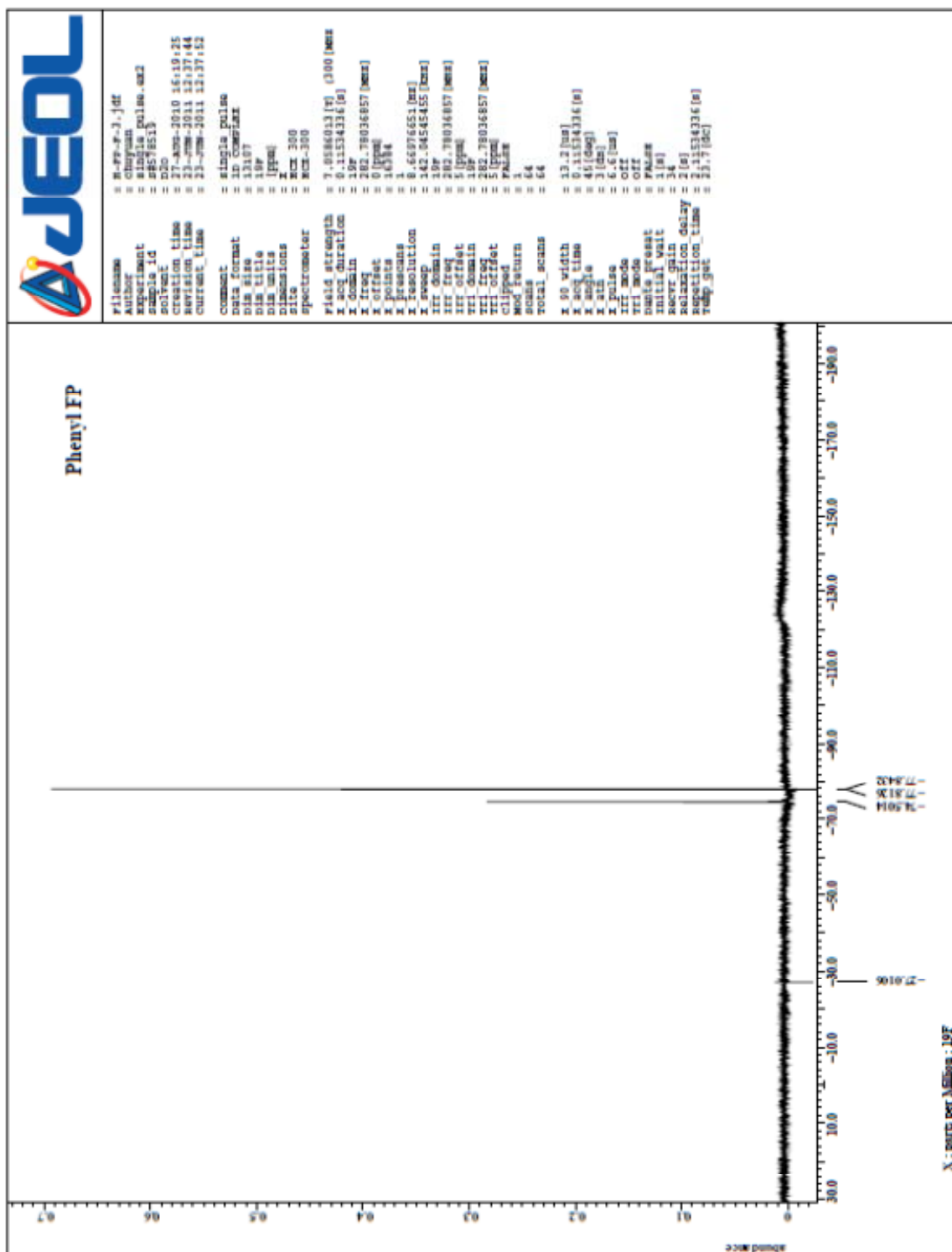


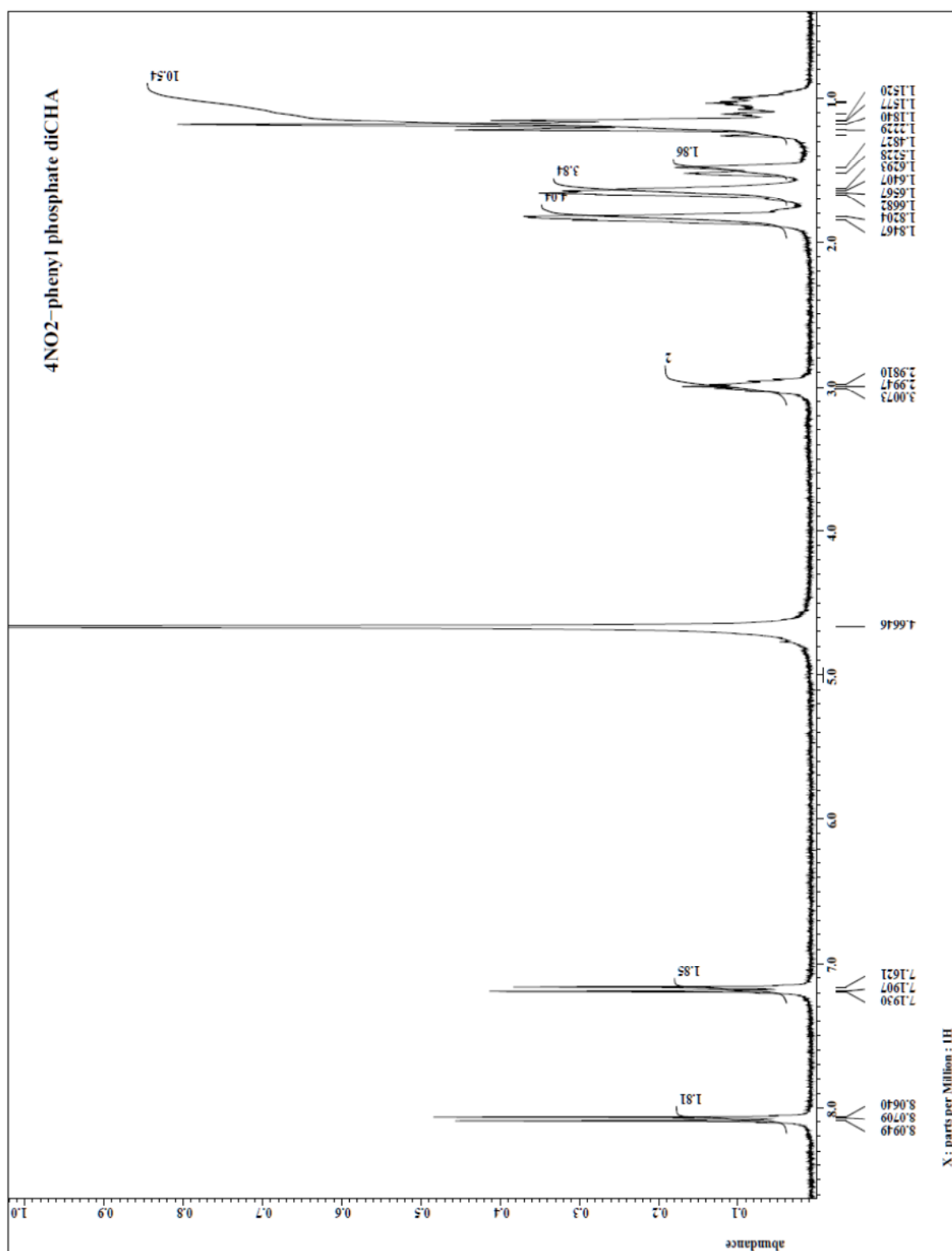






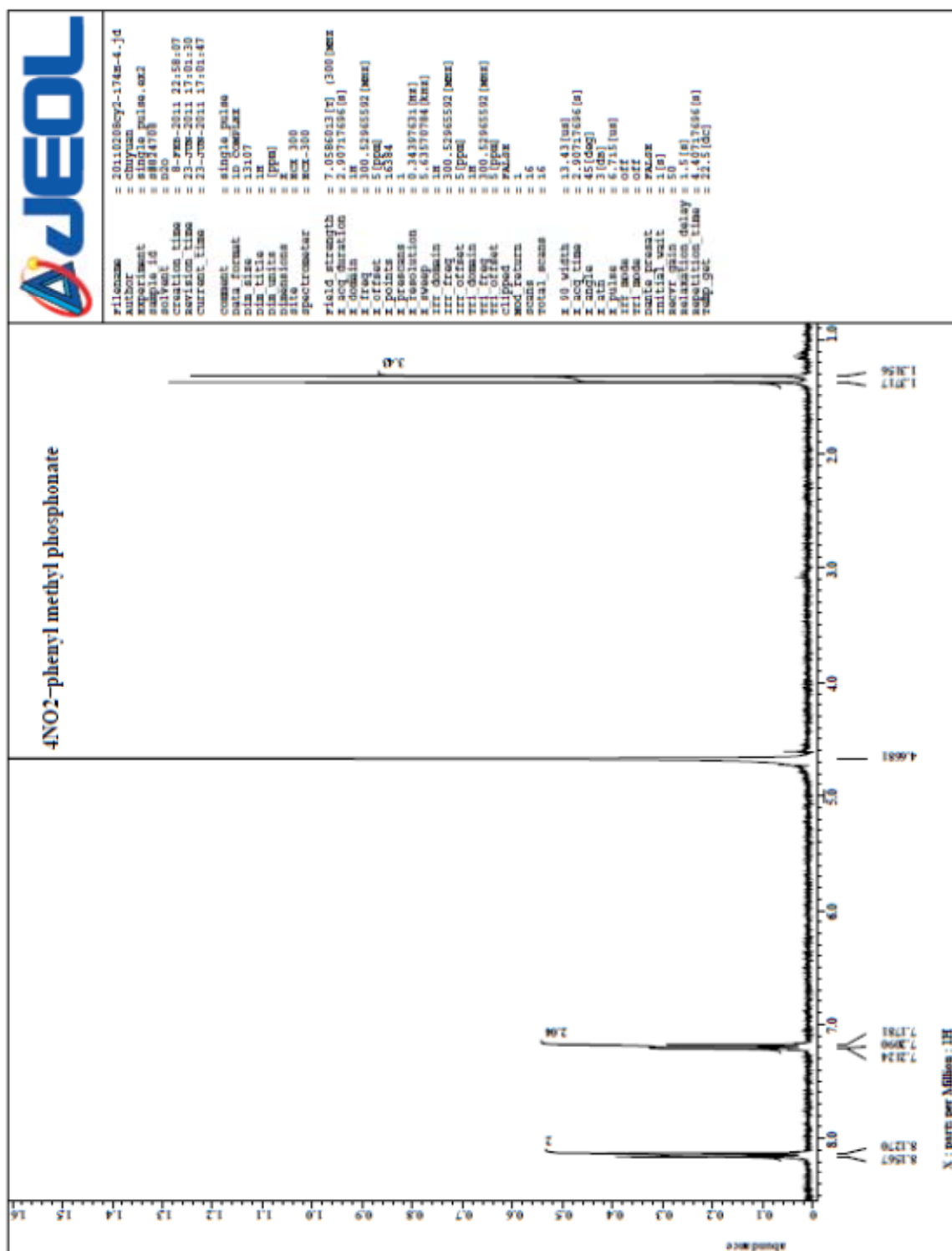


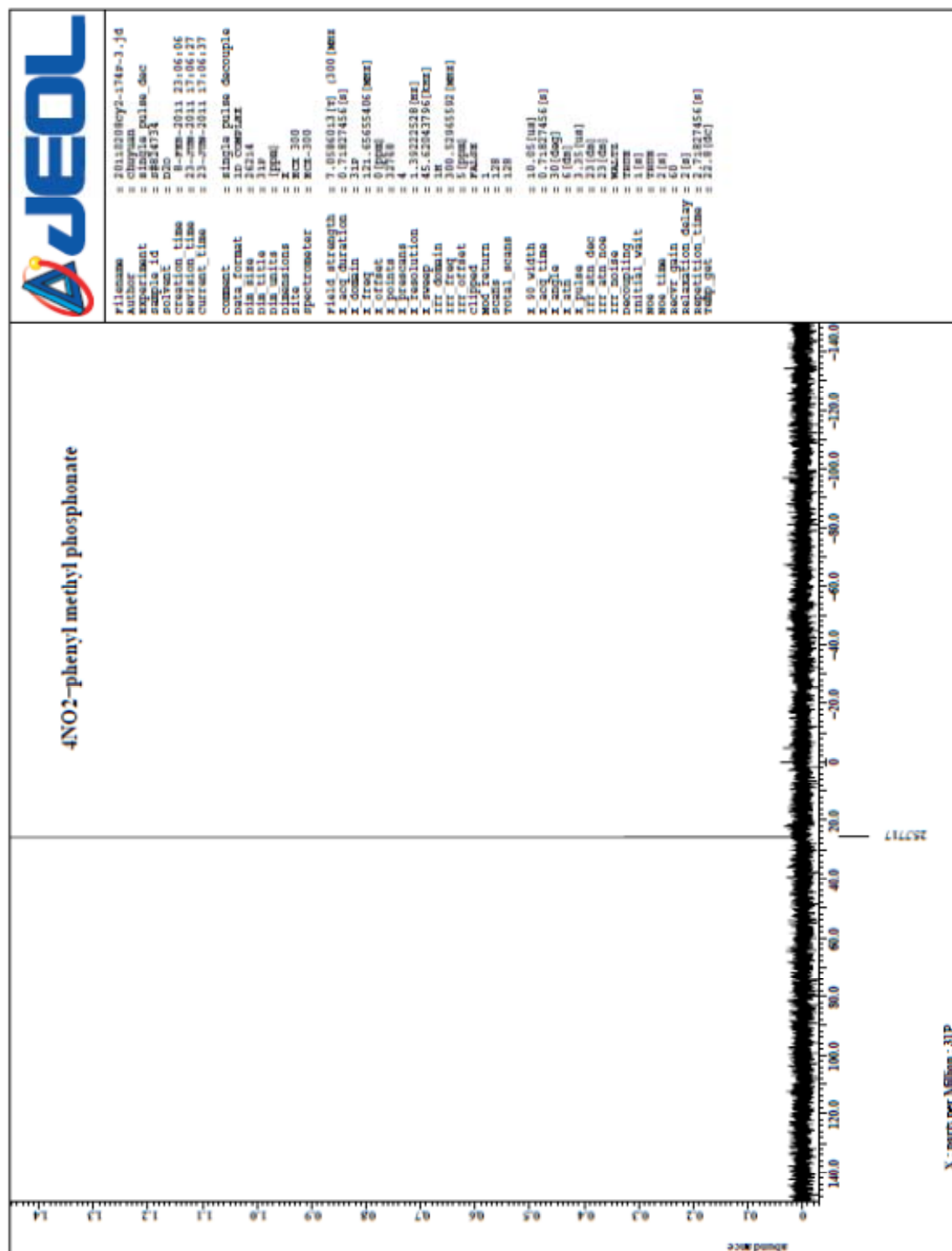
A35.  $^{19}\text{F}$  NMR spectrum of **3f** [Chapter 2]

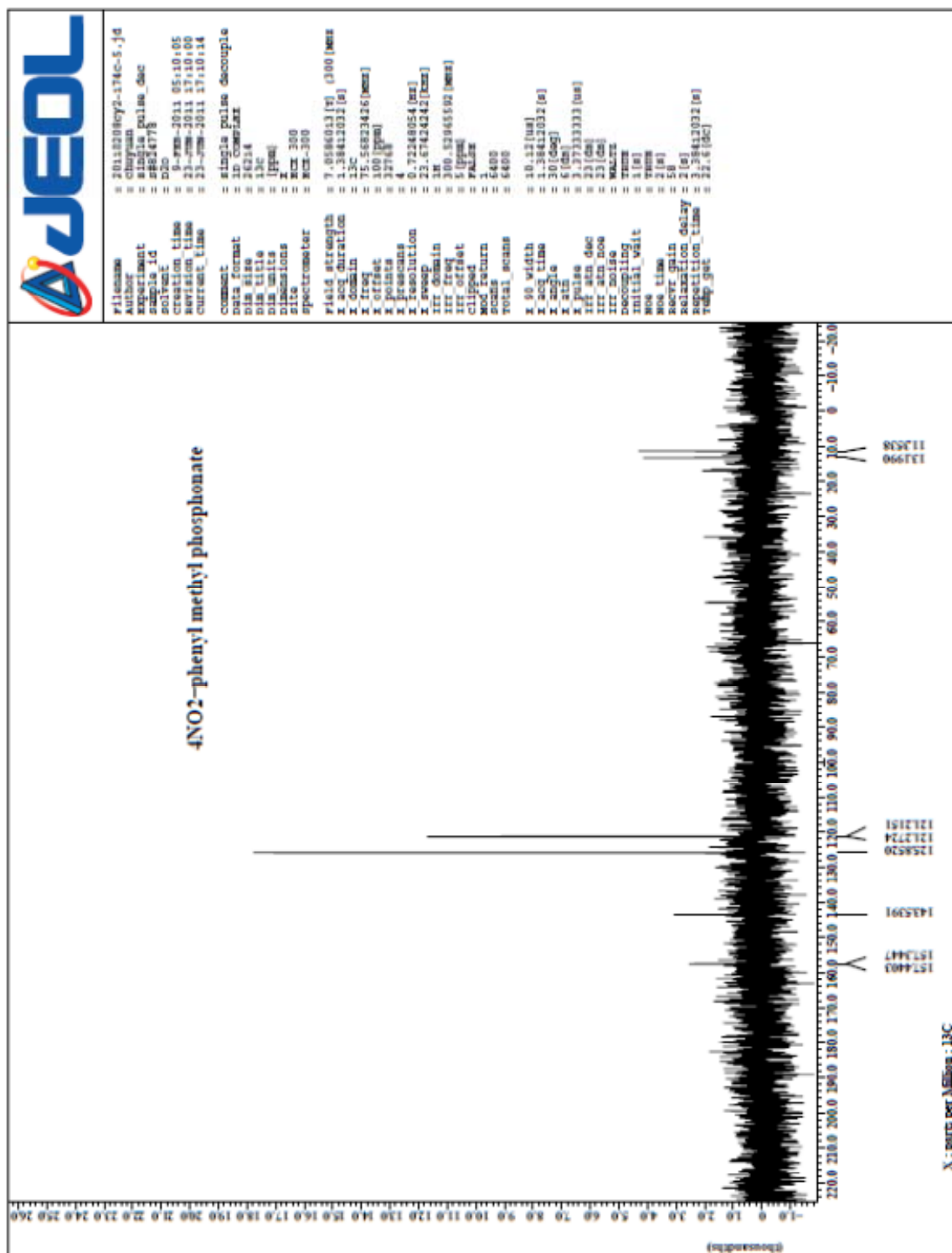


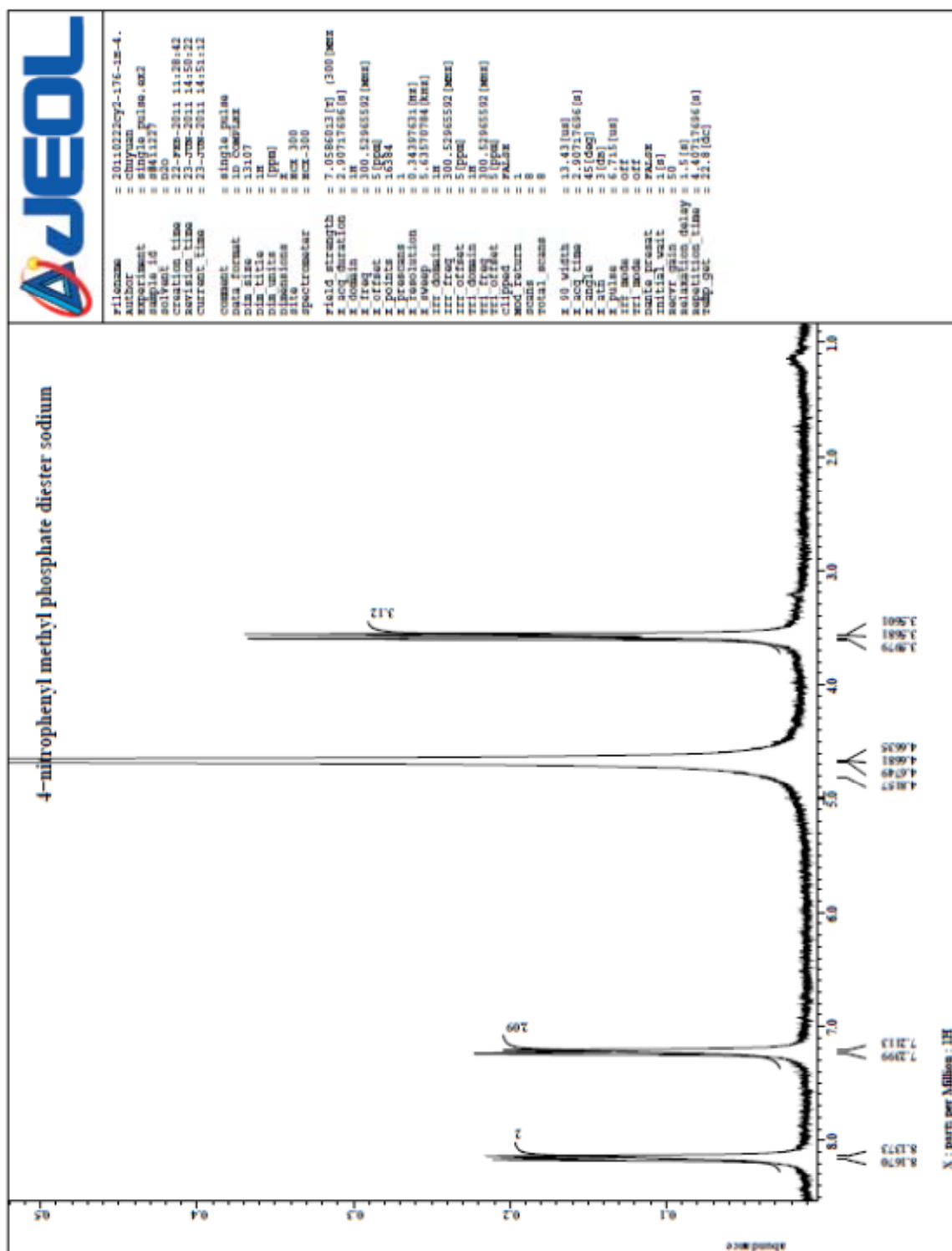
A36. <sup>1</sup>H NMR spectrum of **1a** [Chapter 2]



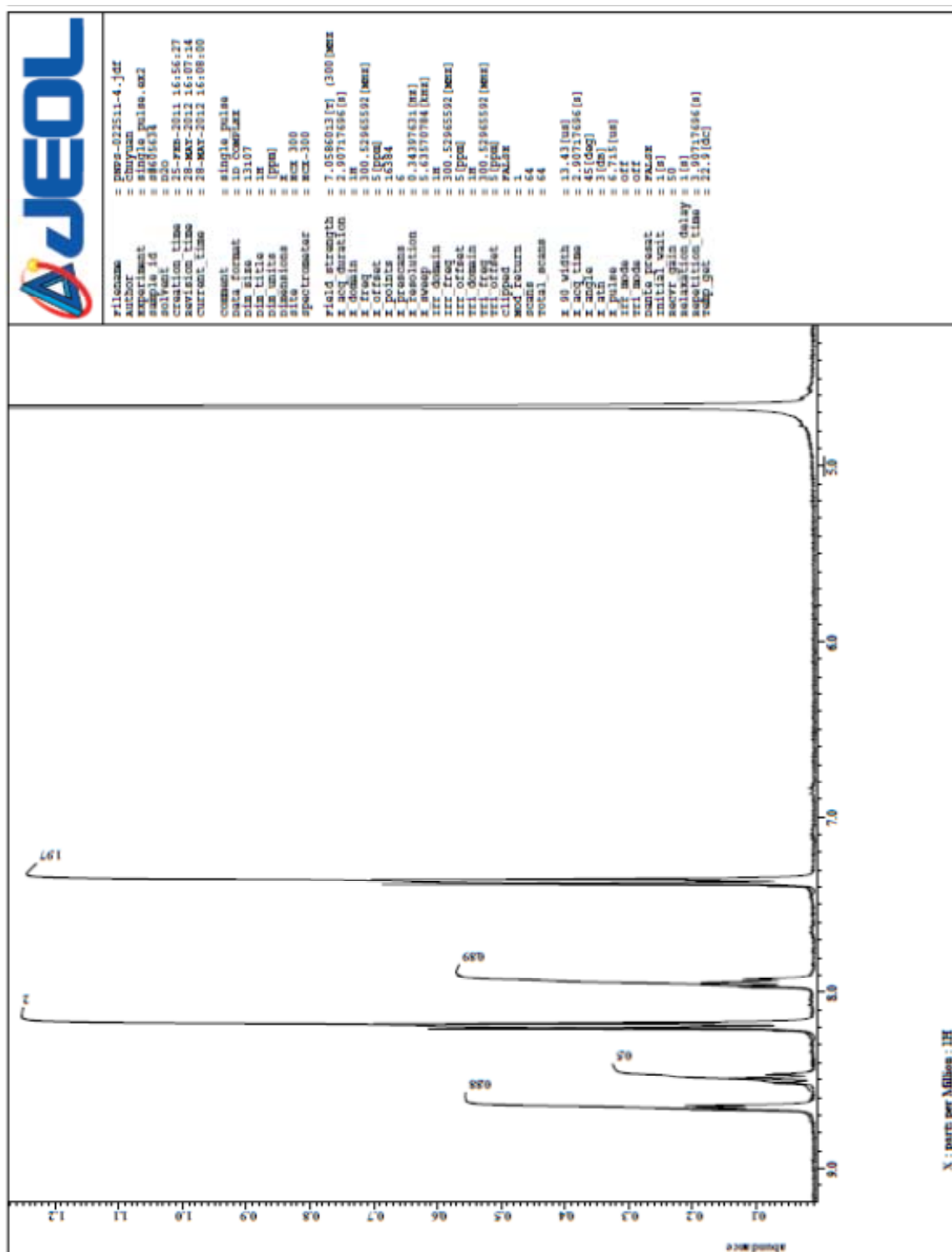
A38. <sup>1</sup>H NMR spectrum of **4a** [Chapter 2]

A39. <sup>31</sup>P NMR spectrum of **4a** [Chapter 2]

A40. <sup>13</sup>C NMR spectrum of **4a** [Chapter 2]

A41.  $^1\text{H}$  NMR spectrum of **5a** [Chapter 2]



A43.  $^1\text{H}$  NMR spectrum of **6a** [Chapter 2]

1 atggcgggatt tagataaaact caacatcgac agcattatcc aacgggctgct ggaagtgaga  
     M A D L D K L N I D S I I Q R L L E V R  
  
 61 gggccaagc ctggtaagaa tgtccagctt caggagaatg aaatcagagg actgtgctta  
     G S K P G K N V Q L Q E N E I R G L C L  
  
 121 aagtctcgtg aaatctttct cagtcagcct atcctactag aacttgaagc accactcaaa  
     K S R E I F L S Q P I L L E L E A P L K  
  
 181 atatgtggtg acatccatgg acaatactat gatttgctgc gactttttga gtacggtggt  
     I C G D I H G Q Y Y D L L R L F E Y G G  
  
 241 ttcccaccag aaagcaacta cctgtttctt ggggactatg tggacAAGgg aaagcagtca  
     F P P E S N Y L F L G D Y V D K G K Q S  
  
 301 ttggagacga tctgcctctt actggcctac aaaataaaaat atcctgagaa ttttttctt  
     L E T I C L L L A Y K I K Y P E N F F L  
  
 361 ctccagagga accatgaatg tgccagcatc aacagaatct atggatttta tgatgaatgt  
     L R G N H E C A S I N R I Y G F Y D E C  
  
 421 aaaagaagat acaacattaa actatggaaa actttcacag actgttttaa ctgtttaccg  
     K R R Y N I K L W K T F T D C F N C L P  
  
 481 atagcagcca tcgtggatga gaagatatcc tgctgtcatg gaggtttatc accagatctt  
     I A A I V D E K I F C C H G G L S P D L  
  
 541 caatctatgg agcagattcg gcgaattatg cgaccaactg atgtaccaga tcaaggtctt  
     Q S M E Q I R R I M R P T D V P D Q G L  
  
 601 ctttngatc ttttgtggtc tgaccccgat aaagatgtct taggctgggg tgaaaatgac  
     L ? D L L W S D P D K D V L G W G E N D  
  
 661 agaggagtgt ccttcacatt tggcgcagaa gtgggtgcaa aatttctcca taagcatgat  
     R G V S F T F G A E V V A K F L H K H D  
  
 721 ttggatctta tatgtagagc ccatcagggtg gttgaagatg gatatgaatt ttttgcaaag  
     L D L I C R A H Q V V E D G Y E F F A K  
  
 781 aggcagttgg tcactctggt ttctgcgccc aattattgcg gagagtttga caatgcaggt  
     R Q L V T L F S A P N Y C G E F D N A G  
  
 841 gccatgatga gtgtggatga aacactaatg tgttcttttc agattttaaa gcctgcagag  
     A M M S V D E T L M C S F Q I L K P A E  
  
 901 aaaaagaagc caaatgccac gagacctgta acgcctccaa ggggtatgat cacaaagcaa  
     K K K P N A T R P V T P P R G M I T K Q  
  
 961 gcaaagaaa  
     A K K

#### A44. DNA sequencing result of R96K mutant of PP1 $\gamma$ [Chapter 2]

```

1  atggcgggatt tagataaaact caacatcgac agcattatcc aacggctgct ggaagtgaga
   M A D L D K L N I D S I I Q R L L E V R

61  gggccaagc ctggtaagaa tgtccagctt caggagaatg aaatcagagg actgtgctta
   G S K P G K N V Q L Q E N E I R G L C L

121 aagtctcgtg aaatctttct cagtcagcct atcctactag aacttgaagc accactcaaa
   K S R E I F L S Q P I L L E L E A P L K

181 atatgtgggtg acatccatgg acaatactat gatttgctgc gactttttga gtacggtggt
   I C G D I H G Q Y Y D L L R L F E Y G G

241 ttcccaccag aaagcaacta cctgtttctt ggggactatg tggacaaaggg aaagcagtca
   F P P E S N Y L F L G D Y V D R G K Q S

301 ttggagacga tctgcctctt actggcctac aaaataaaaat atcctgagaa ttttttctt
   L E T I C L L L A Y K I K Y P E N F F L

361 ctcagagggga accatgaatg tgccagcatc aacagaatth atggatttta tgatgaatgt
   L R G N H E C A S I N R I Y G F Y D E C

421 aaaagaagat acaacattaa actatggaaa actttcacag actgttttaa ctgtttaccg
   K R R Y N I K L W K T F T D C F N C L P

481 atagcagcca tcgtggatga gaagatatcc tgctgtcatg gaggtttatc accagatctt
   I A A I V D E K I F C C H G G L S P D L

541 caatctatgg agcagattcg gcgaattatg cgaccaactg atgtaccaga tcaaggtctt
   Q S M E Q I R R I M R P T D V P D Q G L

601 ctttngatc ttttgtggtc tgaccccgat aaagatgtct taggctgggg tgaaaatgac
   L ? D L L W S D P D K D V L G W G E N D

661 AAAggagtgct ccttcacatt tggcgcagaa gtgggttgcaa aatttctcca taagcatgat
   K G V S F T F G A E V V A K F L H K H D

721 ttggatctta tatgtagagc ccatcaggtg gttgaagatg gatatgaatt ttttgcaaag
   L D L I C R A H Q V V E D G Y E F F A K

781 aggcagttgg tcactctggt ttctgcgccc aattattgcg gagagtttga caatgcaggt
   R Q L V T L F S A P N Y C G E F D N A G

841 gccatgatga gtgtggatga aacactaatg tgttcttttc agattttaaa gcctgcagag
   A M M S V D E T L M C S F Q I L K P A E

901 aaaaagaagc caaatgccac gagacctgta acgcctccaa ggggtatgat cacaaagcaa
   K K K P N A T R P V T P P R G M I T K Q

961 gcaaagaaa
   A K K

```

#### A45. DNA sequencing result of R221K mutant of PP1 $\gamma$ [Chapter 2]

```

1  atggcgggatt tagataaaact caacatcgac agcattatcc aacgggctgct ggaagtgaga
   M A D L D K L N I D S I I Q R L L E V R

61  gggccaagc ctggtaagaa tgtccagctt caggagaatg aaatcagagg actgtgctta
   G S K P G K N V Q L Q E N E I R G L C L

121 aagtctcgtg aaatctttct cagtcagcct atcctactag aacttgaagc accactcaaa
   K S R E I F L S Q P I L L E L E A P L K

181 atatgtggtg acatccatgg acaatactat gatttgctgc gactttttga gtacggtggt
   I C G D I H G Q Y Y D L L R L F E Y G G

241 ttcccaccag aaagcaacta cctgtttctt ggggactatg tggacAAGgg aaagcagtca
   F P P E S N Y L F L G D Y V D K G K Q S

301 ttggagacga tctgcctctt actggcctac aaaataaaaat atcctgagaa tttttttctt
   L E T I C L L L A Y K I K Y P E N F F L

361 ctcagagggga accatgaatg tgccagcatc aacagaatth atggatttth tgatgaatgt
   L R G N H E C A S I N R I Y G F Y D E C

421 aaaagaagat acaacattaa actatggaaa actttcacag actgttttth ctgtttaccg
   K R R Y N I K L W K T F T D C F N C L P

481 atagcagcca tcgtggatga gaagatatth tgctgtcatg gaggtttatc accagatctt
   I A A I V D E K I F C C H G G L S P D L

541 caatctatgg agcagattcg gcgaattatg cgaccaactg atgtaccaga tcaaggtctt
   Q S M E Q I R R I M R P T D V P D Q G L

601 ctttngatc ttttgtggtc tgaccccgat aaagatgtct taggctgggg tgaaaatgac
   L ? D L L W S D P D K D V L G W G E N D

661 AAAggagtg ctttcacatt tggcgcagaa gtgggtgcaa aatttctcca taagcatgat
   K G V S F T F G A E V V A K F L H K H D

721 ttggatctta tatgtagagc ccatcagggtg gttgaagatg gatatgaatt ttttgcaaag
   L D L I C R A H Q V V E D G Y E F F A K

781 aggcagttgg tcactctggt ttctgcgccc aattattgag gagagtttga caatgcaggt
   R Q L V T L F S A P N Y C G E F D N A G

841 gccatgatga gtgtggatga aacactaatg tgttcttttc agattttaaa gcctgcagag
   A M M S V D E T L M C S F Q I L K P A E

901 aaaaagaagc caaatgccac gagacctgta acgcctccaa ggggtatgat cacaaagcaa
   K K K P N A T R P V T P P R G M I T K Q

961 gcaaagaaa
   A K K

```

**A46.** DNA sequencing result of R96K R221K double mutant of PP1 $\gamma$  [Chapter 2]

**<sup>15</sup>N KIE**

Delta TC	Rinf.
-3.84	
-4.16	
-3.53	
-4.4	
-3.98	0.99602

PP1 y 3.37 mg/mL  
pNPPT  
pH 7.0 (Base Mix/0.5 mM DTT)  
30°C

$$\text{isotope effect} = \log(1-f) / \log((1-f)(R_s / R_o))$$

$$\text{isotope effect} = \log(1-f) / \log((1-f)(R_p / R_o))$$

Sample	P Delta	RS Delta	Rp	Rs	f	IE(Rs,Ro)	IE(Rp,Ro)	IE(Rp,Rs)
1	-4.51	-3.40	0.99549	0.99660	0.462	1.00094	1.00073	1.00083
2	-2.65	-3.61	0.99735	0.99639	0.295	1.00107	0.99840	0.99919
3	-3.14	-3.70	0.99686	0.99630	0.284	1.00085	0.99900	0.99952
Mean						1.00095	0.99938	0.99985
Sd						0.00011	0.00121	0.00087
overall						1.00017		<b>1.00006</b>
Sd						0.00116		0.00103
SE						0.00058		0.00042

**Bridge <sup>18</sup>O KIE**

Delta TC	Rinf.
-1.65	
-1.37	
-1.97	
-1.66333	0.99834

y	x	z	b	15-N	number of
fraction	fraction	fraction	fraction	isotope	discrimin.
of 18-O	of 15-N	of 15-N	of 15-N	effect	atoms
in double	in double	in 14-N	in		1
labeled cp	labeled cp	labeled cp	mixture		
0.901	0.99	0.0003	0.00364	1.00006	1

Sample	P Delta	S Delta	Rp	Rs	f	IE(Rs,Ro)	IE(Rp,Ro)	corrected IE(Rs)	corrected IE(Rp)	corrected IE(Rp,Rs)	corrected IE (Rp,Rs)
1	-11.20	3.19	0.98880	1.00319	0.195	1.02287	1.01077	1.02754	1.01290	1.01308	1.01567
2	-11.21	3.23	0.98879	1.00323	0.195	1.02306	1.01078	1.02777	1.01291	1.01313	1.01572
3	-11.18	0.51	0.98882	1.00051	0.163	1.01237	1.01053	1.01483	1.01261	1.01083	1.01295
4	-10.96	0.50	0.98904	1.00050	0.163	1.01232	1.01029	1.01476	1.01232	1.01061	1.01269
Mean						1.01765	1.01059	1.02123	1.01269	1.01191	1.01426
Sd						0.00613	0.00023	0.00742	0.00028	0.00138	0.00166
overall						1.01412		1.01696			<b>1.01606</b>
Sd						0.00551		0.00667			0.00555
SE						0.00225		0.00334			0.00227

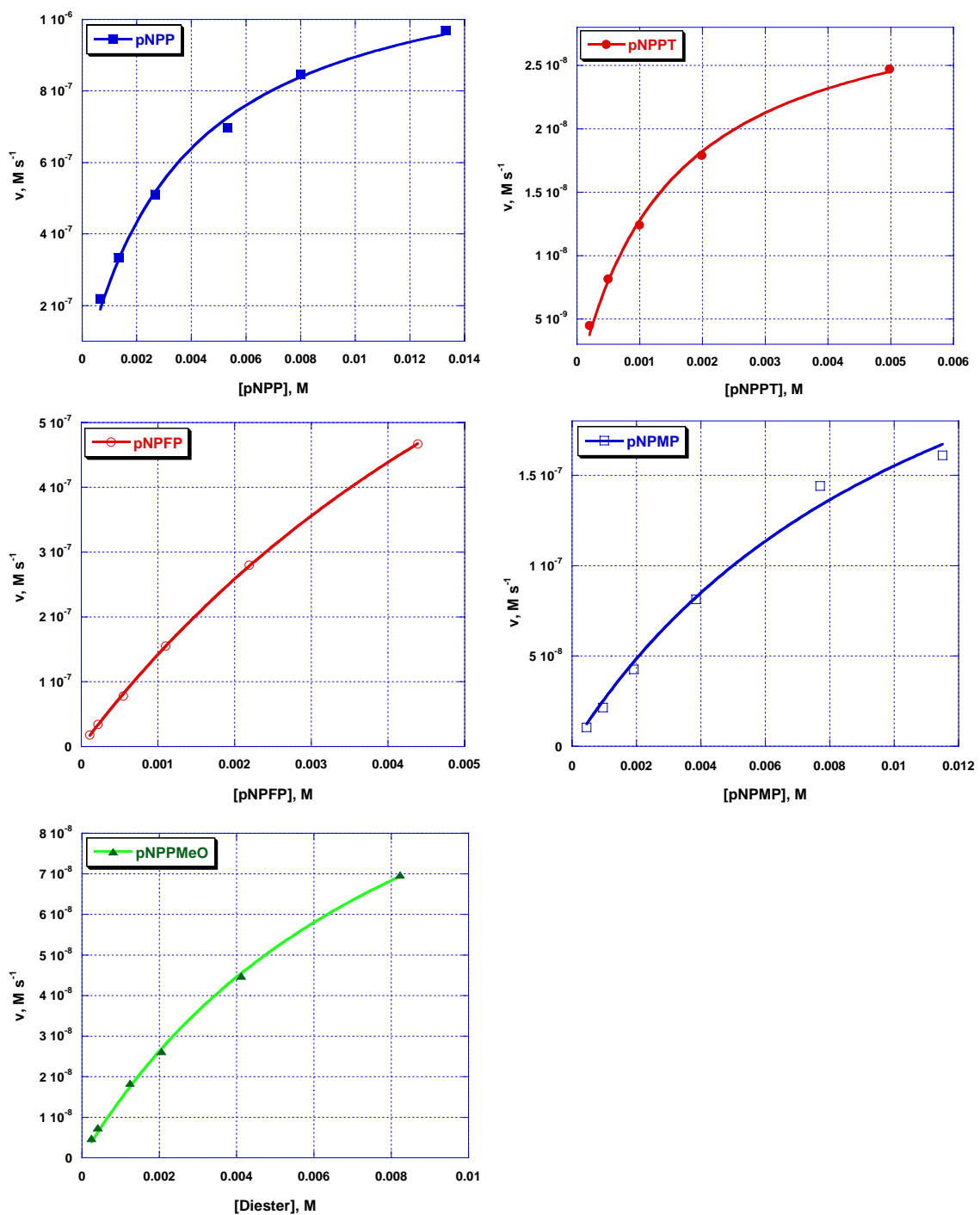
**Nonbridge <sup>18</sup>O KIE**

TC	Rinf.
-35.82	
-34.67	
-35.25	0.96476

y	x	z	b	15-N	number of	Substrate =
fraction	fraction	fraction	fraction	isotope	discrimin.	pNPPT
of 18-O	of 15-N	of 15-N	of 15-N	effect	atoms	fraction
in double	in double	in 14-N	in			Ka at 39°C*
labeled cp	labeled cp	labeled cp	mixture			the reactant
						pH at 25°C
0.895	0.99	0.0003	0.00353	1.00006	2	1.000

Sample	P Delta	S Delta	Rp	Rs	f	IE(Rs,Ro)	IE(Rp,Ro)	corrected IE O <sub>i</sub> (Rs)	corrected IE O <sub>i</sub> (Rp)	corrected IE(Rp,Rs)	corrected IE O <sub>i</sub> (Rp,RS)	corrected IE O <sub>i</sub>	pH correct
1	-1.99	-36.03	0.99801	0.96397	0.195	0.99626	0.96278	0.99782	0.97852	0.96933	0.98234		
2	-2.42	-35.99	0.99758	0.96401	0.195	0.99645	0.96325	0.99793	0.97879	0.96974	0.98258		
3	0.89	-36.03	1.00089	0.96397	0.197	0.99630	0.95962	0.99785	0.97669	0.96687	0.98092		
4	0.73	-36.04	1.00073	0.96396	0.197	0.99626	0.95980	0.99782	0.97679	0.96700	0.98099		
Mean						0.99632	0.96136	0.99786	0.97770	0.96865	0.98195		
Sd						0.00009	0.00192	0.00005	0.00111	0.00151	0.00087		
overall						0.97884		0.98778		0.98575	0.97171	<b>0.97170</b>	
Sd						0.01873		0.01080		0.00913	0.01800	0.01800	
SE						0.00936		0.00540		0.00373	0.00735	0.00735	

**A47. Kinetic isotope effect data of substrate 2a [Chapter 3]**



**A48.** Michaelis-Menten curves for hydrolysis of substrate **1a-5a** catalyzed by PP1 $\gamma$  at pH 7.0. Each figure shows substrate concentration-dependent hydrolytic activity in turn for **1a** (pNPP), **2a** (pNPPT), **3a** (pNPFP), **4a** (pNPMP) and **5a** (phosphate diester).

## CURRICULUM VITAE

Yuan Chu

(June 2012)

## EDUCATION

Ph.D., Organic Chemistry, Utah State University, Logan, Utah, USA .....	08/2012
Ph.D., Organic Chemistry, Nankai University, Tianjin, China .....	12/2007
B. Sc., Chemistry, Nankai University, Tianjin, China .....	07/2002

## PROFESSIONAL EXPERIENCE

- Systematically studied in characterizing the mechanistic details of chemical reactions, especially those of biological interest, with the goal of understanding the origins of the tremendous catalytic power of enzymes. Ongoing projects are examining the chemistry of phosphate esters and sulfate esters to understand how enzymes accomplish this remarkable chemistry.
- Developed a method for determining the relationship between the stability of the imidazolium-type room-temperature ionic liquids under basic conditions and their conjugate bases *N*-heterocyclic carbenes.
- Systematically studied the hydrogen transfer mechanism of reduction of  $\alpha,\beta$ -unsaturated ketone and recycling processes in the yeast by using quantitative isotope tracing close to natural abundance measured by  $^2\text{H}$  NMR.

**By two pH.D experiences, I learn a wide variety of skills than span the fields of chemistry and biochemistry.**

## PUBLICATIONS

**Conference papers:**

1. Yuan Chu, Nicholas H. Williams, Alvan C. Hengge\*. “Mechanistic study of phosphoryl transfer reactions catalyzed by protein phosphatase-1”  
239th ACS National Meeting, San Francisco, CA, March 21-25, 2010, BIOL-92.
2. Yuan Chu, Nicholas H. Williams, Alvan C. Hengge\*. “Mechanistic study of phosphoryl transfer reactions catalyzed by protein phosphatase-1”  
239th ACS National Meeting, San Francisco, CA, March 21-25, 2010, BIOL-92.

**Book chapters:**

3. Alvan C. Hengge, Yuan Chu. “Phosphatases” in Encyclopedia of Catalysis, 2nd edition. Edited by Istvan T. Horvath, Wiley, 2010.

**Journal articles:**

4. Yuan Chu, Ben-Li Zhang\*, Virginie Silvestre, Jin-Pei Cheng\*. “Hydrogen transfer pathways of the asymmetric reduction of  $\alpha,\beta$ -unsaturated ketone mediated by baker’s yeast.” *Bioorganic Chemistry* **2006**, 34,158-166.
5. Yuan Chu, Hui Deng, Zhao Li, Jin-Pei Cheng\*. “An Acidity Scale of 1,3-Dialkylimidazolium Salts in Dimethylsulfoxide Solution.” *Journal of Organic Chemistry* **2007**, 72, 7790-7793.